To the Graduate Council:

I am submitting herewith a dissertation written by Patrick Elliott Perkins entitled "The Application of Non-linear Coherent Optical Processes to the Measurement of Number Density and Temperature." I recommend that it be accepted in partial fulfillment of the requirements for the degree of Doctor of Philosophy, with a major in Physics.

A. A. Mason, Major Professor

We have read this dissertation
and recommend its acceptance:

William H. Fletcher

Robert J. Lovell

Accepted for the Council:

Vice Chancellor
Graduate Studies and Research

Thesis
80b
.P474
Cop.2

THE APPLICATION OF NON-LINEAR COHERENT OPTICAL PROCESSES TO THE MEASUREMENT OF NUMBER DENSITY AND TEMPERATURE

A Dissertation

Presented for the

Doctor of Philosophy

Degree

The University of Tennessee, Knoxville

Patrick Elliott Perkins

March 1980

1113841

ABSTRACT

The functional form of the third-order susceptibility as it relates to Coherent Anti-Stokes Raman Scattering (CARS) and to Stimulated Raman Scattering (SRS) is developed from current literature as it applies to centrosymmetric and isotropic media (gases), including polarization effects. Mixtures of gases are also considered.

The theoretical power functions for CARS and SRS as a function of laser difference frequency are convolved with representative Gaussian laser linewidths. Spectral profiles are generated for N_2 Q-branch CARS and O_2 Q-branch SRS and are compared to experimental data. The effects of different number density and temperature regimes as well as laser linewidths are considered and illustrated.

The utility of CARS and SRS in the measurement of number density and temperature is determined within representative experimental regimes for two possible techniques: (1) fitting observed spectral profiles by the method of minimizing a weighted least squares functions or (2) ratioing the peak height intensity of two selected resonances including a linewidth normalization scheme.

For the method of profile fitting, the functional linewidth derivatives of the convolved power expressions and an assumed (N, T) linewidth dependence are used within the framework of multivariate non-linear regression analysis to predict

realistic measurement errors from Gaussian shot noise, a finite signal-to-noise ratio, and linewidth uncertainties. The resonance linewidth masking due to a comparable order-of-magnitude laser linewidth is demonstrated as beneficial in regards to the error influence of detection noise as well as resonance linewidth uncertainties.

TABLE OF CONTENTS

CHAPTER		PAGE
1.	INTRODUCTION.	1
2.	THEORY.	10
	2.1 Non-Linear Wave Equation	
	2.2 Third-Order Susceptibility	
	2.3 Macroscopic Tensor	
	2.4 Effects of Finite Laser Linewidths	
	2.5 Convolution of $\|X_{CARS}\|^2$	
	2.6 Convolution of $-X''_{SRS}$	
3.	COMPARISON OF EXPERIMENT AND THEORY	38
	3.1 CARS	
	3.2 SRS	
4.	EFFECTS OF PRESSURE AND TEMPERATURE ON RAMAN LINEWIDTH	46
	4.1 Effective Linewidth	
	4.2 Pressure and Temperature Effects	
5.	REPRESENTATIVE SPECTRAL PROFILES.	50
	5.1 N_2 CARS Versus SRS	
	5.2 Effects of Different zl Parameters	
	5.3 Effects of Number Density	
	5.4 Effects of Temperature	
6.	RATIOING TECHNIQUES IN (N, T) MEASUREMENT . . .	78
	6.1 Linewidth Effects	
	6.2 FM Normalization	
7.	PARAMETERIZATION OF NON-LINEAR PROFILE FITTING	84
8.	MULTIVARIATE NON-LINEAR REGRESSION ANALYSIS . .	97
	8.1 Basic Theory	
	8.2 Application to Experimental Error	

CHAPTER PAGE

9. ERROR ANALYSIS. 108

9.1 Explanation of Error Tables
9.2 Count Rate Versus Number Density
9.3 Effects of the zl Parameter
9.4 Influence of X_{NR}
9.5 Effects of Linewidth Uncertainties
9.6 CARS Versus SRS

10. CONCLUSIONS 133

LIST OF REFERENCES. 135

APPENDIXES 139

APPENDIX A. TABLES. 140

APPENDIX B. EXPONENTIALS. 169

APPENDIX C. THE COMPLEX ERROR FUNCTION. 171

APPENDIX D. LINE STRENGTH FACTOR. 174

VITA 178

LIST OF TABLES

TABLE		PAGE
1.	N_2 Error - CARS (T, N), T = 60^oK	141
2.	N_2 Error - CARS (T, N), T = 300^oK	142
3.	N_2 Error - CARS (T, N), T = 1200^oK	143
4.	N_2 Error - CARS (T), (N), T = 60^oK	144
5.	N_2 Error - CARS (T), (N), T = 300^oK	145
6.	N_2 Error - CARS (T), (N), T = 1200^oK	146
7.	N_2 Error - SRS (T, N), T = 60^oK	147
8.	N_2 Error - SRS (T, N), T = 300^oK	148
9.	N_2 Error - SRS (T, N), T = 1200^oK	149
10.	N_2 Error - SRS (T), (N), T = 60^oK	150
11.	N_2 Error - SRS (T), (N), T = 300^oK	151
12.	N_2 Error - SRS (T), (N), T = 1200^oK	152
13.	CO Error - SRS (T, N)	153
14.	CO Error - SRS (T), (N)	154
15.	CO Error - CARS (T, N), T = 60^oK	155
16.	CO Error - CARS (T, N), T = 300^oK	156
17.	CO Error - CARS (T, N), T = 1200^oK	157
18.	CO Error - CARS (T), (N), T = 60^oK	158
19.	CO Error - CARS (T), (N), T = 300^oK	159
20.	CO Error - CARS (T), (N), T = 1200^oK	160
21.	CO Error - CARS (T, N); X_{NR}	161
22.	CO Error - CARS (T), (N); X_{NR}	162
23.	Pressure Broadening Coefficients	163
24.	CARS N_2 Peak Height Error	164

TABLE PAGE

25. N_2 CARS Variance Error, zl = 0.050. 165

26. N_2 CARS Variance Erorr, zl = 0.010. 166

27. N_2 SRS Variance Error, zl = 0.050 167

28. N_2 SRS Variance Error, zl = 0.010 168

LIST OF FIGURES

FIGURE		PAGE
1.	Energy Diagram.	2
2.	CARS Advantages/Disadvantages	4
3.	SRS Advantages/Disadvantages.	5
4.	N_2 Q-Branch CARS Profile: Low Resolution Exp/Theory.	39
5.	N_2 Q-Branch CARS Profile: High Resolution Exp/Theory.	41
6.	O_2 Q-Branch SRS Profile: High Resolution Exp/Theory.	44
7.	N_2 CARS/SRS Profile: (N, T, zl) = 0.2 Amagat, 60°K, 0.200 cm-1.	51
8.	N_2 CARS/SRS Profile: (N, T, zl) = 0.01 Amagat, 300°K, 0.020 cm-1	52
9.	N_2 CARS/SRS Profile: (N, T, zl) = 1.0 Amagat, 1200°K, 0.200 cm-1.	53
10.	N_2 CARS/SRS Profile: (N, T, zl) = 0.10 Amagat, 1200°K, 0.020 cm-1.	54
11.	N_2 SRS: (N, T) = 0.20 Amagats, 60°K.	57
12.	N_2 CARS: (N, T) = 0.002 Amagats, 60°K.	58
13.	N_2 CARS: (N, T) = 0.010 Amagats, 300°K	59
14.	N_2 CARS: (N, T) = 1.0 Amagats, 1200°K.	60
15.	N_2 SRS: (N, T) = 0.10 Amagats, 1200°K.	61
16.	N_2 SRS: (T, zl) = 300°K, 0.020 cm-1.	63
17.	N_2 SRS: (T, zl) = 300°K, 0.200 cm-1.	64
18.	N_2 SRS: (T, zl) = 1200°K, 0.020 cm-1	65
19.	CO/N_2 CARS: (T, zl) = 300°K, 0.020 cm-1.	67
20.	CO/N_2 CARS: (T, zl) = 300°K, 0.200 cm-1.	68

FIGURE PAGE

21. CO/N_2 SRS: (T, z1) = 300°K, 0.020 cm-1. 69

22. CO/N_2 CARS: (T, z1) = 1200°K, 0.020 cm-1. 70

23. CO/N_2 CARS: (T, z1) = 1200°K, 0.200 cm-1. 71

24. N_2 SRS: (N, z1) = 0.2 Amagats, 0.200 cm-1 72

25. N_2 SRS: (N, z1) = 0.002 Amagats, 0.020 cm-1 . . . 74

26. N_2 CARS: (N, z1) = 1.0 Amagats, 0.200 cm-1. . . . 75

27. N_2 CARS: (N, z1) = 0.100 Amagats, 0.020 cm-1. . . 76

28. N_2 CARS: (N, z1) = 1.0 Amagats, 0.020 cm-1. . . . 77

29. CARS (N, T) Error in (N) at 100°K. 113

30. CARS (N, T) Error in (T) at 100°K. 114

31. SRS (N, T) Error in (N) at 100°K 115

32. SRS (N, T) Error in (T) at 100°K 116

33. CARS 100°K, 0.1 Amagat Profile 118

34. SRS 100°K, 0.1 Amagat Profile. 119

LIST OF SYMBOLS

$\vec{P}^{(3)}$	dielectric source polarization
$\vec{E}$	electric field vector
$\chi^{(3)}$	third-order non-linear susceptibility tensor (cm^3/erg)
T_{iJ}	transformation matrix
$\vec{\ell}_i$	unit polarization vector of E_i
$\vec{\ell}_{CARS}$	CARS polarization vector
$\vec{k}$	propagation vector
$\Delta\vec{k}$	phase difference
ω_p	pump laser frequency (cm^{-1})
ω_s	Stokes laser frequency (cm^{-1})
ω_{as}	anti-Stokes laser frequency (cm^{-1})
n_{as}	anti-stokes index of refraction
P_p	pump laser power (ergs)
P_s	Stokes laser power (ergs)
P_{as}	anti-Stokes power
P_{SRS}	stimulated Raman power
X_{NR}	non-resonant susceptibility
X_{CARS}	third-order susceptibility for CARS
X_{SRS}	third-order susceptibility for SRS
$\frac{d\sigma}{d\Omega}$	Raman scattering cross section
a_J	line strength factor
n_J	nuclear spin factor
Δ_J	population difference
δ	frequency different
Γ	Raman linewidth HWHM

β_ℓ	Lorentzian linewidth
β_g	Gaussian linewidth
γ_{ijkl}	microscopic susceptibility
N	number density
T	temperature
ψ	polarization angle
β	analyzer angle
$D'_{nn}, D^{*'}_{nn}$	Resonance denominators
d_{ij}	CARS transition moment
e_{ij}	SRS transition moment
$\overline{P}_J$	normalized resonance denominator
$\overline{Y}_J$	normalized linewidth
$\overline{X}_J$	normalized frequency difference
$\overline{K}_J$	normalized product of linestrength factor and population difference
$\overline{D}_{kjnm}, \overline{Y}_{jm}$	CARS interference functions
X_0	normalized tensor multiplier
zl	R.M.S. laser linewidth parameter
$\overline{W}(\overline{Z})$	complex error function
$Z\vec{K}M$, $Z\vec{K}C$	CARS interference vector functions
$\overline{\beta}$	normalization constant
$\vec{c}$	parameter vector
$\vec{\varepsilon}$	error vector
Ω	variance
$\underline{M}^{-1}$	error matrix
$\underline{\alpha}$	Jacobean matrix

S/N	signal-to-noise ratio
Ω_α	linewidth variance

CHAPTER 1

INTRODUCTION

Coherent scattering processes arising from the third-order non-linear susceptibility [$X^{(3)}$] have received considerable recent attention due to the possible improvement relative to spontaneous Raman scattering in the measurement of number density and temperature (N, T). Reasons cited range from the N^2 signal dependence characteristic of CARS to the achievement of higher intrinsic spectral resolution in both CARS and SRS. Tolles (1) and Owyoung (2) have discussed these subjects extensively.

In actual application, CARS temperature measurement in combustion-like 1500K environments has been achieved by Shaub (3) and Eckbreth (4). Moya (5) and his French associates have reported number density measurements. Experimental SRS has received less attention; Owyoung (2, 6, 7) has reported experiments on hydrogen and methane while Ezekiel (8) has obtained unpublished Q-branch spectra in nitrogen and oxygen.

Although CARS and SRS are both two-photon resonant processes with the implicit dependence on number density, population difference, and phenomenological Raman linewidth, there are decided differences. CARS may be considered as a four-wave parametric mixing process (Fig. 1A) generating a coherent light output at the new frequency $\omega_{as} = 2\omega_p - \omega_s$ and with a power proportional to $|x^{(3)}|^2$ (5, 9, 10, 11). SRS is a different type of mixing process (Fig. 1B) in which a gain (loss) is exhibited at the Stokes (pump) frequency proportional to the imaginary part of $X^{(3)}$ (2, 12).

A. CARS

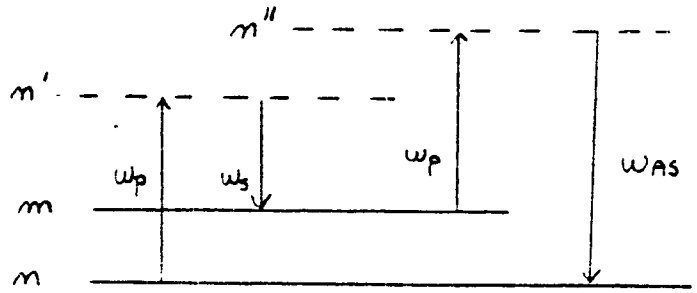

B. SRS

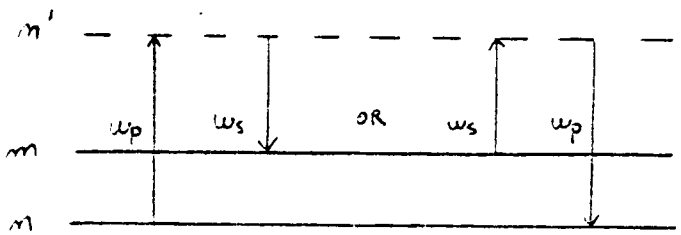

FIGURE 1. ENERGY DIAGRAM

The experimental advantages and disadvantages of CARS and SRS are reproduced from Owyoung (2) in Figures 2 and 3. One important experimental distinction should be emphasized. In the notation of Bloembergen (13), SRS ($-\omega_s$, ω_s, $-\omega_p$, ω_p) is self-phase matching. The wavevector difference is identically zero since

$$\Delta k = -k_s + k_s - k_p + k_p \equiv 0. \tag{1}$$

Power generation is dependent on scattering volume rather than on phase-matching.

However, CARS ($-\omega_{as}$, ω_p, ω_p, $-\omega_s$) is fundamentally different since

$$\Delta k = -k_{as} + 2k_p - k_s. \tag{2}$$

One of the explanations for the large discrepancy between experimental and theoretical power calculations (5) has been the $[\mathrm{SINC}|\Delta k|]^2$ term predicted by theory. For non-zero Δk, one significantly decreases the effective scattering volume with a corresponding decrease in signal.

Although crossed pump beam configurations such as BOXCARS (4) have been used to alleviate the phase matching problem and to allow tighter experimental control of the scattering volume, signal generation is reduced nominally by an order of magnitude due to the reduction of the scattering volume. SRS allows more

ADVANTAGES:

1) Coherent output signal:

   a) Provides good discrimination against background luminescence.
   b) Allows considerable freedom in system design since the sensitivity will not be limited by the geometry of the collection optics.

2) Increased sensitivity over SRS with output signal scaling as the cube of the input power. This results in the highest sensitivities of all of the techniques examined for most of the cases considered. Output power for a given input is orders of magnitude higher than SRS.

3) Output directly reflects the spectrum of the input beams; thus, high spectral resolutions are possible with no loss in sensitivity.

4) Excellent time resolution with no loss in sensitivity is obtained.

DISADVANTAGES

1) Relatively complex optics and critical alignment requirements.

2) Phase matching requirements may produce difficulties at high pressures.

3) Data reflects $|\chi^{(3)}|^2$ and may thus be more difficult to interpret.

4) Nonresonant background signal must be eliminated to see densities $<10^{15}$ cm^{-3}. This is possible but complicates the experimental apparatus.

5) A broadband dye laser probe is necessary to obtain broadband output data. We note, however, that since the output is coherent there is no loss in sensitivity in the process of analyzing this signal with high spectral resolution.

FIGURE 2. CARS ADVANTAGES/DISADVANTAGES

ADVANTAGES

1) Coherent output signal

   a) Provides good discrimination against background luminescence.
   b) Allows considerable freedom in system design since the sensitivity will not be limited by the geometry of the collection optics.

2) The process is self-phase matching; the beams need not be collinear.

3) The output signal is directly proportional to $\mathrm{Im}\chi^{(3)}$ and thus provides a spectral output similar to that of Spontaneous Raman. Data is thus easier to interpret than that obtained by CARS.

4) The signal does not include contirbutions from $\chi^{(3)}_{NR}$.

5) Resolution is determined by the spectrum of the input beams; thus, high spectral resolution can be attained with no loss in sensitivity.

6) The SRS output signal consists of a small perturbation on a probe beam. Thus, since the probe provides a relatively strong signal, alignment is considerable simplified.

7) Excellent time resolution with no loss in sensitivity.

8) Since the signal is proportional to population difference rather than quadratic, SRS exhibits sensitivities quite comparable to CARS without a cubic dependence on input power.

DISADVANTAGES

1) Optics and alignment requirements are stringent.

2) Multichannel acquistion of data is difficult even with a broadband dye probe since the background probe signal puts stringent requirements on the dynamic range of the detection system.

FIGURE 3. SRS ADVANGAGES/DISADVANTAGES

control of the region of experimental interest as it is inherently self-phase matching.

Even so, both methods have received considerable recent attention. Detection problems are alleviated somewhat in CARS since one is detecting a new frequency rather than the usual amplitude modulation impressed on the carrier Stokes beam in an SRS experiment.

Simultaneous measurements of number density and temperature are possible with either method. If one employs the technique of predicting a theoretical spectral profile as a function of (N, T) and minimizing the difference between the projected profile and an experimental one, minimization of the least-squares error is really determined by the functional linewidth dependence of profile height at a given laser difference frequency. To this end, not only is the convolution of theoretical intensity with respect to finite laser linewidths necessary, but also the explicit Raman resonance linewidths dependence on (N, T). The major necessities of profile fitting are then: (1) theoretical power as a function of linewidths, (2) convolution over finite laser linewidths, and (3) linewidth dependence on (N, T).

To implement profile fitting, a closed-form expression relating theoretical intensity as a function of phenomenological Raman linewidths, laser difference frequency, and finite laser linewidth is extremely useful. Not only is required computation time reduced to the level of the small computer, but the error effects

of laser linewidths, Gaussian measurement shot noise, and inherent measurement inaccuracies in the Raman linewidhts may be determined a priori.

Another possible technique for (N, T) measurement is the ratioing of two selected resonance peaks. Since the ratio is a function of the representative linewidths and the temperature dependent partition function, not only is the convolved power function necessary, but a linewidth measurement technique is extremely useful in reducing measurement error.

The purpose of this dissertation is to determine the functional form for the theoretical spectral profiles in CARS and SRS including polarization and mixture effects. By treating laser linewidths and fluctuations as a representative Gaussian function, the closed-form, convolved theoretical power for CARS and SRS is derived.

From these expressions, the technique of multi-variate non-linear regression analysis is applied to profile fitting in estimating measurement errors within different experimental regimes. Selecting N_2 as a molecule with relatively well known Raman linewidths as well as one of major experimental interest, the relative utility of CARS and of SRS is examined for the pure gas case. As an example of trace constituent detection, CO as a trace in N_2 is considered.

Additionally, a normalized linewidth technique is also discussed in the implementation of SRS as a temperature measurement technique.

Chapter 2 contains the basic theoretical development of the convolved power expressions. Section 2.1 summarizes current semi-classical CARS and SRS theory in which the molecular dipole transitions are quantized but the fields are not. Polarization orientation and mixtures are considered.

Section 2.2 treats $\underline{\underline{\chi}}^{(3)}$ quantum mechanically as a two-photon process. From the resulting functional form, $\underline{\underline{\chi}}^{(3)}$ is extended from the quantum mechanical view to a macroscopic measurable quantity in Section 2.3.

Sections 2.4-2.6 present the details of the convolutions of the expressions for $\underline{\underline{\chi}}^{(3)}$ from the preceding section. Laser linewidth effects are included in the source term for non-linear polarization. The final convolved forms are represented as summations of terms involving the complex error function.

Chapter 3 compares experimentally observed and theoretically predicted spectral profiles. Section 3.1 illustrates N_2 CARS resonance peak height data for laser linewidths comparable to and an order of magnitude smaller than a typical Raman linewidth. Section 3.2 depicts an O_2 experimental/theoretical profile from current SRS experiments at M.I.T.

Chapter 4 details current knowledge regarding the (N, T) derivatives of Raman linewidths. Frequency degeneracy in high pressure conditions is discussed.

Chapter 5 discusses representative spectral profiles in which number density, temperature, and effective laser linewidth are varied for regimes of experimental interest.

Chapter 6 presents a discussion of peak height ratioing as applied to (T, N) measurement. Uncertainties in linewidths are reltaed to measurement error in Section 1 while a possible normalization scheme is presented in Section 2.

Chapter7 discusses parameterization of the respective CARS and SRS spectral profiles in regards to non-linear profile fitting. Computational advantages of the closed-form convolution are discussed.

Chapter 8 introduces multivariate non-linear regression theory and weighted least sum errors. Results from statistical theory are applied to an optimized profile fitting technique for CARS and SRS. The function (N, T, Γ) profile derivatives are expressed as a reference to the enclosed profile generating subroutine.

Chapter 9 presents a comprehensive analysis of possible errors in the measured quantities of number density and temperature. Section 1 explains the error tables in Appendix B. Section 2 details the functional (N) dependence of the predicted count rate. The effects of the effective laser linewidth Zl, the non-resonant susceptibility, and linewidth uncertainties are discussed in Sections 3, 4, 5. Section 6 presents an overview of CARS versus SRS in (T, N) measurement.

Chapter 10 restates the objectives of the dissertation and presents an overview of the methods and results of the convolutions and error analysis.

CHAPTER 2

THEORY

2.1 Non-Linear Wave Equation

The classical wave equation with a source term due to polarization may be written in Gaussian units as (5, 9, 13, 14)

$$\nabla \times \nabla \times \vec{E}_i - \frac{\omega_i^2}{c^2} \vec{E}_i = \frac{4\pi\omega_i^2}{c} \vec{P}_i \qquad (2.1.1)$$

where E_i is a Fourier component of the applied fields and the subscript i indicates frequency. The polarization can be phenomenologically written as (13, 14, 15)

$$\vec{P}_i = \Sigma \vec{P}_i^{(k)}. \qquad (2.1.2)$$

The superscript indicating the order of the polarization refers to the multiplicity of the fields. Thus, a k^{th} order term is composed of k field products; one may extend the definition by writing the n^{th} order term as

$$\vec{P}_i^{(N)} = \chi^{(n)}(\omega_1, \omega_2, \ldots \omega_n)\, \vec{E}_1 \vec{E}_2 \ldots \vec{E}_n \qquad (2.1.3)$$

where $\underline{\chi}^{(n)}$ is the susceptibility tensor of rank n+1. Equation (3) implies that the dipole susceptibilities transform as tensors of a given order and type under linear orthogonal transformations (14, 16).

In centrosymmetric media it may be shown from the symmetry transformation that all even-ordered tensors are identically zero. The first non-linear term is $\underline{\underline{\chi}}^{(3)}$. Additionally, $\underline{\underline{\chi}}^{(3)}$ has 21 non-zero elements of which only 3 are independent (11, 16).

$$XXXX = YYYY = ZZZZ$$

$$YYZZ = ZZYY = ZZXX = XXZZ = XXYY = YYXX$$

$$YZYZ = ZYZY = ZXZX = XZXZ = XYXY = YXYX$$

$$YZZY = ZYYZ = ZXXZ = XZZX = XYYX = YXXY$$

$$XXXX = XXYY + XYXY + XYYX. \tag{2.1.4}$$

In Cartesian component form with implied summation over repeated indices, Equation (2.1.3) can be conveniently written as

$$\vec{P}^{(3)}_{i\alpha} = \chi^{(3)}_{\alpha\beta\gamma\delta}(\omega_1, \omega_2, \omega_3)\, E_{1\beta}\, E_{2\gamma}\, E_{3\delta} \tag{2.1.5}$$

where the Greek subscript refers to the Cartesian component. As $\underline{\underline{\chi}}^{(3)}$ is invariant to the six permutations of the pairs $(\beta\omega_1)$, $(\gamma\omega_2)$, and $(\delta\omega_3)$, one may write for n identical frequencies (14, 15)

$$\vec{P}^{(3)}_{i\alpha} = \left(\frac{6}{n!}\right) \chi^{(3)}_{\alpha\beta\gamma\delta}(\omega_1, \omega_2, \omega_3) E_{1\beta} E_{2\gamma} E_{3\delta} \tag{2.1.6}$$

where the implied summation does not include permutations.

Considering four-wave mixing, the preceding equation becomes (10, 14, 15)

$$\vec{P}_{4\alpha} = \left(\frac{6}{n!}\right)[\chi^{(3)}_{1122} E_{1\alpha} E_{2\beta} E_{3\beta} + \chi^{(3)}_{1212} E_{1\beta} E_{2\alpha} E_{3\beta} + \chi^{(3)}_{1221} E_{1\beta} E_{2\beta} E_{3\alpha}]. \tag{2.1.7}$$

The homogeneous solution to the wave equation is given by traveling waves with exponential $[ik_i r]$ dependence. Assuming these

solutions are not appreciably perturbed, Equation (2.1.7) may be simplified to the following expression involving explicit magnitudes (10, 14)

$$\vec{p}^{(3)} = (\frac{6}{n!})[X^{(3)}_{1122}\ \vec{\ell}_1(\vec{\ell}_2\cdot\vec{\ell}_3) + X^{(3)}\ \vec{\ell}_2(\vec{\ell}_1\cdot\vec{\ell}_3) + X^{(3)}_{1221}\ \vec{\ell}_3(\vec{\ell}_1\cdot\vec{\ell}_2)]E_1E_2E_3\ \mathrm{EXP}[i\Delta\underset{\sim}{k}\cdot\underset{\sim}{r}] \qquad (2.1.7)$$

with

$$\Delta\underset{\sim}{k} = \vec{k}_1 + \vec{k}_2 + \vec{k}_3 \qquad (2.1.8)$$

and $\hat{\varepsilon}_i$ is defined as the unit polarization vector of E_i.

Noting that by definition $E_1 = E^*_{-i}$ and that the frequencies are defined in CARS such that

$$\omega_1 = \omega_2 = \omega_p \qquad (2.1.9a)$$

$$\omega_3 = -\omega_s. \qquad (2.1.9b)$$

Equation (2.1.7) in final form is

$$\vec{p}^{(3)}_{CARS} = X_{CARS}\hat{\ell}_{CARS}E_p^2E_S\ \mathrm{EXP}[i(2\vec{k}_p - \vec{k}_s)\cdot\vec{r}] \qquad (2.1.10a)$$

where

$$X_{CARS}\hat{\ell}_{CARS} = 3[(X_{1122} + X_{1212})\vec{\ell}_p(\vec{\ell}_p\cdot\vec{\ell}_s) + X_{1221}\ \vec{\ell}_s]. \qquad (2.1.10b)$$

A similar expression may be derived for SRS except that the frequencies are

$$\omega_2 = \omega_p = -\omega_3 \qquad (2.1.11a)$$

$$\omega_1 = \omega_s. \qquad (2.1.11b)$$

and Equation (2.1.7) becomes

$$\vec{P}_{SRS} = X_{SRS}\vec{\ell}_{SRS}E_p^2E_s \ EXP[i\ \vec{k}_s \cdot \vec{r}] \qquad (2.1.12)$$

with

$$X_{SRS}\hat{\ell}_{SRS} = 6[X_{1122}\hat{\ell}_s + (X_{1221} + X_{1212})\hat{\ell}_p(\hat{\ell}_p \cdot \hat{\ell}_s)]. \qquad (2.1.13)$$

In strictly isotropic rather than centrosymmetric media, one has only two non-zero independent tensor elements since (18)

$$2X_{1122} = X_{1111} - X_{1221}. \qquad (2.1.14)$$

Thus, if one measures any two of the non-zero terms, the rest of the tensor elements are uniquely determined.

For general polarization vectors $\hat{\ell}_s$, $\hat{\ell}_p$ one may write for clarity

$$\hat{\ell}_p = \hat{x}$$

$$\hat{\ell}_s = COS\psi\ \hat{x} + SIN\psi\ \hat{y}. \qquad (2.1.15)$$

The result of making these substitutions in Equation (2.1.13) is

$$X_{CARS}\hat{\ell}_{CARS} = 3\hat{x}\ COS\psi[X_{1221} + X_{1122} + X_{1212}] +$$

$$3\hat{y}\ SIN\psi\ X_{1221}. \qquad (2.1.16)$$

According to Equation (2.1.4), the quantity within brackets is simply X_{1111} for centrosymmetric media. Thus, the simplified version is

$$X_{CARS}\hat{\ell}_{CARS} = 3\hat{x}\ COS\psi\ X_{1111} + 3\hat{y}\ SIN\psi\ X_{1221}. \qquad (2.1.17)$$

Similarly for the case of SRS,

$$X_{SRS}\hat{\ell}_{SRS} = 6\hat{x}\ COS\psi\ X_{1111} + 6\hat{y}\ SIN\psi\ X_{1122}. \qquad (2.1.18)$$

For either strictly parallel or strictly perpendicular polarizations of the pump and Stokes lasers, either the cos or the sin term are unity with the result

$$X_{CARS\ 11} = 3X_{1111}$$

$$X_{SRS\ 11} = 6X_{1111}, \qquad (2.1.19a)$$

and

$$X_{CARS\ \perp} = 3X_{1221}$$

$$X_{SRS\ \perp} = 6X_{1122}. \qquad (2.1.19b)$$

As only two independent components of the third-order susceptibility tensor exist in the isotropic case, a Stokes laser polarized at an angle neither zero nor $\pi/2$ with respect to the pump laser is sufficient to completely determine the $\underline{\chi}^{(3)}$ tensor. If one uses a polarization analyzer at an anble β with respect to the pump polarization or x axis, one obtains

$$P_\beta = P_x\ COS\beta - P_y\ SIN\beta. \qquad (2.1.20)$$

Combining terms, one then has an expression for both P_{CARS} and P_{SRS} given by

$$X_{\beta\ CARS} = 3COS\psi COS\beta\ X_{1111} - 3SIN\psi SIN\beta\ X_{1221} \qquad (2.1.21a)$$

$$X_{\beta\ SRS} = 3COS\psi COS\beta\ X_{1111} - 3SIN\psi SIN\beta\ X_{1122}. \qquad (2.1.21b)$$

Taking the spectral profiles at any two rotational angles ψ or β will completely determine the third-order tensor; i.e. two equations, two unknowns. A simple determination may be achieved by taking the spectral profiles for parallel and perpendicular pump-Stokes polarization orientations, but the mixed polarization has certain advantage for CARS that will be discussed in Chapter 2.

Expecting the field amplitudes to be relatively constant over an optical wavelength implies $|\nabla^2 E| << |k\frac{\partial E}{\partial z}|$ (5); or physically, one is not saturating. The wave equation then becomes (2, 5, 9)

$$2i\frac{\partial \vec{E}}{\partial z} = -\frac{4\pi k}{n^2}\vec{p}\ \ell^{i\Delta kz}. \qquad (2.1.22)$$

For a relatively phase matched CARS experiment, $|\Delta k| << |k_{as}|$; the solution to Equation (2.1.27) is then (5, 9, 11)

$$E_{as\hat{\beta}} = \frac{2\pi\omega_{as}}{n_{as}C} X_{CARS} E_p^2 E_s^* [\frac{\ell^{i\Delta kz} - 1}{\Delta k}] \qquad (2.1.23)$$

where $\hat{\beta}$ is the observation polarization vector.

Including focusing effects, the time averaged power is (9, 11)

$$P_{as\hat{\beta}} = \left[\frac{16\pi^3}{n_{as}C\lambda_{as}\lambda_p}\right]^2 |X_{CARS\hat{\beta}}|^2 P_p^2 P_s. \qquad (2.1.24)$$

For SRS, only the polarization component parallel to the polarization vector of E_s will be amplified as shown by the wave equation in vector form

$$2i\frac{\partial E_s}{\partial z} = -\frac{4\pi k}{n^2}\vec{P}_{SRS}\ell^{ik_s z}. \qquad (2.1.25)$$

Since the component of P_{SRS} perpendicular to E_s will not be amplified, a polarization analyzer is not useful in an SRS experiment performed to determine $\underline{\underline{\chi}}^{(3)}$. The simpler use of a polarization rotator in either the pump or Stokes lasers will suffice, however.

The solution to Equation (2.1.25) written as

$$\vec{E}_s = \vec{E}_s\, \ell^{ik'_s z}\, \ell^{k''_s z} \qquad (2.1.26)$$

with

$$k'_s = k_s\left(1 + \frac{2\pi E_p^2 \chi'_{SRS}}{n_s^2}\right)$$

$$k''_s = k_s\left(\frac{-2\pi E_p^2 \chi''_{SRS}}{n_s^2}\right) \qquad (2.1.27)$$

indicates a gain associated with $-\chi''_{SRS}$ and a self-focusing effect due to χ'_{SRS} (2, 12). Equation (2.1.22) suggests a power gain per unit length of (12, 17)

$$G = \frac{-4\pi k_s E_p^2 \chi''_{SRS}}{n_s^2}. \qquad (2.1.28)$$

For two beams of frequency ω_p and ω_s, treating the problem in the paraxial ray expression gives the expression for power gain as (2, 6, 7)

$$P_{SRS} = \frac{-64\pi^3}{\lambda^2 cn} \chi''_{SRS} P_p P_s. \qquad (2.1.29)$$

Since $\chi''_{SRS}(\omega_s, \omega_p, -\omega_p)$ will be shown to be negative at resonance, Equation (2.1.29) implies a gain (loss) at the Stokes (pump) frequency in agreement with experiment (6, 7).

2.2 Third-Order Susceptibility

A quantum mechanical derivation of $\underline{\underline{\chi}}^{(3)}$ may be done in second order perturbation theory within the dipole approximation, i.e., the characteristic molecular diameter is small compared to the wavelengths of the incident electric fields or

$$\text{EXP}[i \vec{k} \cdot \vec{r}\,] \simeq 1. \qquad (2.2.1)$$

Flytzanis (13) has devoted an extensive amount of his text to third and second order non-linear tensor calculations.

Using the results of Flytzanis lengthy calculations, one may write the functional form considering a single resonance for the microscopic resonant third-order susceptibility as

$$\gamma_{iJKL} = \frac{\Delta nm}{3!D_{mn}(\omega_p-\omega_s)} \times \{\langle n|d^{(2)}_{ij}(\omega_{as},\omega_p)|m\rangle\langle m|d^{(2)}_{kl}(\omega_s,-\omega_p)|n\rangle$$

$$+ \langle n|d^{(2)}_{ik}(\omega_{as},\omega_p)|m\rangle\langle m|d^{(2)}_{jl}(-\omega_s,\omega_p)|n\} \qquad (2.2.2)$$

and

$$\gamma_{iJKL} = \frac{\Delta nm}{3!D^*_{nm}(\omega_s-\omega_p)} \langle m|\ell^{(2)}_{iJ}(\omega_s,\omega_p)|n\rangle\langle n|\ell^{(2)}_{KL}(-\omega_p,\omega_s)|m\rangle. \qquad (2.2.3)$$

The denominators are defined by

$$D_{nn'}(\omega) = \frac{1}{n}(\omega_{nn'} - \omega - i\Gamma nn')$$

$$D^*_{n'n}(\omega) = \frac{1}{n}(\omega_{nn'} + \omega + i\Gamma nn'), \qquad (2.2.4)$$

and the respective CARS and SRS two-photon transition operators are

$$d^{(2)}_{iJ}(\omega',\omega'') = \sum_{n'} \frac{P_i|n'\rangle\langle n'|P_j}{D_{n'n}(\omega')} + \sum_{n'} \frac{P_J|n'\rangle\langle n'|P_i}{D^*_{n'm}(\omega'')} \qquad (2.2.5)$$

and

$$\ell^{(2)}_{iJ}(\omega',\omega'') = \sum_{n'} \frac{P_i|n'\rangle\langle n'|P_J}{D_{n'n}(\omega')} + \sum_{n'} \frac{P_J|n'\rangle\langle n'|P_i}{D^*_{n'm}(\omega'')}. \qquad (2.2.6)$$

As usual, Δ is the population difference arising from the diagonal elements of the density matrix corresponding to the states coupled by a Raman transition. P_i is the i^{th} Cartesian component of the

polarization vector operator; n, m, and n' are the initial, final, and intermediate states.

An examination of the functional form is quite instructive. As

$$\gamma_{SRS} \simeq D^{*-1}_{nm}(\omega_s-\omega_p) \simeq [\omega_J - \omega_p + \omega_s + i\Gamma_J]^{-1}$$

$$\gamma_{CARS} \simeq D^{-1}_{nm}(\omega_p-\omega_s) \simeq [\omega_J - \omega_p + \omega_s - i\Gamma_J]^{-1}, \qquad (2.2.7)$$

the imaginary part of the microscopic susceptibility for SRS has the opposite sign as that related to CARS. Additionally assuming that the magnitudes of the two-photon transition operators are essentially equal, since

$$|\gamma_{SRS}| = \frac{\Delta_J}{6D^*_J(\omega_s-\omega_p)} |\ell_{iJ}||\ell_k\ell|$$

$$|\gamma_{CARS}| = \frac{\Delta_J}{6D_J(\omega_p-\omega_s)}\{|d_{iJ}||dk\ell| + |d_{ik}||d_J\ell|\}; \qquad (2.2.8)$$

then, at resonance

$$\omega_J = \omega_p - \omega_s$$

and

$$\gamma_{SRS} \simeq -\frac{1}{2}\gamma_{CARS} \qquad (2.2.9)$$

in accordance with Nibler (10) and Owyoung (2).

The nature of the transition operators reveal the possibility of electronic enhancement of the tensor. Both CARS and SRS will be electronically enhanced if

$$\omega_{nn'} = \omega_p. \tag{2.2.10}$$

Double enhancement is possible in CARS if one satisfies Equation (2.2.10) and additionally

$$\omega_{nn''} = \omega_{as}. \tag{2.2.11}$$

Signal enhancement is quite possible in either coherent process, but CARS does offer the unique prospect of double resonant enhancement. In physical terms, electronic enhancement is tantamount to accessing a real electronic state rather than a virtual one. Since the denominator will now be of order Γ rather than $\Delta\omega$, an extremely large increase in signal level is easily possible since $\Gamma \leq 1\ cm^{-1}$ and $\Delta\omega \simeq 10^3\ cm^{-1}$.

Including the effects of far electronic states as a slowly varying non-resonant term, the macroscopic susceptibility must have the same functional form in the denominator. As is usual for finite lifetime transitions, Γ is the phenomenlogical damping factor which may be affected by not only the natural lifetime of the state, but also, and importantly, molecular collisions. Including the effects of interfering resonances, the resulting expression for $X^{(3)}$ must be summed over all resonances with the result (1, 3, 11)

$$X^{1111}_{CARS} = X_{NR} + \sum_J K_J \Delta_J \left[\omega_J - \omega_p + \omega_s - i\Gamma_J\right]^{-1}, \tag{2.2.12}$$

$$X^{1111}_{SRS} = X'_{NR} + \sum_J K'_J \Delta_J [\omega_J - \omega_p + \omega_s + i\Gamma_J]^{-1} \qquad (2.2.13)$$

where j represents a Raman transition and K_J, K'_J are the CARS and SRS transition moments.

2.3 Macroscopic Tensor

Relating transition moments to scattering cross sections (4, 15, 20) it may be shown that macroscopically (20) for a single species

$$X^{1111}_{CARS} = X_{NR} + \frac{n_p C^4 N}{6\hbar n_s \omega_s^4} \sum_J \frac{n_J \left(\frac{d\sigma}{d\Omega}\right)_J \Delta_J}{\omega_J - \omega_p + \omega_s - i\Gamma_J}, \qquad (2.3.1)$$

$$X^{1111} = X_{NR} + \frac{n_p C^4 N}{12\hbar n_s \omega_s^4} \sum_J \frac{n_J \left(\frac{d\sigma}{d\Omega}\right)_J \Delta_J}{\omega_J - \omega_p + \omega_s - i\Gamma_J}. \qquad (2.3.2)$$

Additionally, Yuratich (20) has demonstrated that due to the similarities in transition moments, CARS and SRS obey the same selection rules and Γ_J is indeed the Raman linewidth (14, 15, 20).

Rewriting X^{1111} in terms of real and imaginary parts.

$$X^{1111} = X' + iX'', \qquad (2.3.3)$$

$$X' = X_{NR} + \alpha \sum_J \frac{K_J(\omega_J - \omega_p + \omega_s)}{(\omega_J - \omega_p + \omega_s)^2 + \Gamma_J^2}, \qquad (2.3.4a)$$

$$X'' = \alpha \sum_J \frac{K_J \Gamma_J}{(\omega_J - \omega_p + \omega_s)^2 + \Gamma_J^2}. \qquad (2.3.4b)$$

Noting that $X_{CARS} = 3X_{1111}$ and defining

$$\delta = \omega_p - \omega_s$$

$$D_J = (\omega_J - \delta)^2 + \Gamma_J^2$$

$$\alpha = n_p C^4 N/2\hbar n_s \omega_s^4$$

$$K_J = n_J \Delta_J \frac{d\sigma}{d\Omega} a_J \qquad (2.3.5)$$

where a_j is the linestrength factor then gives

$$|X_{CARS}|^2 = X_{NR}'^2 + 2\alpha X_{NR}' \sum_J K_J(\omega_J - \delta)/D_J$$

$$+ \alpha^2 \sum_J \sum_K K_J K_K[\Gamma_J\Gamma_K + (\omega_J - \delta)(\omega_K - \delta)]/D_J D_K. \qquad (2.3.6)$$

The prime, hereafter dropped for convenience, indicates the factor of three. The population difference and line strength factor are calculated for diatomic molecules in Appendix D.

The double summation can be put in a more computationally convenient form since the quantity within brackets is equal to

$$\frac{1}{2}\{D_J + D_K - [(\omega_J - \omega_K)^2 + (\Gamma_J - \Gamma_K)^2]\} \qquad (2.3.7)$$

allowing one to simply the double summation as

$$\alpha^2[\sum_J K_J][\sum_K K_K/D_K] - \frac{1}{2}\alpha^2 \sum_{J,K} K_J K_K[(\omega_J-\omega_K)^2 + (\Gamma_J-\Gamma_K)^2]/D_J D_K. \qquad (2.3.8)$$

Using the method of partial fractions, the new double summation may be written as

$$-\frac{1}{2}\alpha^2 \sum_{J,K} K = K_K M_{(J,K)}\left[\frac{\delta + B_{(J,K)}}{D_J} - \frac{\delta + B_{(K,J)}}{D_K}\right] \qquad (2.3.9)$$

with

$$M_{(J,K)} = \frac{2(\omega_K - \omega_J)}{(\omega_K - \omega_J)^2 + (\Gamma_K + \Gamma_J)^2}$$

$$B_{(J,K)} = \frac{1}{2}\left[(\omega_K - \omega_J) + \frac{\Gamma_K^2 - \Gamma_J^2}{\omega_K - \omega_J}\right] - \omega_J. \qquad (2.3.10)$$

From the above equation, it is immediately clear that M(j, k) = -M(k, j) and since j, k are interchangeable dummy indices, the double summation becomes

$$-\alpha^2 \sum_{J,K} K_J K_K M_{(J,K)}[\delta + B_{(J,K)}]/D_J \qquad (2.3.11)$$

which by writing it again as

$$-\alpha^2 \sum_{J} K_J/D_J \sum_{K} K_K M_{(J,K)}[\delta + B_{(J,K)}] \qquad (2.3.12)$$

further simplifies Equation (2.3.8).

The preceding argument is then condensed in the final equation for $|X_{CARS}|^2$ as

$$|X_{CARS}|^2 = X_{NR}^2 + 2\alpha X_{NR} \sum_{J} K_J(\omega_J - \delta)/D_J$$

$$+ \alpha^2 \sum_{J} K_J/D_J \sum_{K} K_K\{1 - M_{(J,K)}[\delta + B_{(J,K)}]\}. \qquad (2.3.13)$$

The imaginary part of X_{SRS}^3 may be simply stated as

$$-X''_{SRS} = \alpha \sum_{J} K_J\Gamma_J/D_J. \qquad (2.3.14)$$

Writing ω, Γ as wavenumbers rather than inverse seconds redefines α as

$$\alpha = n_p N/32\lambda C\pi^4 n_s \omega_s^2. \tag{2.3.15}$$

Dimensional analysis demonstrates at least self consistency--α has now the units of inverse ergs with $\frac{d\sigma}{dr}$ in cm^2/SR; h, erg-sec; and X_{NR}, cm^3/erg. Since K has the units of cm^2 and D_J, cm^{-2}; term by term Equation (2.3.13) has the units of cm^6/erg^2. For a two species mixture, since Equation (2.1.3) is linear in $\underline{\chi}^{(3)}$,

$$\chi^{(3)} = \chi^{(3)}_{(1)} + \chi^{(3)}_{(2)} \tag{2.3.16a}$$

with the result

$$\chi_{1111} = \chi_{1111}^{(1)} + \chi_{1111}^{(2)}. \tag{2.3.16b}$$

Equation (2.3.4) may then be written for two species as

$$\chi' = \chi_{NR} + \alpha_{(1)} \sum K_{J(1)}[\omega_{J(1)} - \delta]/D_{J(1)}$$

$$+ \alpha_{(2)} \sum K_{J(2)}[\omega_{J(2)} - \delta]/D_{J(2)} \tag{2.3.17}$$

$$\chi'' = \alpha_{(1)} \sum_J K_{J(1)}\Gamma_{J(1)}/D_{J(1)} + \alpha_{(2)} \sum_J K_{J(2)}\Gamma_{J(2)}/D_{J(2)}. \tag{2.3.18}$$

For an n species mixture, the generalization is clear.

Equation (2.3.13) becomes with the inclusion of n species,

$$|X_{CARS}|^2 = X_{NR}^2 + 2X_{NR} \sum_m \alpha_m \sum_J K_{Jm}[\omega_{Jm} - \delta]/D_{Jm}$$

$$+ \sum_m \sum_n \alpha_m \alpha_n \sum_J K_{Jm}/D_{Jm} \sum_K K_{Kn} \times$$

$$[1 - M_{JKmn}][\delta + B_{JKmn}]. \qquad (2.3.19)$$

The addition of the m, n indices to the D_J, M_{JK}, and B_{JK} terms reflects the fact that Raman transition frequency ω_J and Raman linewidth Γ_J now have an additional index m associated with the type of species. Additionally, it should be clear that

$$X_{NR} = \sum_n X_{NR}(n). \qquad (2.3.20)$$

For the SRS process, it is simple to write Equation (2.3.14) for n species as

$$-X''_{SRS} = \sum_m \alpha_m \sum K_{Jm} \Gamma_{Jm}/D_{Jm}. \qquad (2.3.21)$$

In a typical n species case, excluding isotopic mixtures, Raman transitions are not close enough to interfere except in a single species. One then duplicates Equations (2.3.13) and (2.3.14)

if the Raman transitions are not particularly close except for the important fact that in CARS, X_{NR} is given by Equation (2.3.20).

If one is interested in trace gas constituent detection, the presence of a large non-resonant component will mask low concentrations of the constituent in which one is interested. This can be more clearly understood by examining Equation (2.1.29) along with Equation (2.3.13). These clearly indicate a large constant signal level will be generated proportional to X_{NR}^2 for the case $X_{NR} >> \alpha \frac{d\sigma}{d\Omega}/\Gamma$. As α is directly proportional to N, the number density of the species under consideration, the presence of low concentrations will indeed be masked. The SRS process will not be so affected; X_{NR} does not contribute to the detected signal.

However, the advantages of the polarization formulation of X_{CARS} in Equation (2.1.23) can now be demonstrated. One may eliminate the non-resonant part of X_{CARS} by defining the angle β such that

$$\text{TAN}\beta = \text{CTN}\psi \frac{X_{1111}}{X_{1221}}_{NR}^{NR} \tag{2.3.22}$$

with the result that

$$X_{CARS} = 3\ \text{COS}\psi\text{COS}\beta\ X_{1111}_{R}\left(1 - \frac{X_{1221_R}}{X_{1111_R}} \frac{X_{1111_{NR}}}{X_{1221_{NR}}}\right). \tag{2.3.23}$$

From Ecbreth (4) and Andersen (13), the resonant part of the $\underline{\underline{\chi}}^{(3)}$ tensor is expressed for isotropic media in terms of p, the depolarization ratio, as

$$X_{IJKL_R}(-\omega_{as}, \omega_p, \omega_p, -\omega_s) = X_{1111_R}[(1 - 2p)\delta_{IJ}\delta_{KL}$$

$$+ P(\delta_{IK}\delta_{JL} + \delta_{IL}\delta_{JK})]. \qquad (2.3.24)$$

Equation (2.3.24) may be simplified as

$$X_{CARS\hat{\beta}} = 3COS\psi COS\beta\ X_{1111_R}(1 - P\frac{X_{1111_{NR}}}{X_{1221_{NR}}}). \qquad (2.3.25)$$

The maximum signal will be received at an angle of pump-Stokes polarization for $X_{1111_{NR}} \simeq X_{1221_{NR}}$, thus

$$\psi_{MAX} \simeq \pi/4. \qquad (2.3.26)$$

For N_2, p = 0.022 (4), with the result that

$$X_{CARS\hat{\beta}} \simeq \frac{1}{2}X_{1111_R}. \qquad (2.3.27)$$

For the choice β as in Eq. (2.3.22), one may reduce the effective non-resonant contribution so that it is negligible with a corresponding reduction in the Raman resonant part by a factor of 4. With this technique, it has been suggested that much lower levels of trace gases may be detected with the CARS process (4, 5).

2.4 Effects of Finite Laser Linewidths

Equation 2.1.5 may be more formally considered to be true for the Fourier components of E_1, E_2, E_3, respectively. The

Fourier components $\vec{P}^{(3)}_{(\omega)}$ are given by (21, 22)

$$\vec{P}^{(3)}_{(\omega)} = \int d\omega' \vec{E}_1(\omega') \int d\omega'' \underline{\chi}^{(3)}(\omega'-\omega'') \vec{E}_2(\omega-\omega'+\omega'') \vec{E}_3(-\omega'') \quad (2.4.1)$$

where E_i is the complex amplitude of an incident laser field. Assuming uncorrelated modal phases, both the CARS and SRS spectral distributions are expressible in terms of the spectral energy densities $P_p(\omega)$, $P_s(\omega)$ as (22)

$$P_{as}(\omega) \simeq \int P_p(\omega_1) d\omega_1 \int P_s(\omega_1-\delta) P_p(\omega-\delta) \times$$

$$[|\chi_{CARS}(\delta,\omega-\delta)|^2] d\delta \quad (2.4.2)$$

$$P_{SRS}(\omega) \simeq \int P_p(\omega_1) d\omega_1 P_s(\omega) \quad -\chi''_{SRS} \, d\omega' \quad (2.4.3)$$

where $P_p = \int P_p(\omega) d\omega$, $P_s = \int P_s(\omega) d\omega$

and similarly for P_{as}, P_{SRS}.

These spectral energy densities are typicall represented as Gaussian functions with a characteristic width. Since the Gaussian fairly accurately represents modal energy distribution, contributing laser line broadening sources will be included in a Gaussian width.

2.5 Convolution of $|X_{CARS}|^2$

Characterizing the normal spectral energy distribution of the pump and Stokes lasers as Gaussian with $'/\ell$ parameters Δp and Δs respectively, it is possible to convolve Equation (2.1.5) over both linewidths by performing the integration in Equation (2.4.2). Defining ω_p, ω_s as the center frequencies of the pump and Stokes lasers, Equation (2.4.2) implies (Appendix B)

$$P_{as}(\omega) \simeq \frac{P_p^2 P_s}{\Delta p^2 \Delta s \pi^{3/2}} \int \mathrm{EXP}[\omega_1, \omega_p; \Delta p] d\omega_1 \; x$$

$$\int \mathrm{EXP}[\omega_2, \omega_s; \Delta_s] \; \mathrm{EXP}[\omega-\omega_1 + \omega_2, \omega_p; \Delta p] \; x$$

$$|X_{CARS}(\omega_2, \omega-\omega_1)|^2 d\omega_2. \qquad (2.5.1)$$

In terms of the explicit functional dependence on ω_2, Equation (2.3.19) may be written formally as

$$|X_{CARS}|^2 = C_0 + \omega_2^{-4} \, u(\omega-\omega_1) + \omega_2^{-8} v(\omega-\omega_1). \qquad (2.5.2)$$

Equation (2.5.1) becomes

$$P_{as}(\omega) \simeq \int \mathrm{EXP}[\omega_1, \omega_p; \Delta p] \; \mathrm{EXP}[(\omega-\omega_1), (\omega_p-\omega_s); z1]$$

$$x \{ y_1 C_0 + u(\omega-\omega_1) \int \mathrm{EXP}[\omega_2, \omega_\alpha; y_1] d\omega_2$$

$$+ v(\omega-\omega_1) \int \omega_2^{-8} \, \mathrm{EXP}[\omega_2, \omega_2; y_1] d\omega_2 \} \qquad (2.5.3)$$

with the following variable definitions

$$z_1^2 = \Delta_s^2 + \Delta_p^2,$$

$$y_1^2 = \Delta_s^2 \Delta_p^2 / z_1^2,$$

$$\omega_\alpha = \omega_s + \Delta_s(\omega_1 + \omega_p - \omega - \omega_s)/z_1^2. \qquad (2.5.4)$$

There is no formal method of integrating the expressions involving ω_2^{-n}. Even with extremely broad Stokes lasers on the order of 100 cm^{-1} FWHM centered near 1.7×10^4 cm^{-1}, for errors less than 0.1%, it is sufficient to expand the negative exponent in a first order Taylor series with the usual result

$$\omega_2^{-4} \simeq \omega_s^{-4}[1 - 4(\frac{\omega_2 - \omega_s}{\omega_s})],$$

$$\omega_2^{-8} \simeq \omega_s^{-8}[1 - 8(\frac{\omega_2 - \omega_s}{\omega_s})]. \qquad (2.5.5)$$

To complete the closed form convolution, the experimental arrangement becomes the determining factor. A general CARS experiment is done in one of two ways:

A) The pump laser typically has a narrow linewidth while the Stokes laser is broad enough (30-100 cm^{-1}) to excite multiple Raman resonances. A spectrometer is used to scan the spectrum; the limiting linewidth is now a function of the spectrometer resolution and the pump linewidth (4, 5).

B) The pump laser is again narrow, but a narrow but tunable Stokes dye laser is scanned to excite successive Raman resonances. A photon counting apparatus is preceded by some type of blocking filter to reduce stray light from the Stokes and pump lasers (22, 23).

Case B) has a much higher achievable resolution with present-day laser sources and spectrometers. A dye laser driven by a pulsed

nitrogen pumping source achieves resolution on the order of 3×10^{-3} cm^{-1}; it is difficult to achieve a resolution less than 1×10^{-1} cm^{-1} in a spectrometer with reasonable throughput.

The Taylor expansion is unnecessary in B) for even moderate resolution (2×10^{-1} cm^{-1}) dye lasers with a central frequency on the order of 1.7×10^{4} cm^{-1}. In case A), $Y_1^2 \simeq \Delta p^2$ with the result

$$\omega_\alpha(\omega) \simeq \omega_1 + \omega_p - \omega. \tag{2.5.6}$$

Proceeding with case A),

$$P_{as}(\omega) \simeq P_p^2 P_s \, X_{NR}^2 + \frac{P_p^2 P_s}{\Delta p \Delta s} \int d\omega_1 [EXP\ \omega_1, \omega_p; \Delta p] \times$$

$$EXP[(\omega-\omega_1), (\omega_p-\omega_s); \Delta s] \{u(\omega-\omega_1)\omega_s^{-4} g_u$$

$$+ v(\omega-\omega_1) g_c \}, \tag{2.5.7}$$

where g_u, g_v are function of $\omega(\omega)$ given by

$$g_u \simeq 1 - \frac{4(\omega_2 - \omega_s)}{\omega_s},$$

$$g_v \simeq 1 - \frac{8(\omega - \omega_s)}{\omega_s} \tag{2.5.8}$$

in case A); in the high resolution case B),

$$g_s \simeq g_u \simeq 1. \tag{2.5.9}$$

Letting $\delta = \omega - \omega_1$, the integration equation now becomes

$$\int d\delta EXP[\delta, (\omega-\omega_p); \Delta p]\ EXP[\delta, (\omega_p-\omega_s); \Delta s] \times \{ \quad \}. \tag{2.5.10}$$

Writing Equation (2.5.10) in a form that more explicitly reflects the dependence on $\omega_{as} = 2\omega_p - \omega_s$ gives

$$\frac{p_p^2 p_s}{\Delta p \Delta s} \; EXP[\omega, \omega_{as}; \Delta_s] \int d\delta \; EXP[\delta, \delta_w; \Delta p] \mathcal{E} \; \mathcal{E} \tag{2.5.11}$$

where the assumption $\Delta_s >> \Delta_p$ is maintained throughout the derivation and

$$\delta_w \simeq \omega - \omega_p. \tag{2.5.12}$$

With the inclusion of g_u, g_v, Equation 2.2.25 is more usefully written

$$|X_{CARS}|^2 = X_{NR}^2 + 2g_u X_{NR} \alpha \sum_J K_J(\omega_J - \delta)/D_J(\delta)$$

$$+ \alpha^2 g_v \sum_J K_J \sum_K K_K\{1 - M_{(J,K)}[\delta + B_{(J,K)}]\}/D_J(\delta). \tag{2.5.13}$$

It is convenient to write Equation (2.5.13) in terms of dimensionless terms. Defining

$$\overline{K}_J = \eta_J a_J \Delta_J \tag{2.5.14a}$$

$$\overline{z}_J = [\omega_J + \omega_p - \omega_s]/\Delta p + i\Gamma_J/\Delta p$$

$$\overline{z}_J = \overline{X}_J + i\overline{Y}_J, \tag{2.5.14b}$$

the variable of integration in Equation (2.5.11) may be changed to

$$\overline{t} = \frac{\delta - \delta_w}{\Delta p} \tag{2.5.15a}$$

with

$$\delta_w = \omega - \omega_p. \tag{2.5.15b}$$

It is also convenient to rewrite g_u, g_v in terms of the central CARS frequency ω_{as} as

$$g_v = 1 + 8\left(\frac{\omega - \omega_{as}}{\omega_s}\right) \tag{2.5.16a}$$

$$g_u = 1 + 4\left(\frac{\omega - \omega_{as}}{\omega_s}\right). \tag{2.5.16b}$$

Rewriting Equation (2.5.13) in dimensionless terms,

$$\begin{aligned} |X_{CARS}|^2 = {} & X_{NR}^2 + 2g_u(\omega)\, X_{NR} X_0 \sum_J \overline{K}_J(\overline{X}_J - \overline{t})/\overline{D}_J(\overline{t}) \\ & + g_v(\omega)\, X_0^2 \sum_J \overline{K}_J \sum_K \overline{K}_K\{1 + \overline{M}(J,K)(\overline{X}_J - \overline{t}) \\ & - \overline{M}(J,K)\,\overline{[\omega_J + B(J,K)]}\}/\overline{D}_J(\overline{t}) \end{aligned} \tag{2.5.17}$$

where $X_0 = \alpha\frac{d\sigma}{d\Omega}/\Delta p$ (cm^3/erg),

and the new dimensionless terms are

$$\overline{D}_{KJ} = (\omega_K - \omega_J)/\Delta p,$$

$$\overline{D}_J(\overline{t}) = (\overline{X}_J - \overline{t})^2 + \overline{Y}_J^2,$$

$$\overline{M}(J,K) = 2\overline{D}_{KJ}/[\overline{D}_{KJ}^2 + (\overline{Y}_K + \overline{Y}_J)^2],$$

$$\overline{M}(J,K)\,\overline{[\omega_J + B(J,K)]} = \frac{\overline{D}_{KJ}^2 + \overline{Y}_K^2 - \overline{Y}_J^2}{[\overline{D}_{KJ}^2 + (\overline{Y}_K + \overline{Y}_J)^2]},$$

$$\overline{C}(J,K) = 1 - \overline{M}(J,K)\overline{[\ ]} = 2\overline{Y}_J(\overline{Y}_J + \overline{Y}_K)/[\ ]. \tag{2.5.18}$$

Equation (2.5.17) can be rewritten in a more physically recognizable form as

$$|X_{CARS}|^2 = X_{NR}^2 + 2g_u(\omega)\ X_{NR}X_0\ \Sigma\ \bar{K}_J(\bar{Y}_J - \bar{t})/\bar{D}_J(t)$$

$$+ X_0^2 g_v(\omega)\ \sum_J \bar{K}_J^2/\bar{D}_J(\bar{t})$$

$$+ X_0^2 g_v(\omega)\ \sum_J \sum_K \bar{K}_J\bar{K}_K\ x$$

$$[\bar{M}(J,K)(\bar{X}_J - \bar{t}) + \bar{C}(J,K)]/\bar{D}_J(t). \qquad (2.5.19)$$

The terms may be clarified for a single resonance. In that case, the double summation is ignorable and one has as expected

$$|X_{CARS}|^2 \simeq X_{NR}^2 + 2X'X_{NR} + (X'^2 + X''^2). \qquad (2.5.20)$$

The double summation term is then solely due to the interference of neighboring resonances. In a usual experimental situation, $\bar{D}_{KJ} > \bar{Y}_K > 1$ with the result that the $\bar{M}$, $\bar{C}$ terms are much smaller than unity. The advantage of this formulation is that true interference effects can be included in closed form.

The integration in Equation (2.5.10) may then be performed ala Abramowitz and Stegun (25) with the result

$$P_{as}(\omega) \simeq \frac{P_p{}^2 P_s}{\Delta s\ \pi}\ EXP(\omega, \omega_{as}; \Delta_s)\ x$$

$$\{X_{NR}^2 + 2g_u(\omega)\ X_{NR}X_0\ \Sigma\bar{K}_J\sqrt{\pi}\ Im\bar{W}(\bar{Z}_J)$$

$$+ g_v(\omega)\ X_0^2\ \sum_J K_J^2\ \sqrt{\pi}\ Re\ \bar{W}(Z_J)/\bar{Y}_J$$

$$+ 2g_v(\omega)\ X_0^2\ \sum_J \bar{K}_J\ \sqrt{\pi}\ x\ \xi Im\bar{W}(Z_J)\ x$$

$$\sum_{\substack{K \\ K\neq}} \bar{K}_K \bar{D}_{KJ}/[D_{KJ}^2 + (\bar{Y}_K + \bar{Y}_J)^2] +$$

$$\text{Re } \bar{W}(Z_J) \sum_{K\neq} \bar{K}_K(\bar{Y}_K + \bar{Y}_J)/[\ ]\ \exists\}. \qquad (2.5.21)$$

For case B) a similar result may be derived. However, since the variable of experimental interest is P_{as}, the convolution equation becomes

$$P_{as}(\omega) \simeq \int d\ _2 d\int \text{EXP}[\omega_2, \omega_s; \Delta s] \times$$

$$\text{EXP}[\omega_2, \omega_{p-}\delta; \Delta p]\ |X_{CARS}(\delta)|^2 \qquad (2.5.22)$$

by changing variables from ω, ω_1, ω_2 to δ, ω_1, ω_2 with $\delta = \omega - \omega_1$. Defining $\delta_{ps} = \omega_p - \omega_s$, combining the exponentials involving ω_2 gives

$$\omega_z = (\Delta p^2\omega_s + \Delta s^2(\omega_p - \delta))/zl^2, \qquad (2.5.23)$$

$$P_{as} \simeq \int d\delta |X_{CARS}(\delta)|^2\ \text{EXP}[\delta,\ \delta_{ps}; zl] \times$$

$$\int d\omega_2\ \text{EXP}[\omega_2; \omega_z; \frac{\Delta p \Delta s}{zl}]. \qquad (2.5.24)$$

Integrating the variable ω,

$$P_{as}\ \ \frac{p_p{}^2 p_s}{zl\ \ \pi} \int \text{EXP}\ [\delta,\ \delta_{ps}; zl]|X_{CARS}|^2 d\delta \qquad (2.5.25)$$

where

$$zl^2 = \Delta s^2 + \Delta p^2. \qquad (2.5.26)$$

One may again integrate the result identical to Equation (2.5.21) except the g_u, g_v multipliers are replaced by unity and Δp is replaced by the effective laser linewidth zl.

To examine the resonance behavior, in the high resolution limit $\bar{Y}_{RES} >> 1$ (laser linewidths are very small compared to the Raman linewidths) with the result

$$P_{as}^{RES} \simeq P_p^2 P_s \; N^2/\Gamma_{RES}^2 \tag{2.5.27}$$

since $\sqrt{\pi}\, \bar{Y}_{RES}\, \bar{\omega}(i\bar{Y}_{RES}) \simeq 1$ (24). One essentially reproduces the non-convolved form; the N^2/Γ^2 resonant behavior has been well noted (1, 2, 9, 10).

Considering mixtures again,

$$\begin{aligned} P_{as} \simeq P_p^2 P_S \{ & X_{NR}^2 + 2X_{NR} \sum_{m,j} X_m \sqrt{\pi}\, \bar{K}_{JM} \mathrm{Im}\bar{W}(Z_{JM}) \\ & + \sum_{m,J} X_m^2\, \bar{K}_{JM}^2 \sqrt{\pi}\, \mathrm{Re}\, \bar{W}(Z_{JM})/\bar{Y}_{JM} \\ & + 2 \sum_{\substack{m,n \\ \neq}} X_m X_n \sum_J \bar{K}_{Jm} \sqrt{\pi}\, x \\ & [\mathrm{Dm}\bar{W}(\bar{Z}_{JM}) \sum_K \bar{K}_{Kn}\, \bar{D}_{KJnm}/\, D_{KJNm}^{-2} + (\bar{Y}_{Jn} + \bar{Y}_{Kn})^2 \\ & + \sum_K \bar{K}_{Kn}(\bar{Y}_{Jm} + \bar{Y}_{Kn})/[\;]\;]\} \end{aligned} \tag{2.5.28}$$

with the constraint on the double sums that $(J, m) \neq (K, n)$.

2.6 Convolution of $-X''_{SRS}$

Experimentally (6, 7), SRS has typically been of type B) nature--i.e., tunable narrow Stokes and narrow pump linewidths. Therefore, only case B) will be considered although an A) type is possible. Equation (2.4.3) becomes

$$P_{SRS} \simeq \frac{P_p P_s}{\pi \Delta p \Delta s} \int EXP[\omega_1, \omega_p; \Delta p]\ EXP\ [\omega_2, \omega_s; \Delta s]\ x$$

$$-X''_{SRS}\ d\omega_1 d\omega_2. \qquad (2.6.1)$$

Changing variables to ω_1 and δ

$$P_{SRS} \simeq \int EXP[\omega_1, \omega_p; \Delta p]\ \ EXP\ [(\omega_1 - \omega_s), \delta; \Delta s]\ x$$

$$[-X''_{SRS}]d\omega_1 d\delta. \qquad (2.6.2)$$

Integrating over ω_1,

$$P_{SRS} \simeq \int EXP\ [\delta, \delta_{ps}; zl]\ [-X''_{SRS}]d\delta. \qquad (2.6.3)$$

From (2.3.21)

$$-X''_{SRS} = X_0 \sum_J \bar{K}_J/\bar{D}_J(\bar{t}) \qquad (2.6.4)$$

with

$$\bar{Z}_J = (\omega_J - \delta)/zl + i\Gamma_J/zl \qquad (2.6.5)$$

the convolution integral yields

$$P_{SRS} \simeq P_p P_s X_0 \sum_J \bar{K}_J \sqrt{\pi}\ Re\bar{W}(Z_J). \qquad (2.6.6)$$

As will be discussed in Chapter 3, computational advantages exist. Note also if Δp, $\Delta s \ll \Gamma_{RES}$, asymptoticly (24) $P_{SRS} \simeq P_p P_s \frac{K_R}{\Gamma_R}$ as one expects (16). Again considering the case of mixtures,

$$P_{SRS} \simeq P_p P_s \sum_m X_m \sum_J \bar{K}_{Jm}\ \sqrt{\pi}\ Re\ \bar{W}(ZJm). \qquad (2.6.7)$$

CHAPTER 3

COMPARISON OF EXPERIMENT AND THEORY

3.1 CARS

When one predicts a theoretical profile as an explicit function of the pump laser, Stokes laser, and Raman transition linewidths, the agreement between the experimentally observed profiles and theoretically predicted profiles is of paramount importance CARS spectral profiles of N_2 as air at atmospheric room temperature conditions have been done in a low resolution (Moya) and a high resolution (Nitsch) case.

The low resolution spectral profile in Fig. 4 was generated using a combined laser FWHM linewidth of 0.14 cm^{-1} which is equal to a zl factor of 0.050 cm^{-1}. The experimentally observed peak heights were plotted versus the theoretically generated profile using the pressure broadening coefficients furnished by W. H. Fletcher (33) in Table 23.* Only the Q(J) values up to J = 12 were plotted. The experimental data were renormalized to the $S\ell_{MAX}$ = 10.0 log scale in the graph.

As one would hopefully expect, relatively little peak height error exists in Fig. 4. Whatever error that does exist is perhaps over emphasized in the tabular form since the principal source of error is lateral displacement of the peak values rather than any real difference in magnitude. This is probably more due to the grid size and error in reducing the Moya data rather than to explicit

---

*All tables are in Appendix A.

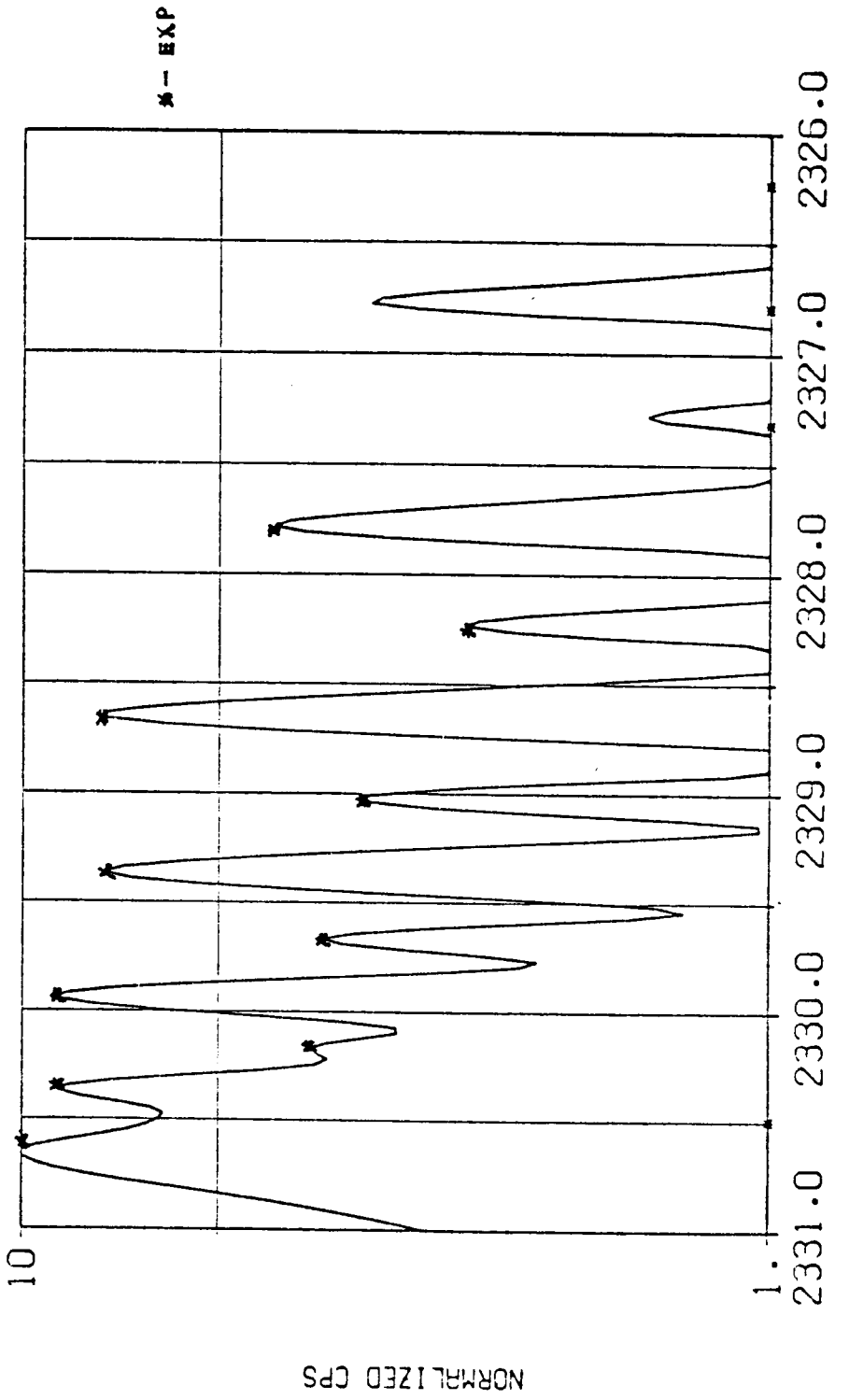

FIGURE 4. N_2 Q-BRANCH CARS PROFILE: LOW RESOLUTION EXP/THEORY

error in the theoretical profile. Regardless, the Moya peak data is well within the peak height errors due to the mean square error in the pressure broadening coefficients as shown in Table 24.

However, the agreement in the high resolution case is not really as good in Fig. 5. Although the peak value is located correctly at the Q(6) point, outside of the Q(8) point the experimental versus theoretical peaks diverge substantially. Since Nitsch used pulsed nitrogen lasers with a zl factor of 0.010 cm^{-1}, the higher resolution data is much more sensitive to the actual Raman linewidth.

In the asymptotic limit for $\overline{Y}_J >> 1$, the peak CARS intensity varies as

$$P_J \simeq (N\Delta_J/\Gamma_J)^2. \tag{3.1.1}$$

The HWHM nitrogen Raman linewidths are on the order of 0.070 cm^{-1} which would give a $\overline{Y}$ value of 7, large enough to use the asymptotic expansion for $\overline{W}jl$. The error then in Equation (3.1.1) is

$$ERR - P_J \simeq P_J\left(\frac{2\ ERR - \Gamma_J}{\Gamma_J}\right) \tag{3.1.2}$$

which is equal to in the collisionally broadened regime for $\overline{\alpha}$, the broadening coefficient,

$$ERS - P_J/P_J \simeq 2\ ERR - \overline{\alpha}/\overline{\alpha}. \tag{3.1.3}$$

Although the general agreement between the high resolution experimental and theoretical peak values is poor, the functional

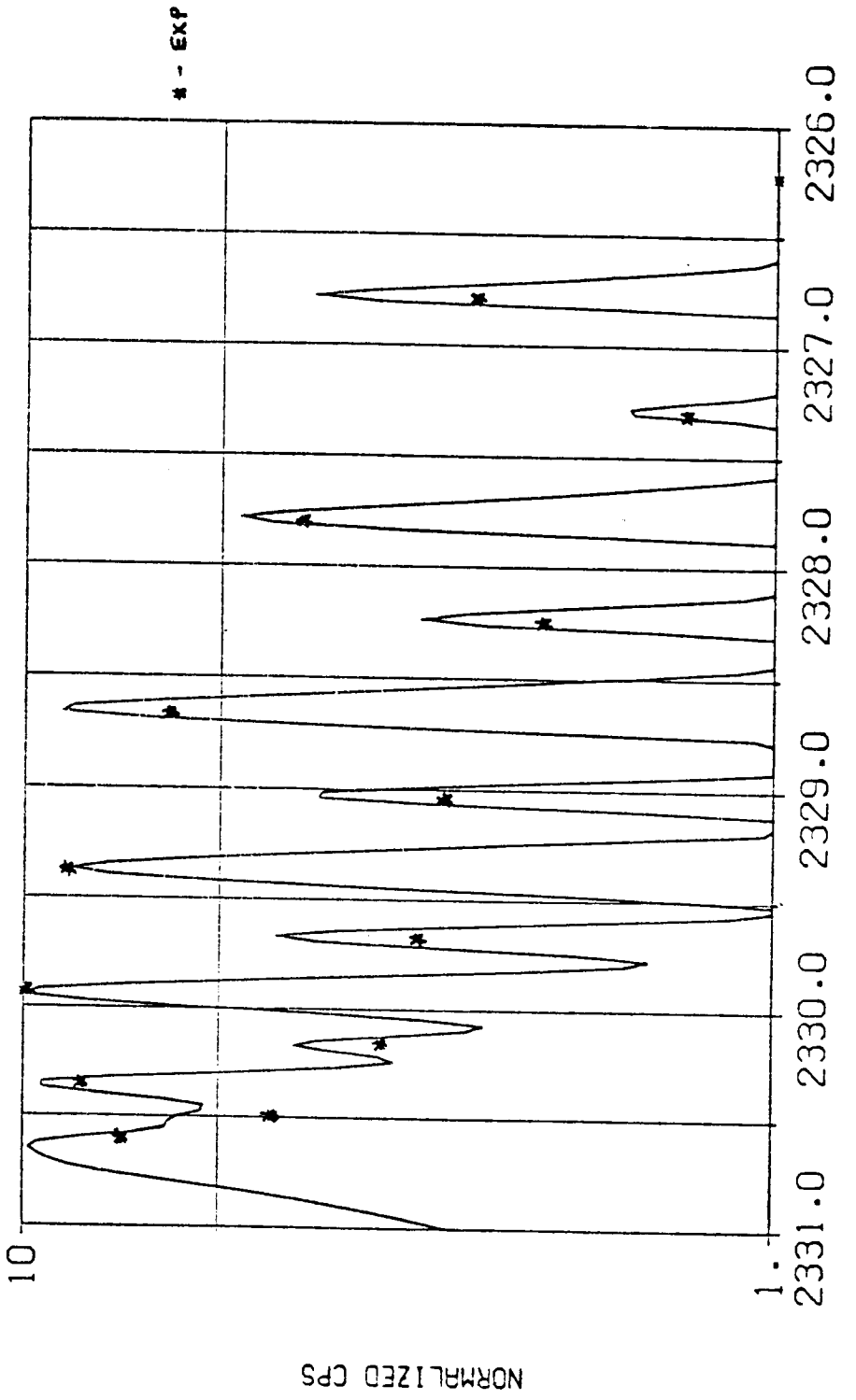

FIGURE 5. N_2 Q-BRANCH CARS PROFILE: HIGH RESOLUTION EXP/THEORY

dependence on the linewidth squared is much greater in the high resolution case since the asymptotic expansion is essentially valid. As one can see from Table 23, even the relatively poor agreement in the high resolution case is within the experimental error in the broadening coefficients.

However, since the CARS signals were generated from an atmospheric mixture of N_2, the use of pressure broadening coefficients for pure N_2 is quite suspect since the foreign gas broadening effect of O_2 is neglected. To explain the better agreement for the low resolution case requires a more detailed mathematical analysis. From Equation (2.6.7), the resonant term is given in the non-asymptotic case by

$$P_J \simeq \frac{N^2 \Delta J^2}{z1^2} \quad \pi \text{ Re } \overline{W}(i\overline{Y}_J)/\overline{Y}_J. \tag{3.1.4}$$

The $\overline{Y}_J$ derivative from Abramowitz is

$$P_J)y \simeq P_J\{(2\overline{Y}_J - 1/\overline{Y}_J) - 2/[\sqrt{\pi} \text{ Re } \overline{W}(i\overline{Y}_J]\} \tag{3.1.5}$$

or expressed in terms similar to Equation (2),

$$(ERR - P_J)/P_J = [\frac{2 \text{ ERR} - \overline{Y}_J}{\overline{Y}_J}][-\overline{Y}_J^2 + \frac{1}{2} + \frac{\overline{Y}_J}{\sqrt{\pi} \text{ Re } \overline{W}}]. \tag{3.1.6}$$

Since $ERR - \overline{Y}_J/\overline{Y}_J = ERR - \overline{\alpha}/\overline{\alpha}$ in the collisionally broadened regime, Equation (3.1.6) becomes

$$(ERR - P_J)/P_J \simeq 2[ERR - \overline{\alpha}/\overline{\alpha}][-\overline{Y}_J^2 + \frac{1}{2} + \frac{\overline{Y}_J}{\sqrt{\pi} \text{ Re } \overline{W}}]. \tag{3.1.7}$$

In the low resolution case, a typical Y_J value is about 1.4 versus 7.0 for the high resolution case. For $Y_J = 1.4$,

$$\%ERR - P_J = 2 \times \%ERR\ \bar{\alpha} \times 0.87175, \qquad (3.1.8)$$

but for $Y_J = 7.0$,

$$\%ERR - P_J = 2 \times \%ERR\ \bar{\alpha} \times 0.99751 \qquad (3.1.9$$

which demonstrates that the low resolution case is indeed less sensitive to Q(J) peak error due to the implicit uncertainty in the pressure broadening coefficients. Additionally, note that the asymptotic expansion is quite sufficient for Y = 7.0 as one obtains an error of only about 0.3% in Equation (3.1.9).

3.2 SRS

Although Owyoung (33) at Sandia and Ezekial (34) at M.I.T. have both done N_2 SRS experimental work, experimental confidence has not been established in the preliminary data. Since SRS is only presently achieving renewed interest, there have been no published N_2 spectral profiles.

In O_2, an illustration of an experimental/theoretical Q-branch spectral profile at room temperature, one atmosphere partial pressure is displayed in Fig. 6. The match is quite good except for the region near the first peak which is the coalesced Q(1) and Q(3) peaks.

The experimentally observed spectrum was a high resolution experiment with a zl value of 7×10^{-3} cm^{-1} or roughly 300 MHz FWFM.

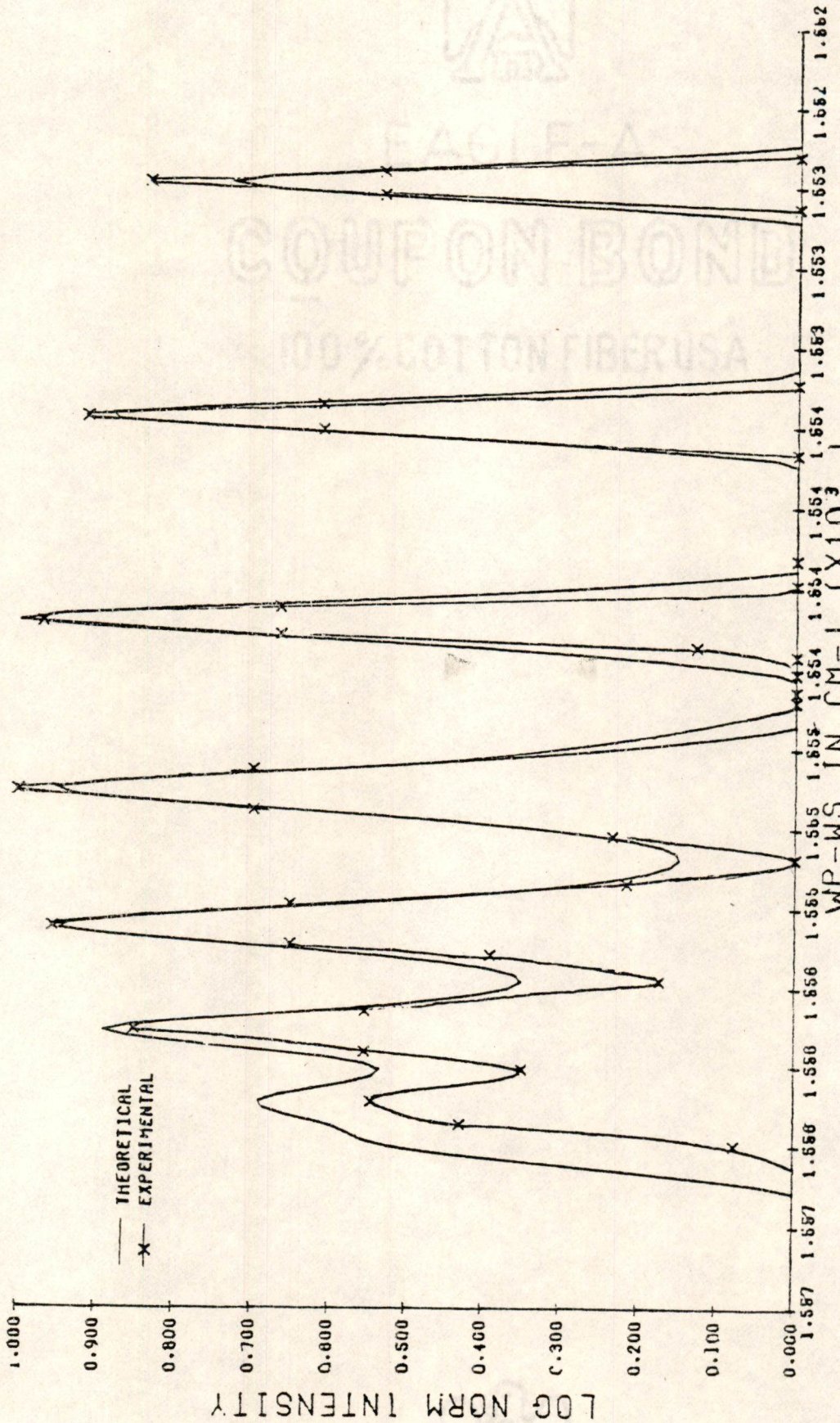

FIGURE 6. O_2 Q-BRANCH SRS PROFILE: HIGH RESOLUTION EXP/THEORY

The data furnished by S. Ezekial (8) at M.I.T. has been unpublished from lack of confidence in experimental quality of the dye laser tracking and linearity of the phase-lock amplifier. Thus, within the limits of the profile, agreement is quite good as regards the SRS linewidths and those of W. H. Fletcher used to generate the theoretical profile.

A comparison of high and low resolution peak height error is possible similarly to Equations (3.1.8) and (3.1.9). The peak value at a resonance point is

$$P_J \simeq \frac{N\Delta_J}{z\bar{1}} \sqrt{\pi}\ \mathrm{Re}\ \bar{W}(i\bar{Y}_J) \qquad (3.2.1)$$

with the result that

$$\%ERR - P_J = \% - ERR - \bar{\alpha} \times [-2\bar{Y}_J^2 + \frac{2\bar{Y}_J}{\sqrt{\pi}\ \mathrm{Re}\ \bar{W}}]. \qquad (3.2.2)$$

The ratio of the $Y_J = 1.4$ and $Y_J = 7.0$ Q(J) peak errors can then be calculated to be 0.743 which again demonstrates that the peak error is less in the low versus high resolution cases. Asymptotically, the quantity within brackets approaches 1 as one would expect.

One comparison between the implicit error in CARS versus SRS profiles can be made. Not only is the peak height error due to linewidth uncertainties halved in SRS, but SRS also has the advantage that the low/high error ratio is less. Thus, in the collision broadened regime, SRS peak errors are better masked by the lower resolution experimental apparatus than the CARS errors.

CHAPTER 4

EFFECTS OF PRESSURE AND TEMPERATURE ON RAMAN LINEWIDTH

4.1 Effective Linewidth

The profile of a spectral line broadened by both thermal motion (Doppler broadening, β_g) and collisional interruption (pressure broadening, β_ℓ) is represented by a Voight function (26) which convolves Gaussian and Lorentzian broadening.

$$\nu(\beta\ell/\beta g/\nu) = \int \frac{\beta\ell/\pi}{\beta\ell^2 + (\nu - \nu')^2} \frac{1}{\beta g \sqrt{\pi}} \ell^{\frac{\nu'^2}{\beta g^2}} d\nu' \qquad (4.1.1)$$

Kielkopf (26) has derived an expression quadratically accurate for the HWHM as

$$\beta = \frac{1}{2}\beta\ell\{1 + \varepsilon\ell n2 + [(1 - \varepsilon\ell n2)^2 + \frac{4\beta g^2}{\beta\ell^2}\ ]^{1/2}\} \qquad (4.1.2)$$

for $\beta\ell$ and βg both in HWHM, and with $\varepsilon = 0.0990$.

4.2 Pressure and Temperature Effects

Determining the broadening coefficients is not an easy task theoretically. For a particular vibrational manifold, the Q branch rotational lines receive contributions from the isotropic ($J = 0$) and ($J = 2$) anisotropic parts of the Raman tensor, except for the $J = 0$ line for which the anisotropic component is

absent. The vibrational Q branch lines consist superposition of the anisotropic and isotropic lines. Clearly, any other branch than Q will not have an isotropic component (27).

Defining the optical cross section as σ, the HWHM and shift of maximum intensity are given by $n\bar{v}\sigma'$ and $n\bar{v}\sigma''$ respectively where as usual n is the number density and $\bar{v}$ is the average velocity between two colliding molecules. Since the superposition of the isotropic and anisotropic lines is incoherent (27, 38), the Q branch optical cross section is the sum of $\sigma_i f(0)$ and $\sigma_i f(2)$ while any other branch is characterized by $\sigma_i f(2)$, i and f the initial and final states. Since the rotational lines arise from the j = 2 part of the Raman tensor, these lines are characterized by $\sigma_i f(2)$.

Examining the line strength factors in Appendix D, the Q branch line strength isotropic part is determined by a_0, the trace scattering constant. For N_2, CO, and O_2, a_0 is significantly greater than asymptotic (high J) value of Q_J in the ratio of 2.24:0.25. Furthermore, since the S and O branch high J line strength factors are 0.275 asymptoticly, the Q branch intensity is much greater than S or O and additionally, the isotropic contribution is much greater.

For the heavier molecules such as N_2 and O_2, the rotation-vibration interaction is generally fairly small with the result that under sufficiently high pressure conditions, the Q(J) lines

are not distinctly resolved. Since the Q branch transitions are nearly frequency degenerate, and additionally, the $|J_m>$ states are complete in terms of rotational motion, there will no collisional change of radiation from a $\Delta\nu = 1$ transition. Under high enough pressure conditions, no collisional Q isotropic broadening should occur. In lower pressure regimes, the low J values are partially degenerate which makes determination of the broadening coefficients difficult. Anisotropic broadening does not occur if $<\nu J|\alpha|\nu' J'>$ is J independent which is the case in frequency degeneracy. Thus, the determination of the Q branch coefficients is difficult in any precision in fairly heavy molecules. Certainly, the n density dependence in $\sigma_i f$ will not be obeyed in degenerate or partially degenerate regimes.

Rotational, O, and S transitions are in general not frequency degenerate; since the $<\nu J|\alpha|\nu' J'>$ element is not J independent, the n dependence in $\sigma_i f(2)$ is relatively good for moderate pressures (27).

The quadrupolar and anisotropic dispersion forces predominate in diatomic molecules (27). Using a modified Andersen treatment depending on the strength of the anisotropic interaction, Van Kranendonk's (27) expression for the broadening coefficient is

$$a_1 = \Delta\nu/P = (\bar{\nu}\sigma'/2\pi ckT) \qquad (4.2.1)$$

which demonstrates a temperature dependence of $\bar{\nu}/T$, varying for a perfect gas as $T^{-\frac{1}{2}}$.

Implicit in this derivation is the dependence on the intermolecular potential used in calculating σ, where the rotational constant is given by

$$\beta\nu = \beta\ell - \alpha(J + \tfrac{1}{2}). \tag{4.2.2}$$

The potential used was

$$4\varepsilon[(\sigma/d)^2 - (\sigma/d)^6] = kT, \tag{4.2.3}$$

and

$$\alpha = 2\pi c\beta\ell d/\bar{\nu}. \tag{4.2.4}$$

The resulting $n/T^{\frac{1}{2}}$ dependence of the boradening coefficient is relatively accurate for non-Q branch transitions. However, since Q branch transitions are an order of magnitude stronger than O, S transitions in N_2, CO, and O_2 the advantages in signal generation are obvious. An $n/T^{\frac{1}{2}}$ collisional linewidth is assumed even for Q branch for error calculation and profile operating in order to determine the total HWHM linewidth derivatives with respect to (N, T) although a power series expansion could be incorporated in either variable. Additionally, analysis will be restricted to Q branch transitions.

The usual Doppler HWHM linewidth is (11)

$$\beta g = \left[\frac{2\ell n\ 2kT}{m}\right]^{\frac{1}{2}} \omega. \tag{4.2.5}$$

CHAPTER 5

REPRESENTATIVE SPECTRAL PROFILES

5.1 N_2 CARS versus SRS

Using the results of Chapter 4, normalized profiles of CARS and SRS for (high zl, high N); (low zl, low N) and the temperature regimes of 60°K, 300°K, and 1200°K are displayed in Figs. 7-10. The normalizing factors in terms of quanta/sec irregardless of alignment or system inefficiencies are displayed on the intensity axis; the scaling factors were calculated for a pump power of 1 watt and a Stokes power of 100 mW. For other systems, the maximum count rate should be scaled as $(P_p^2)_{AVG}\ (P_s)_{AVG}$ for CARS and $(P_p)_{AVG}\ (P_s)_{AVG}$ for SRS. Since the unlabeled lines parallel to the $(\omega_p - \omega_s)$ axis represent half maximum points, the convoluted FWHM linewidth may be obtained graphically from the intersection points of the profile and the highest unlabeled line. The low zl case was calculated with a broad laser line characterized by zl = 0.200 cm^{-1} the high zl case, a narrow line with zl = 0.002 cm^{-1}.

From the succession of experimental regimes, it is clear from the graph that one obtains somewhat broader lines with SRS than one does with CARS. Considering the respective $1/\Gamma$, $1/\Gamma^2$ asymptotic dependence, the profiles agree with theory. From the ratio of the error factors from Equations (3.1.7), (3.2.2) one would also expect a broader line in the SRS case.

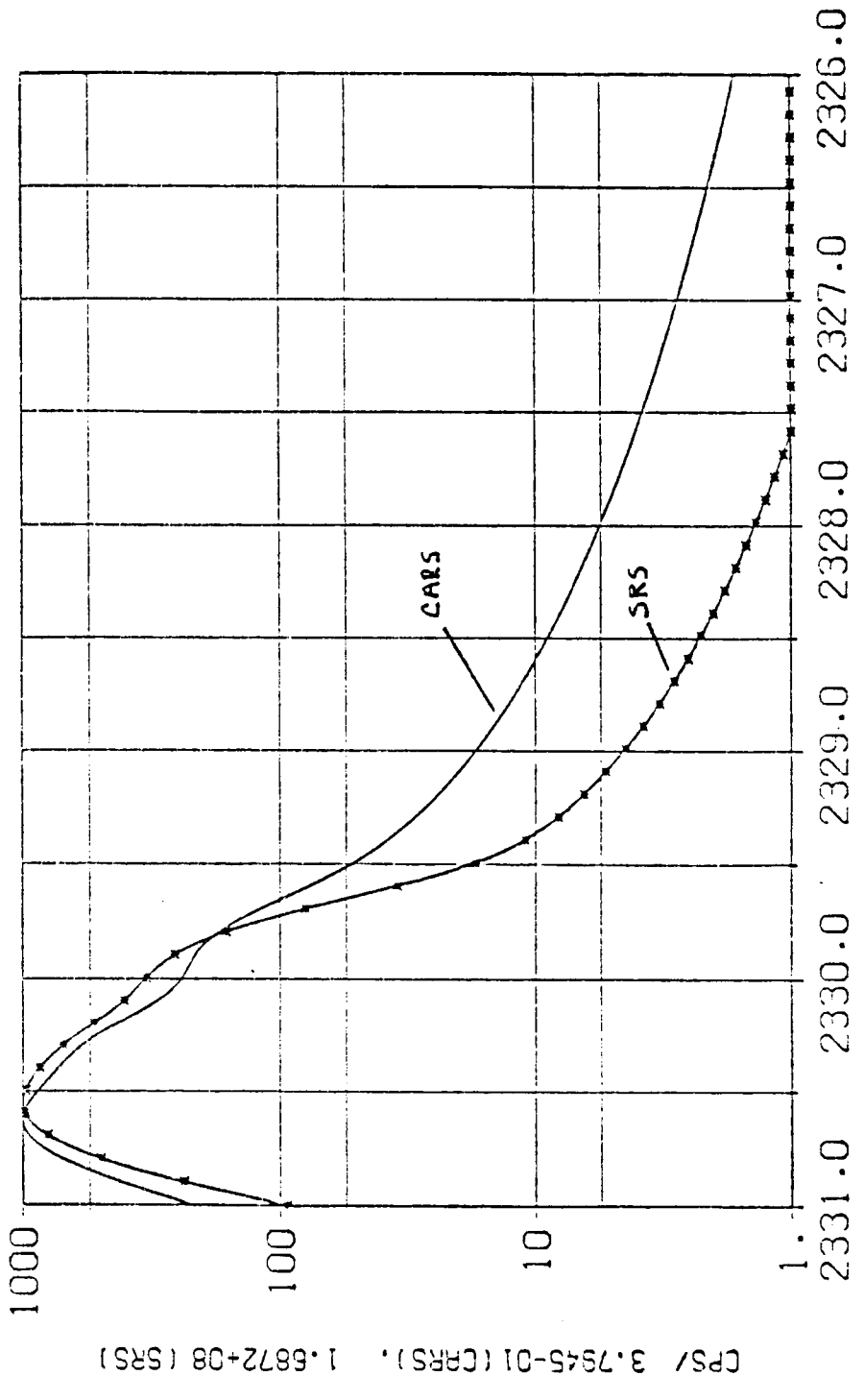

FIGURE 7. N_2 CARS/SRS PROFILE: (N,T,21) = 0.2 AMAGAT, 60°K, 0.200 CM-1

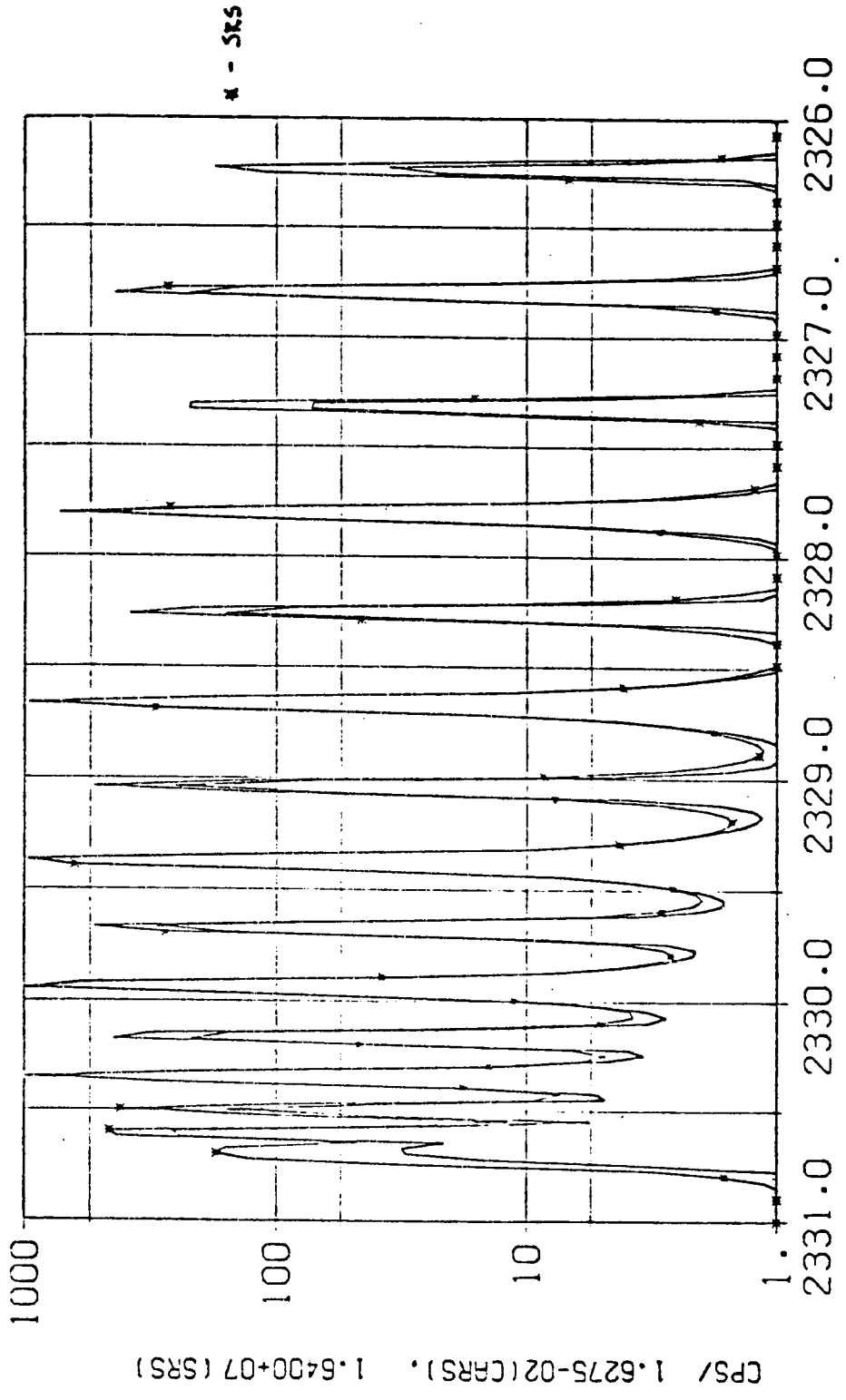

FIGURE 8. N_2 CARS/SRS PROFILE: (N,T,Z1) = 0.01 AMAGAT, 300°K, 0.020 CM-1

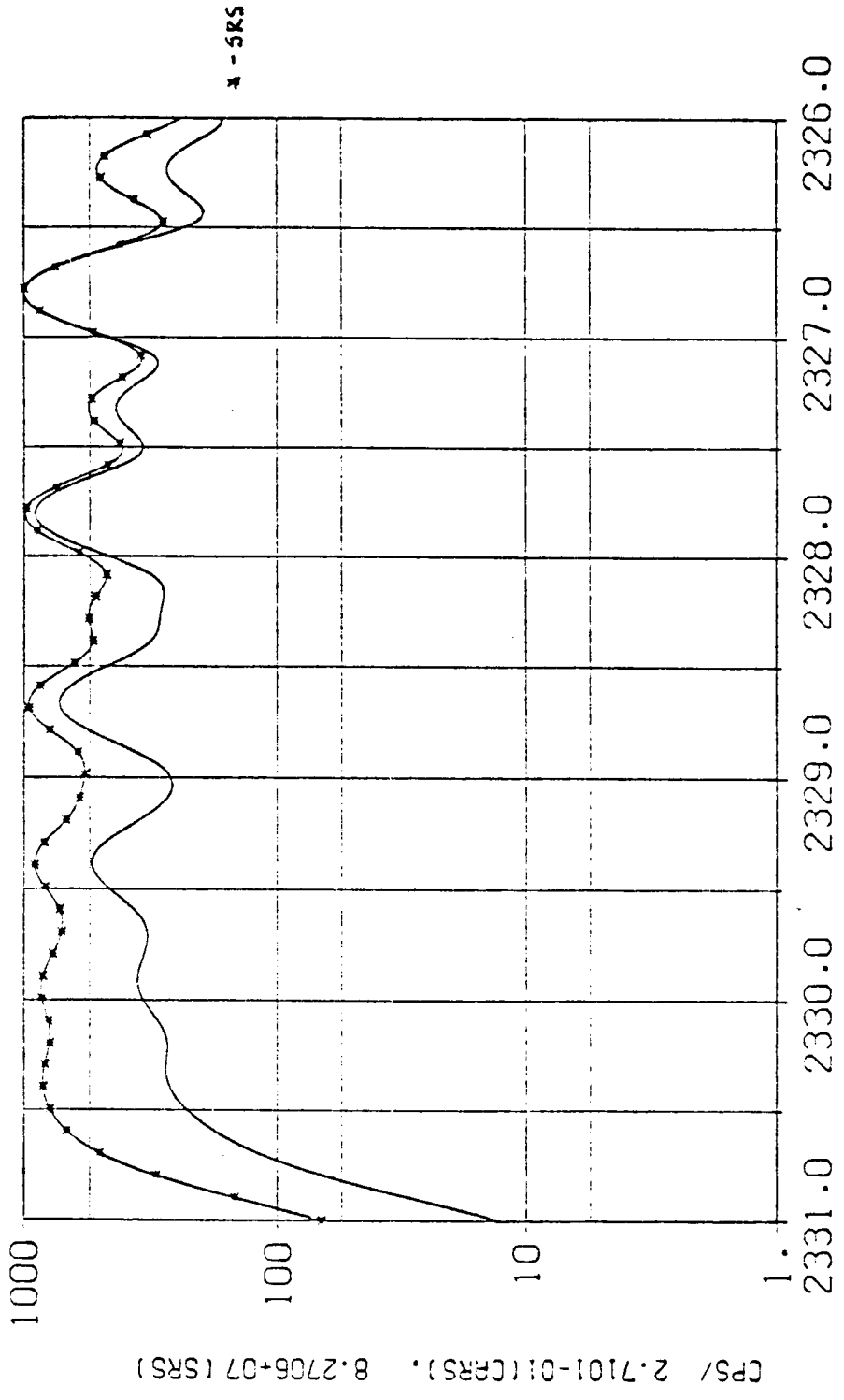

FIGURE 9. N_2 CARS/SRS PROFILE: (N,T,Z1) = 1.0 AMAGAT, 1200°K, 0.200 CM-1

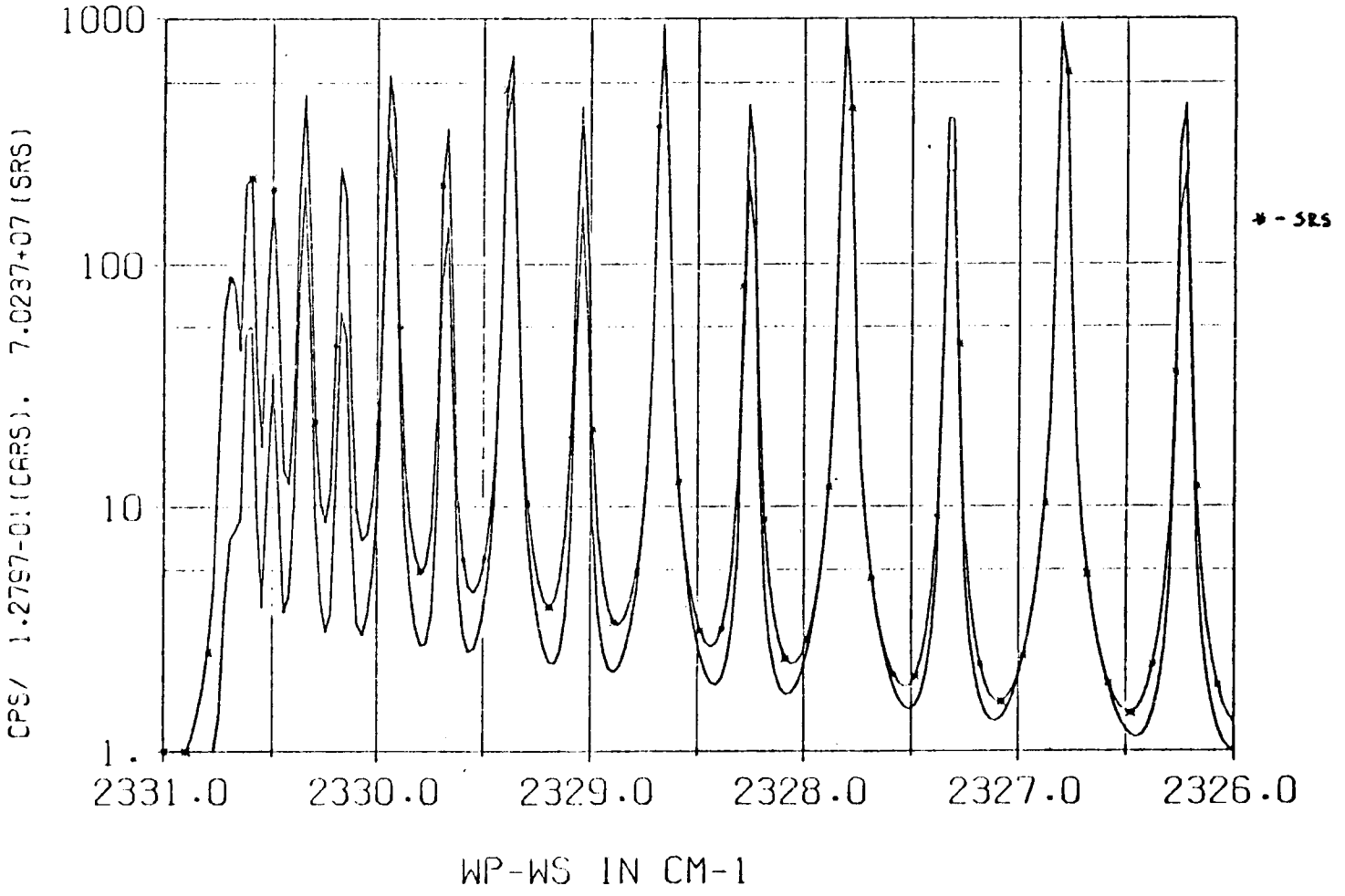

FIGURE 10. N_2 CARS/SRS PROFILE: (N,T,Z1) = 0.10 AMAGAT, 1200°K, 0.020 CM-1

For the given pump and Stokes laser powers, the SRS signal intensity is roughly a factor of 10^5 greater than the CARS signal. To date, high resolution CW CARS N_2 data has been very scarce with the only published data by Hirth (33), done intracavity with the usual two orders of magnitude or so increase in the pump power and Stokes power. However for benzene, since the peak value of X" is about 3.5 orders of magnitude greater than nitrogen (6), the SRS and CARS signal levels are much closer. Owyoung (6) has reported benzene SRS data while Henesian has attempted CARS experimental data (35).

In generating N_2 profiles, the scattering volume was considered only to contain pure N_2, another reason for the marked similarity in profile. In the case of pure N_2, X_{NR} is about three orders of magnitude less than the peak value of X" (1). Since no other constituents are present, the contribution of X_{NR} is essentially ignorable. However, the CO profiles were generated under a worse case quasi-resonant assumption where CO is a trace constituent in N_2 with a correspondingly large value of X_{NR}.

For the CO/N_2 mixture case, the profiles are radically different since the X_{NR}^2 term dominates the CARS profile while the SRS profiles are not a function of the non-resonant term. This is discussed further in section 4.

From the comparative CARS/SRS profiles, the rough similarity in the profiles for ignorable X_{NR} indicates that both behave somewhat the same for different zl parameters; i.e. if one profile is broadened, so is the other and vice versa.

5.2 Effects of Different zl Parameters

From the preceding discussions, zl is a critical parameter in generating a CARS or SRS spectral profile. The value of zl significantly effects the fit between experimental and theoretical data; depending on the typical values of Y_J, the intrinsic error due to measurement uncertainties is altered. In the preceding illustrations, Fig.s 11-15, the effects of three zl parameters of 2×10^{-1}, 2×10^{-2}, and 2×10^{-3}, are displayed for the three temperature regimes considered and different (N) values at each temperature which reflect a linewidth dominated by (collisional-high N) or (Doppler-low N). Since the CARS and SRS N_2 profiles are very similar, one or the other is displayed.

Although the log dependence of the intensity axis suppresses high value differences, for all six graphs, there is little appreciable visual difference between the 2×10^{-2} and 2×10^{-3} values of zl except where Doppler widths predominate. Considering the relative values of Y offers a reasonable explanation.

With zl = 2×10^{-2} and 2×10^{-3}, in a collisionally broadened regime, Γ is on the order of 5×10^{-2} giving respective Y values of 2.5 and 25. The asymptotic expansion of the complex error function, $1/Y^2$, exhibits errors of $5 \times 10^{-1}\%$ and $4 \times 10^{-3}\%$ for Y values of 2.5 and 25. Thus, one would expect relatively little difference in the profiles for Y values greater than 2 as demonstrated in Figures 11 and 14.

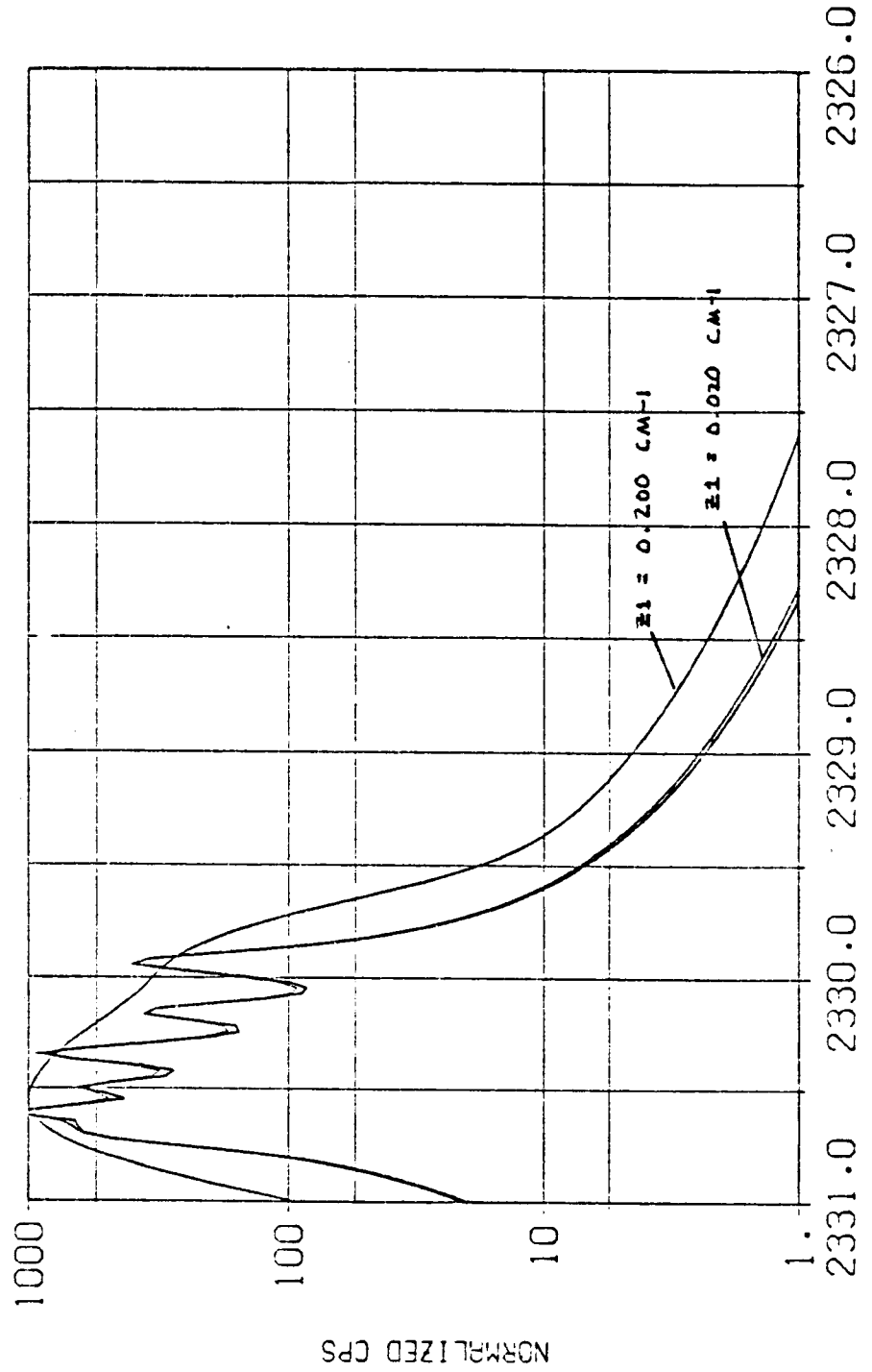

FIGURE 11. N_2 SRS: (N,T) = 0.20 AMAGATS, 60°K

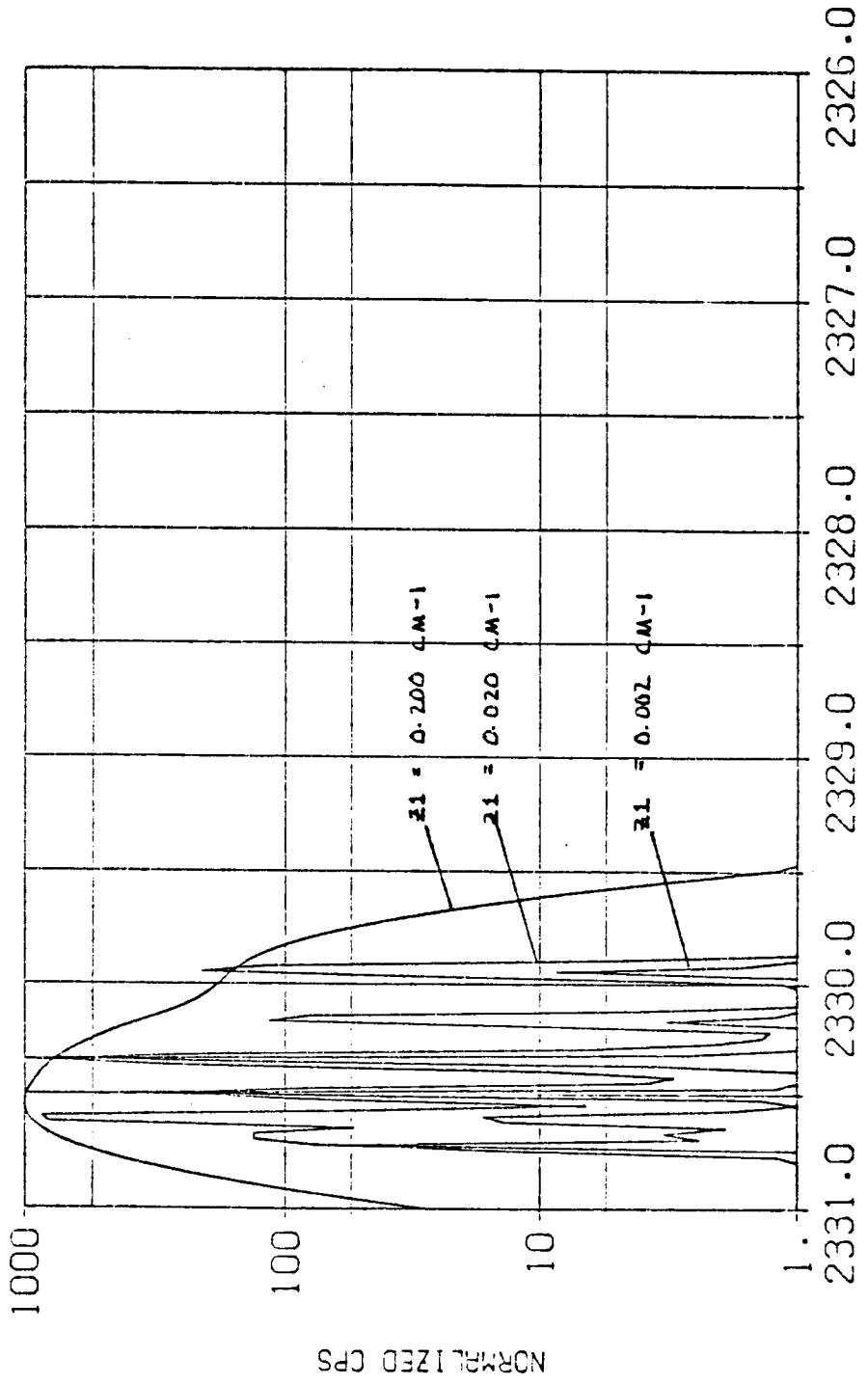

FIGURE 12. N_2 CARS: (N,T) = 0.002 AMAGATS, 60°K

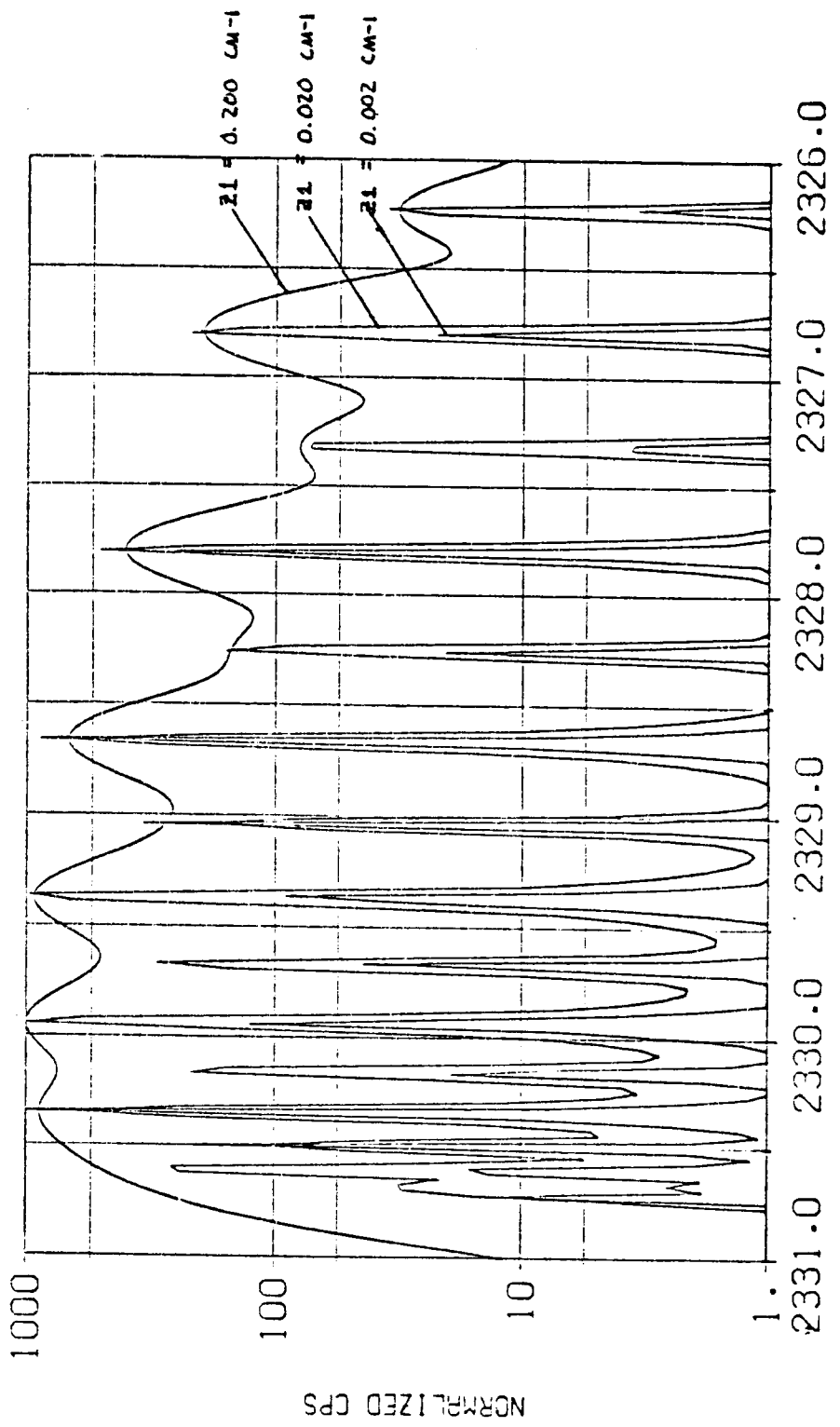

FIGURE 13. N_2 CARS: (N,T) = 0.010 AMAGATS, 300°K

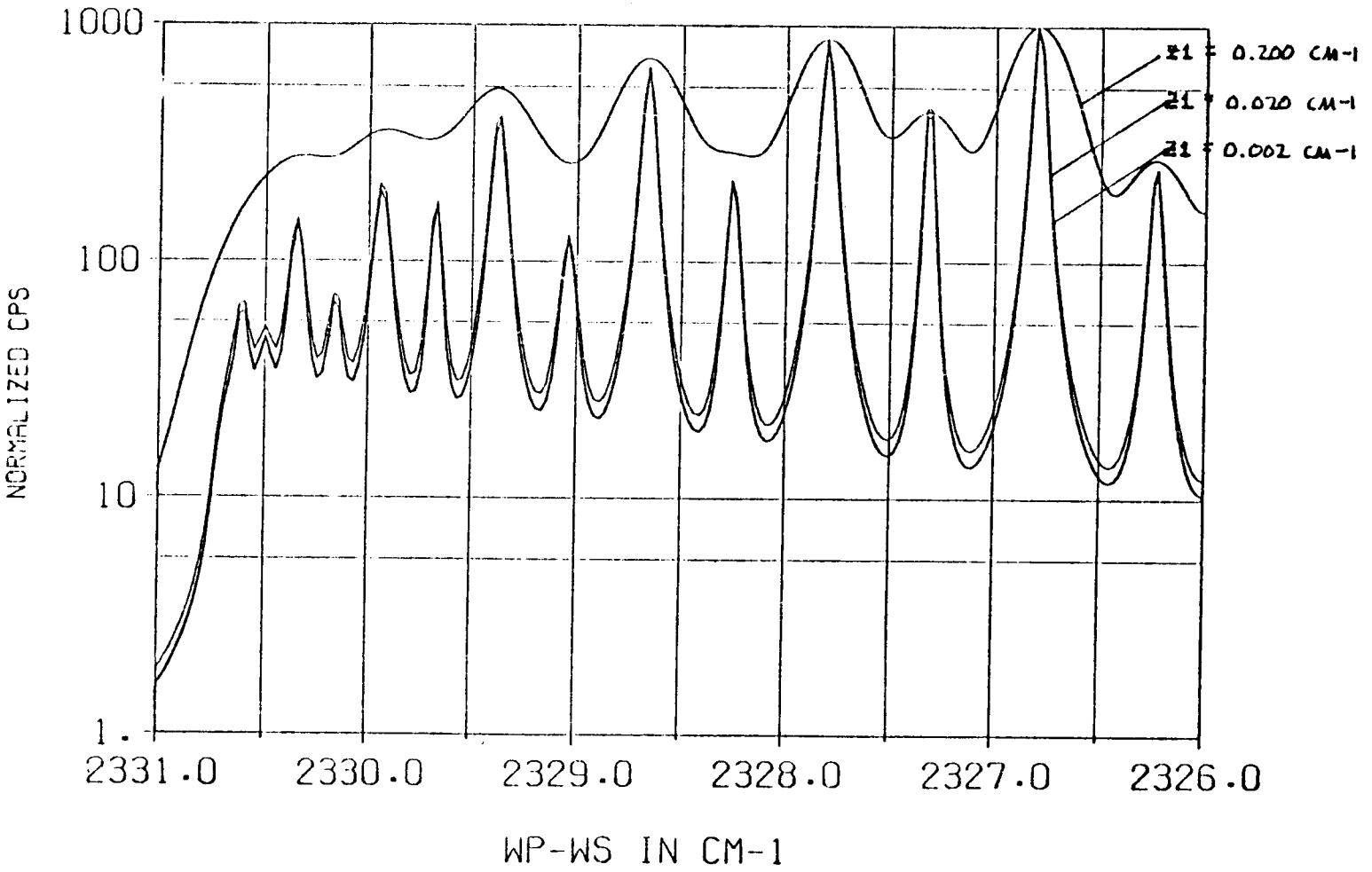

FIGURE 14. N_2 CARS: (N,T) = 1.0 AMAGATS, 1200°K

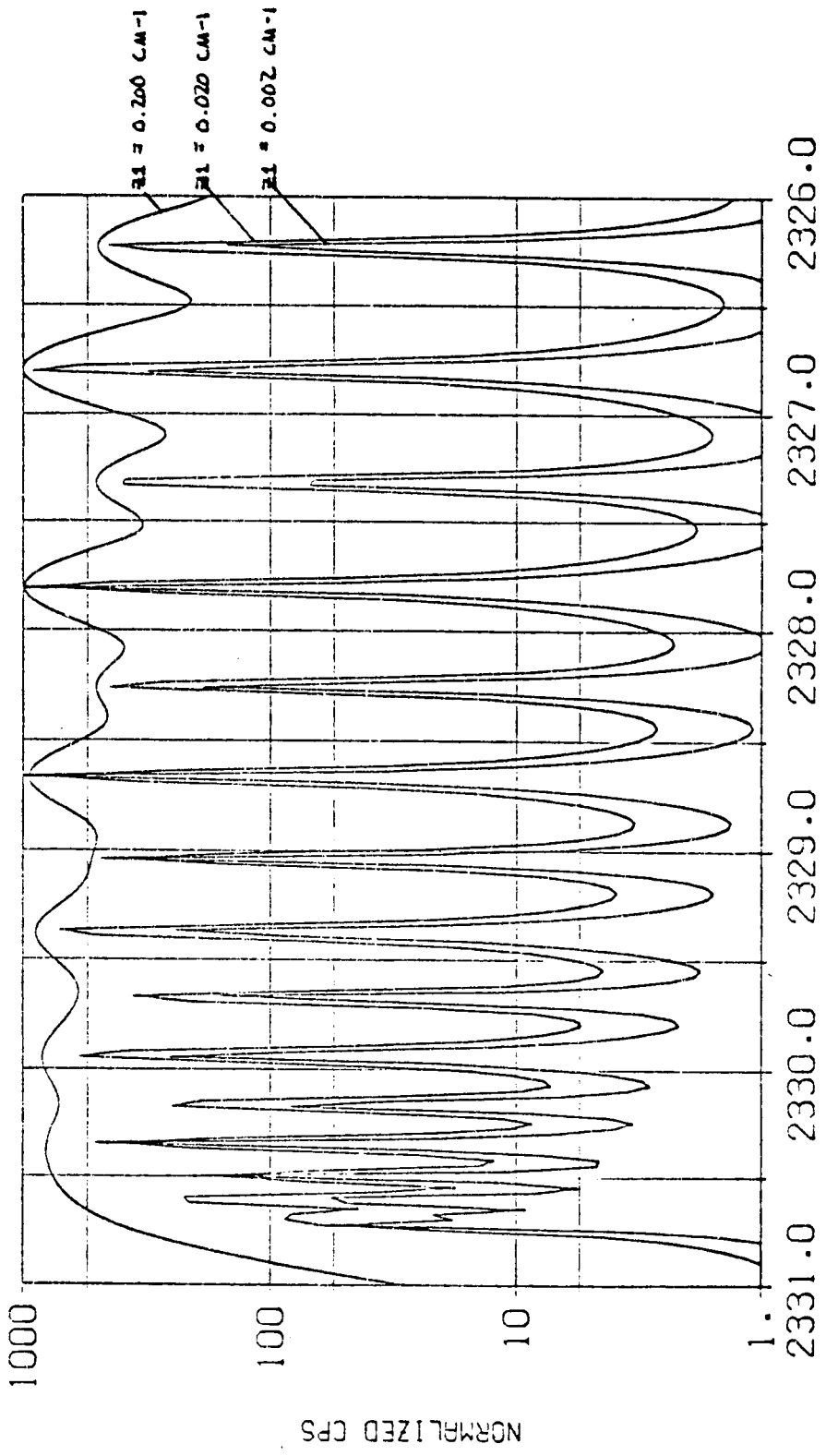

FIGURE 15. N_2 SRS: (N,T) = 0.10 AMAGATS, 1200°K

In the experimental regimes characterized by a Doppler HWHM of 2.5×10^{-3} cm^{-1}, Y is 0.125 and 1.25 for zl = 2×10^{-2} and 2×10^{-3}. One should therefore expect a substantial difference in the profile as is demonstrated in Figures 12, 13 and 15. These profiles are generated under experimental regimes of (T, N) given by (60K, 10^{-3}), (300K, 10^{-2}) and (1200K, 10^{-1}) where the $N/T^{\frac{1}{2}}$ dependence of the pressure broadening coefficients will cause the regime to be typically Doppler broadened.

The zl = 2×10^{-1} case is presented as a counterpoint; even for significantly broadened regimes, the asymptotic expansion error is on the order of 40%. As one would expect, the lowest resolution case differs visibly in all regimes.

5.3 Effects of Number Density

Considering only pure N_2, Figs. 16-18 display number densities of 1.0, 10^{-1}, and 10^{-2} amagats over different experimental regimes of (T, zl). The three values of N are displayed to illustrate the decidedly different N dependence for the high resolution (zl = 2×10^{-2}) and low resolution (zl = 2×10^{-1}) cases. The difference between N = 1.0 and N = 10^{-1} is quite visible for both cases. However, the visible difference between N = 10^{-1} and N = 10^{-2} is much less for the low resolution case than the high, particularly in the T = 1000°K regime. This phenomenon is in accordance with one's expectations due to the linewidth masking in the low resolution case. However, the log vertical scale suppresses the true differences; for the T = 1000°K, the N = 10^{-2}, 10^{-3} comparison

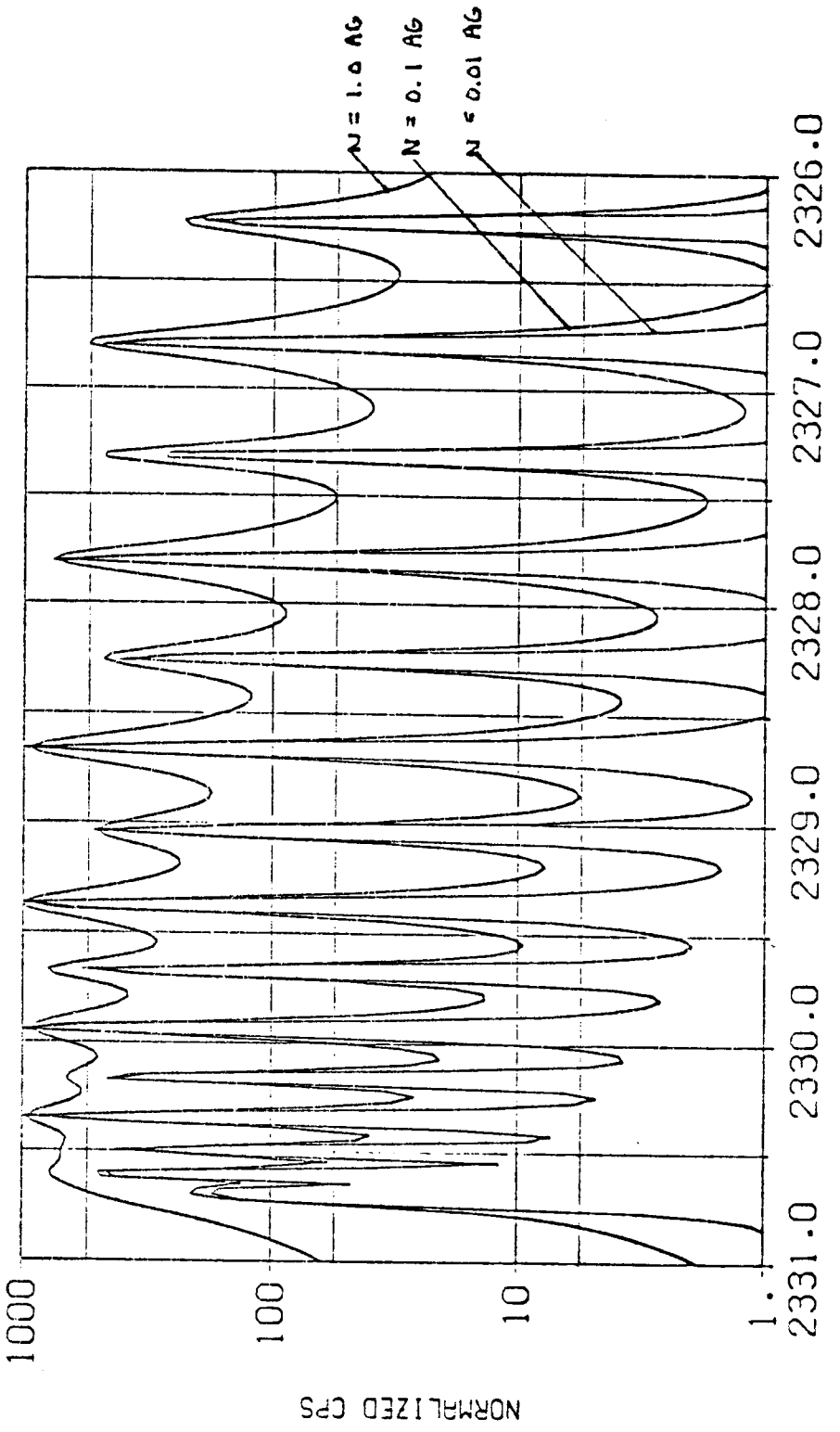

FIGURE 16. N_2 SRS: (T,21) = 300°K, 0.020 CM-1

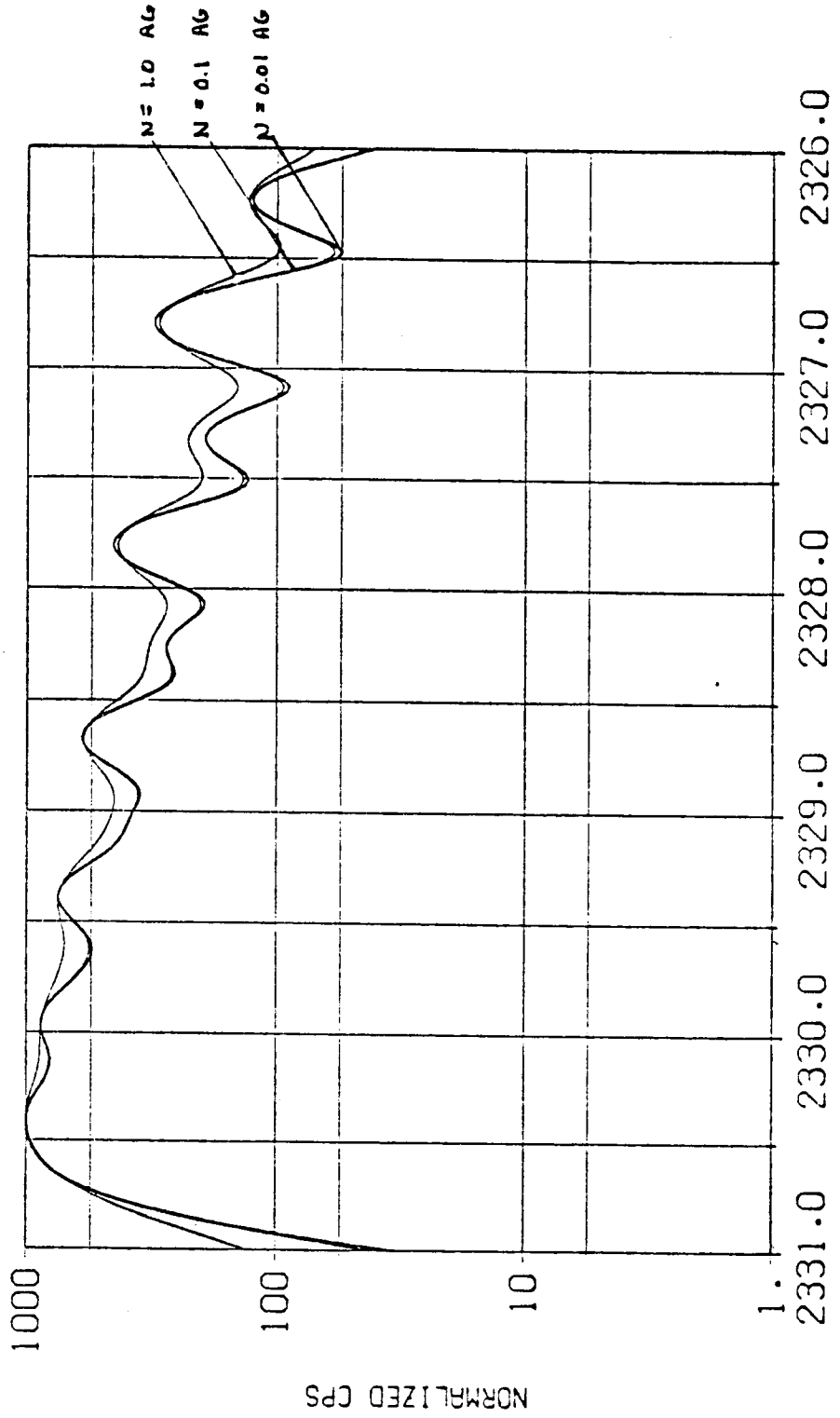

FIGURE 17. N_2 SRS: (T,Z1) = 300°K, 0.200 CM-1

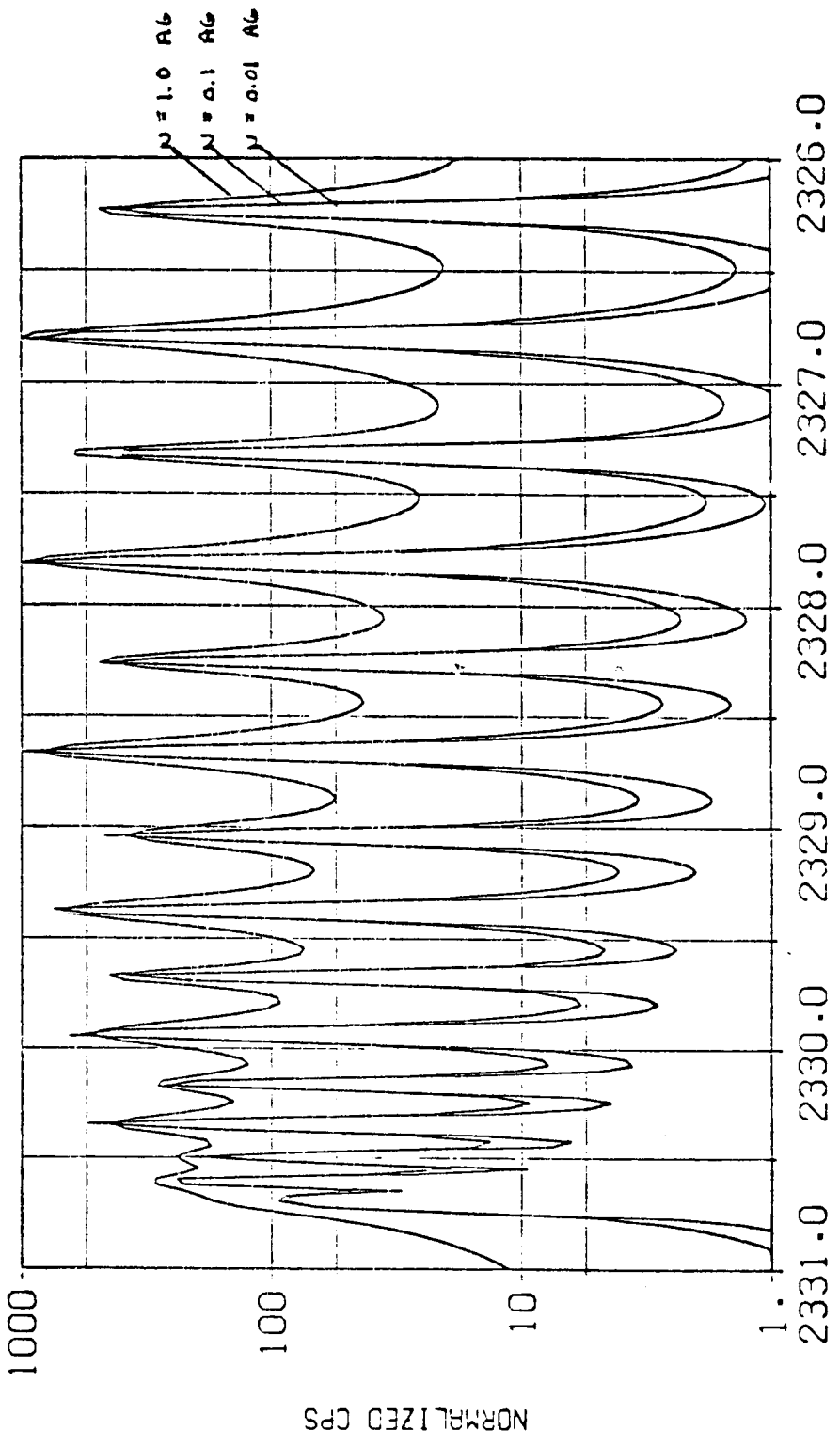

FIGURE 18. N_2 SRS: (T,Z1) = 1200°K, 0.020 CM-1

is not as extreme as one might first imagine from Fig. 18. Not the differences in the two number densities for the high resolution case occur in the low count rate ≈5 cps part of the graph. This is about the same as the low resolution differences.

The mixture case, CO in N_2, exhibits in Figs. 19-23 a different aspect for CARS than for SRS due to the masking influence of a large non-resonant susceptibility. The SRS spectra displayed in Fig. 21 differ primarily from the N_2 profiles in that the even-J, odd-J nuclear spin factor difference of 2:1 one sees in N_2 is absent from the CO profiles. For a pure CO case, again the SRS and CARS profiles will not differ radically. However, the CO/N_2 CARS spectra fully exhibit the visible utility of reducing the non-resonant contribution to the third-order susceptibility. The CARS spectra exhibit the large signal generated due to X_{NR} which, regardless of Y, demonstrates the difficulty of signal detection for low N levels. The profile is now primarily dominated by the $2X_{NR}X'$ term. This will be discussed further in the error analysis. One point is worth further consideration; at least visibly, for the high and low resolution cases, number density differences of 10^{-1} amagats are equally detectable.

5.4 Effects of Temperature

Figs. 24-28 exhibit the effects of temperature on the evolution of N_2 spectral profiles. In the low temperature regime, the profiles are displayed in 20°K increments. In Fig. 24, a typical value of Y is less than 2; one is constrained to a non-asymptotic

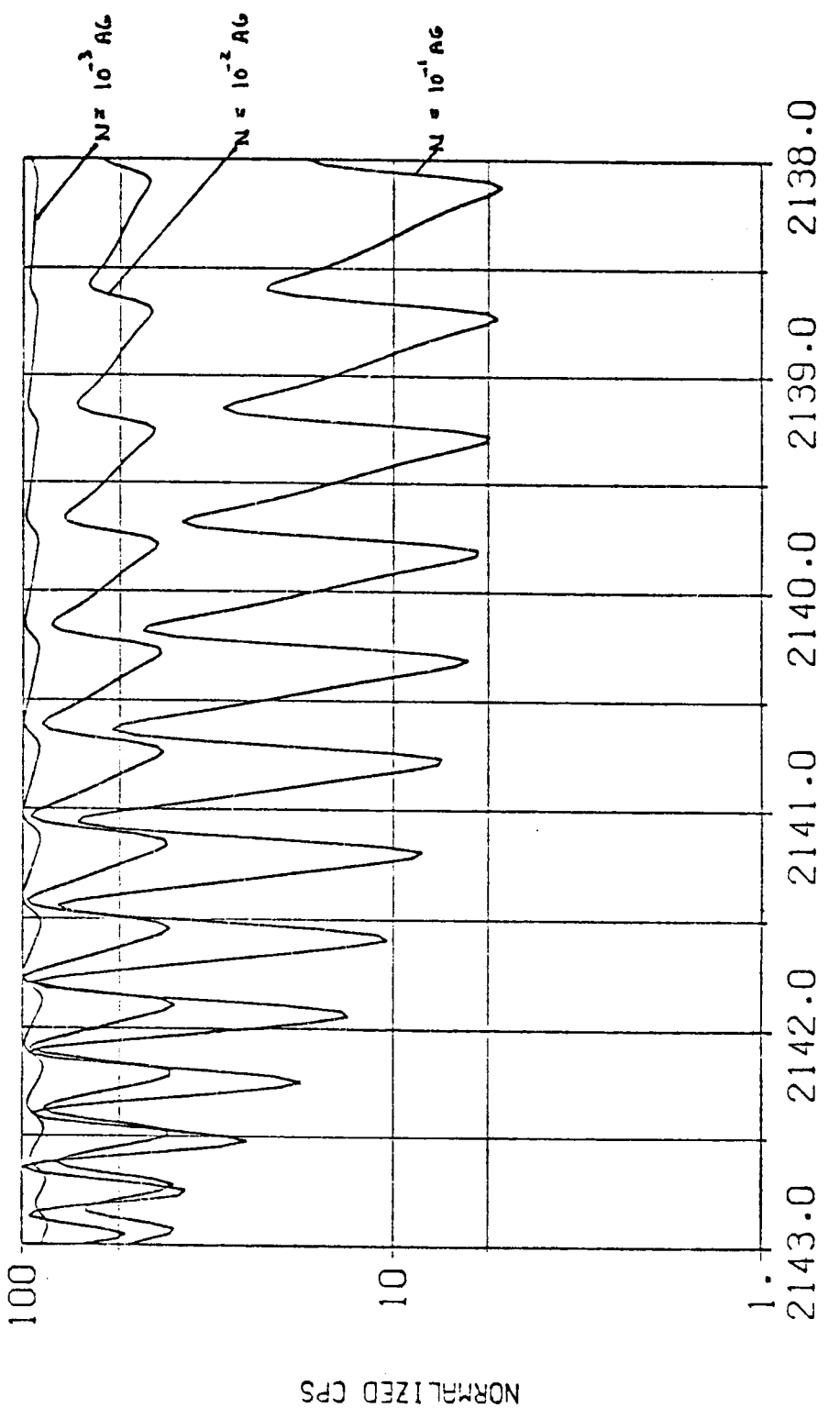

FIGURE 19. CO/N_2 CARS: (T,Z1) = $300^{O}K$, 0.020 CM-1

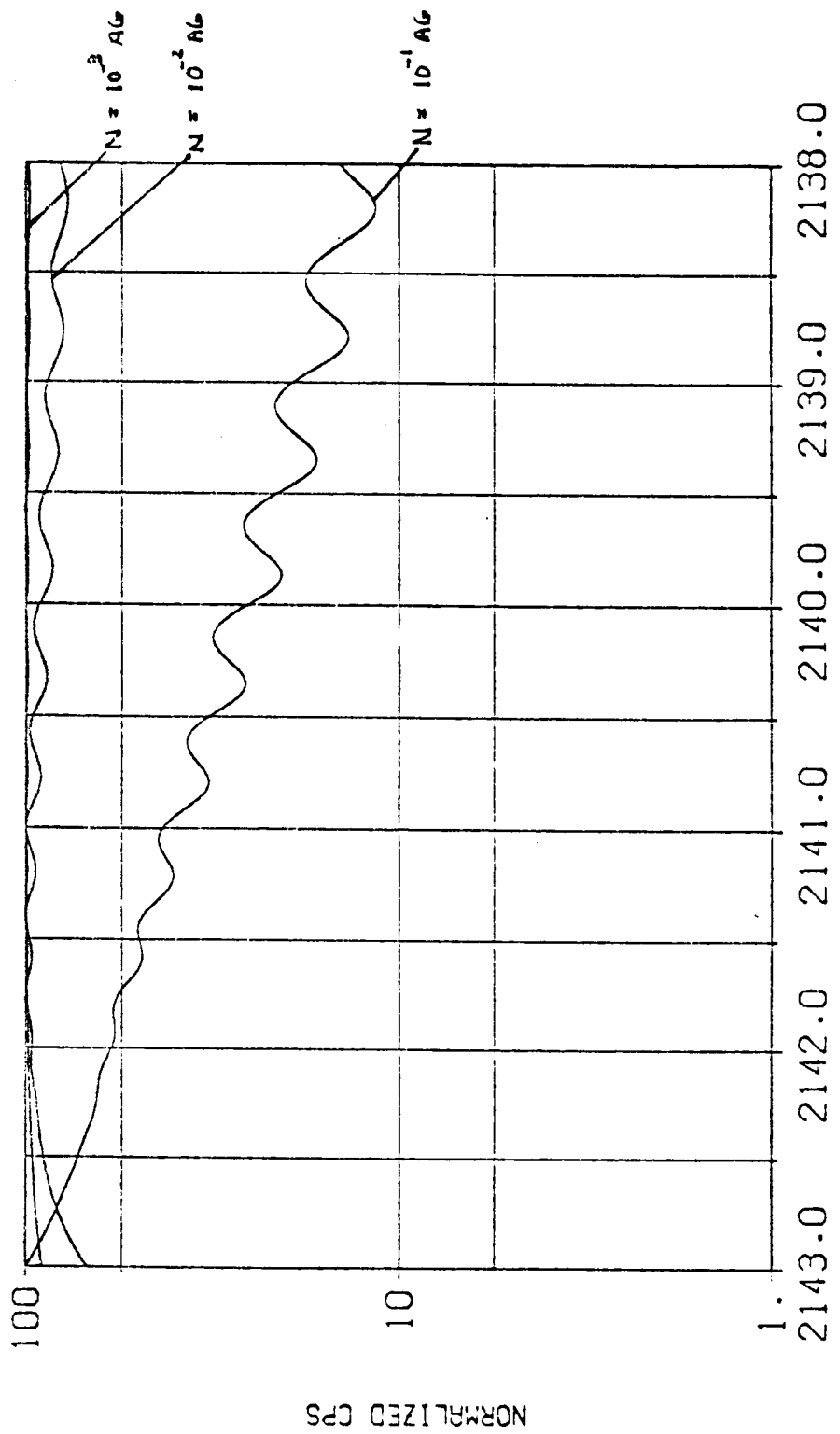

FIGURE 20. CO/N_2 CARS: (T,Z1) = $300^{O}K$, 0.200 CM-1

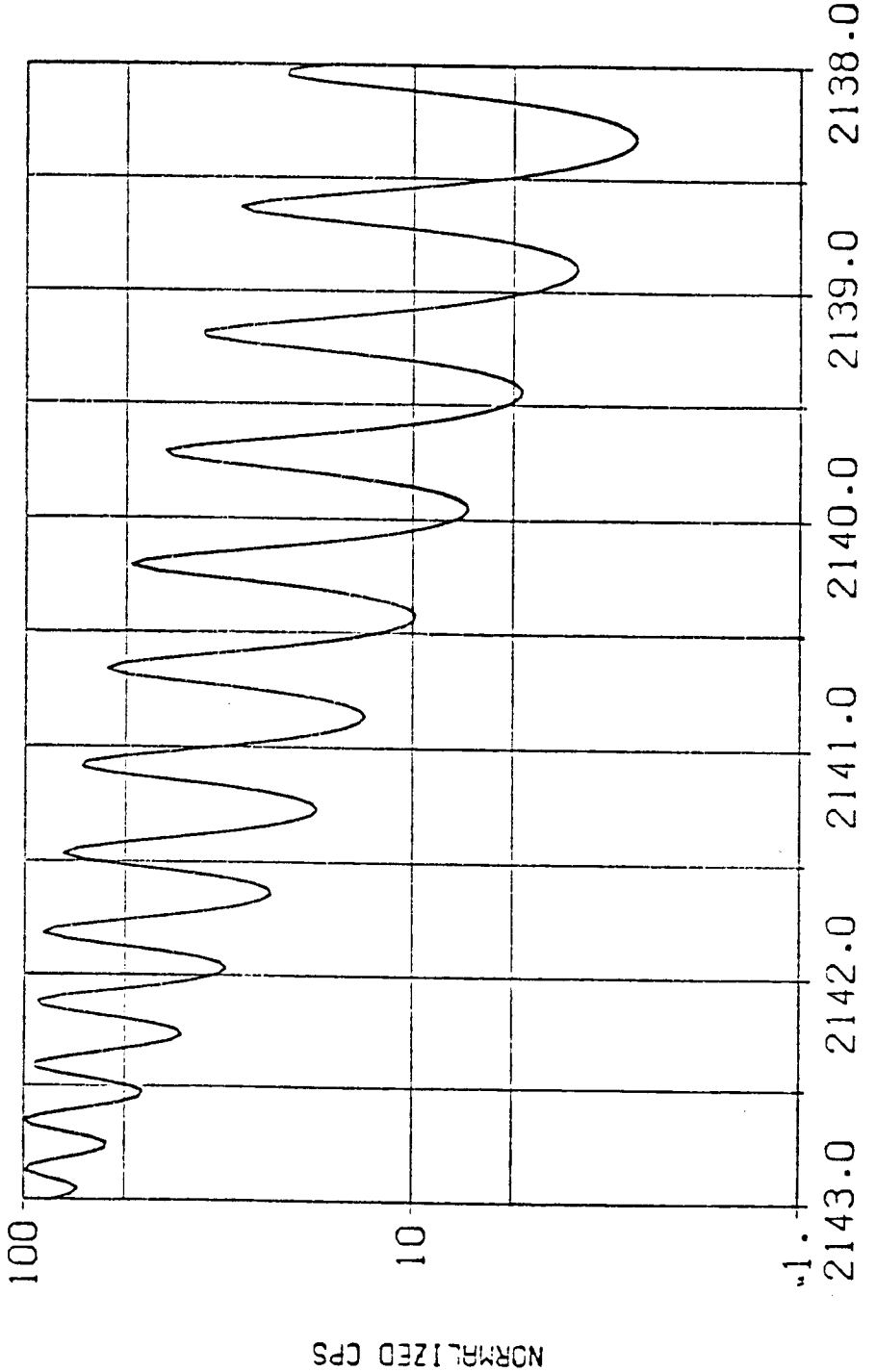

FIGURE 21. CO/N_2 SRS: (T,Z1) = $300^{o}K$, 0.020 CM-1

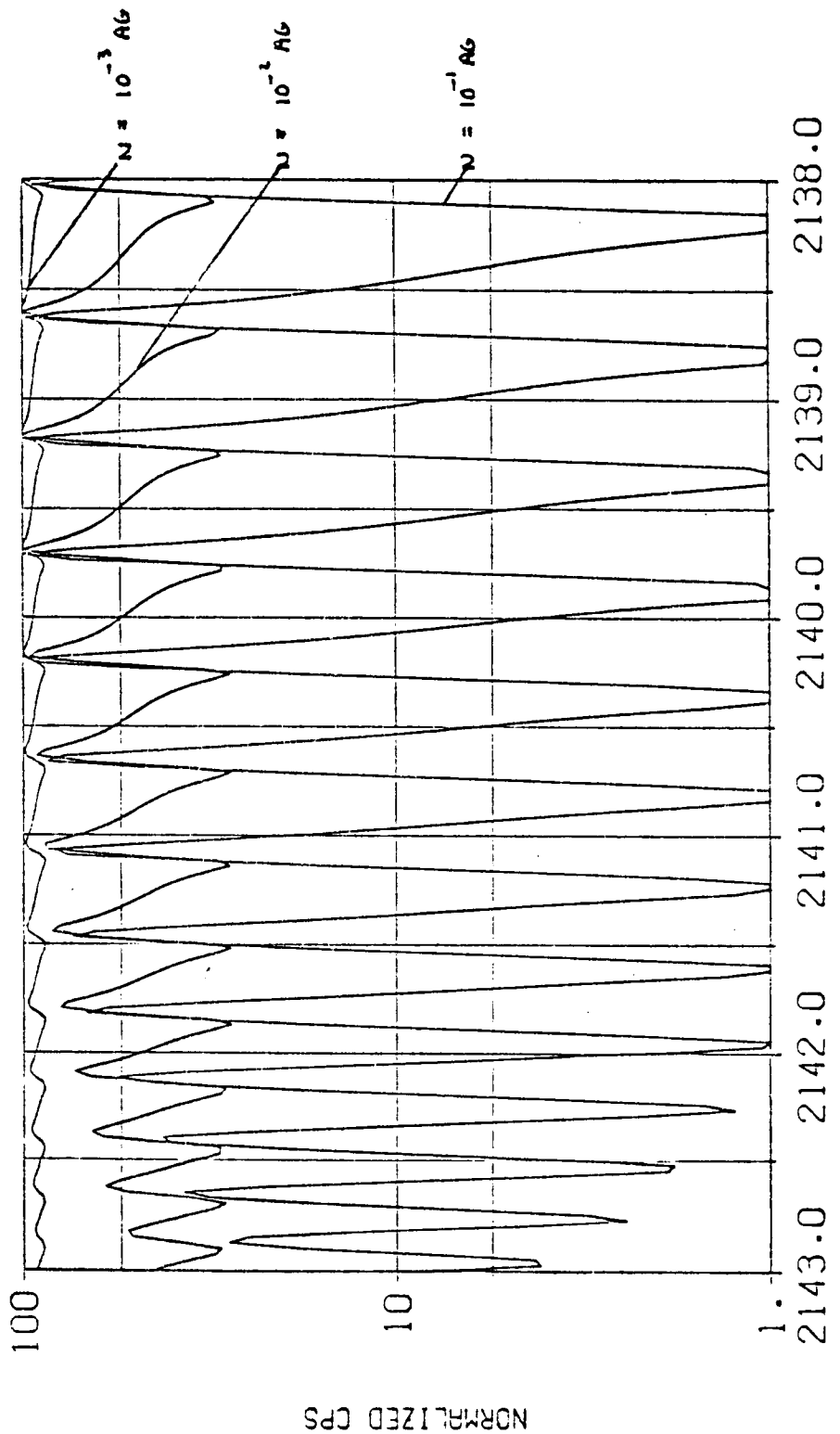

FIGURE 22. CO/N_2 CARS: (T,Z1) = 1200°K, 0.020 CM-1

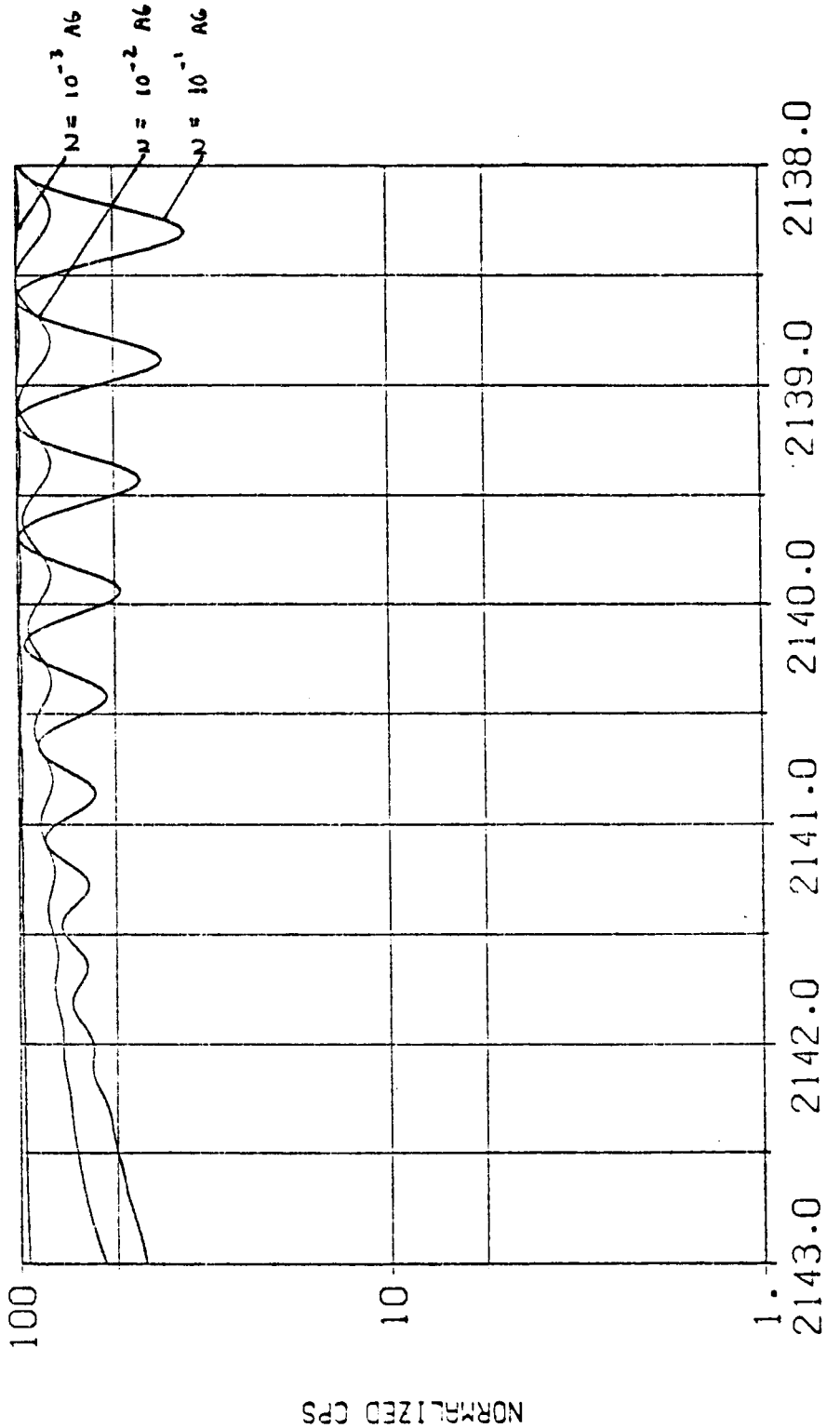

FIGURE 23. CO/N_2 CARS: (T,21) = 1200°K, 0.200 CM-1

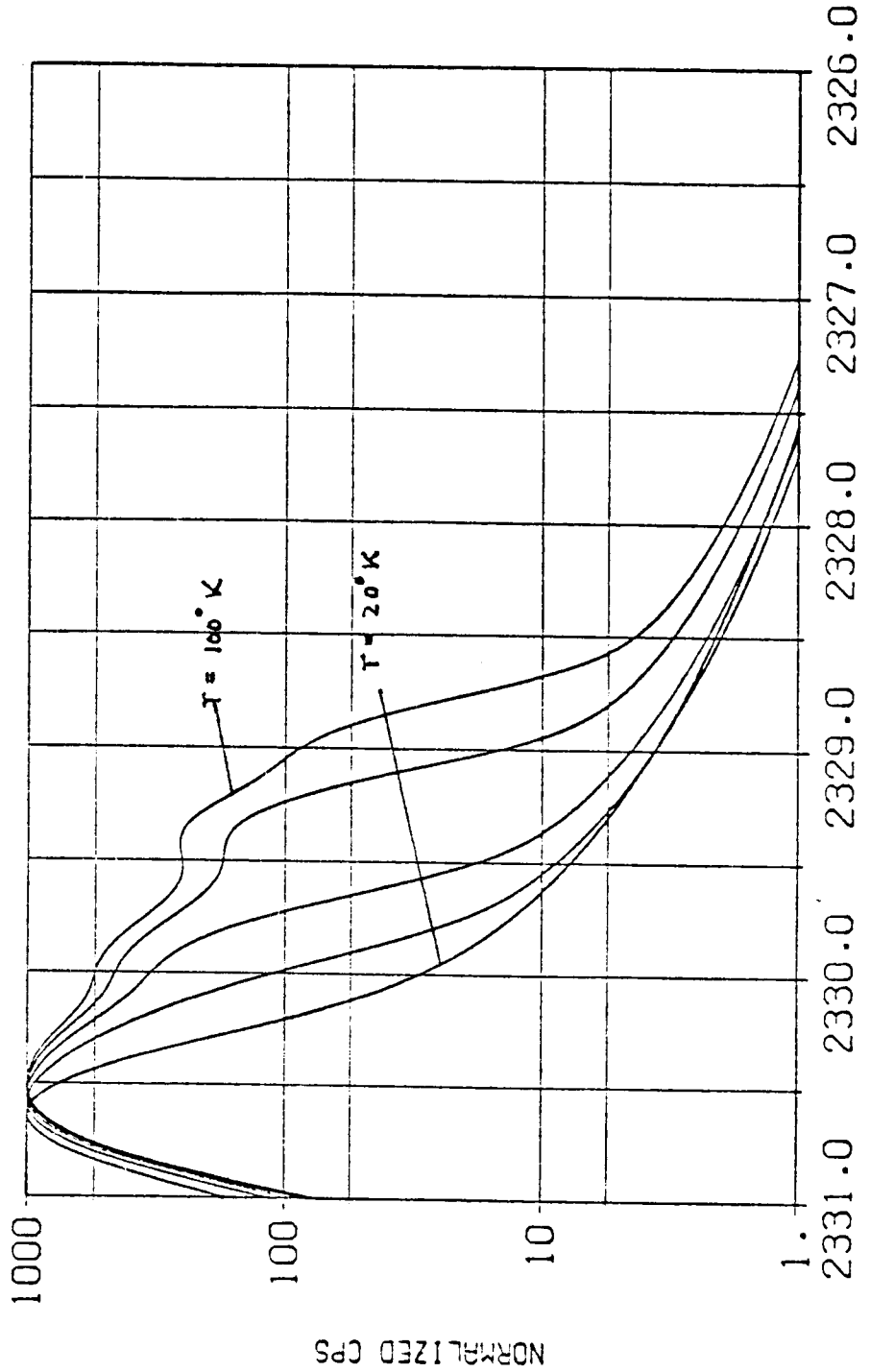

FIGURE 24. N_2 SRS: (N,21) = 0.2 AMAGATS, 0.200 CM-1

region dominated by collisional broadening. The temperature variation in the profiles is visually clear from the evolution of the higher J level which does indeed broaden the entire profile.

Fig. 25 is also a non-asymptotic regime, but Doppler and collisional broadening both contribute to the Raman linewidth. Again, the temperature effect is predominately evolution of the higher J levels.

Figs. 26 and 27 are higher temperature analogs of A and B respectively considering the Raman linewidths. The intensity ratios of the J levels change as temperature increases in each case. The EXP $[-E_J/kT]$ functional dependence would essentially determine the ratios for a solely doppler broadened regime.

An asymptotic Y case is displayed in Fig. 28 in which again the (T) evolution of the J states is still the predominate visual factor.

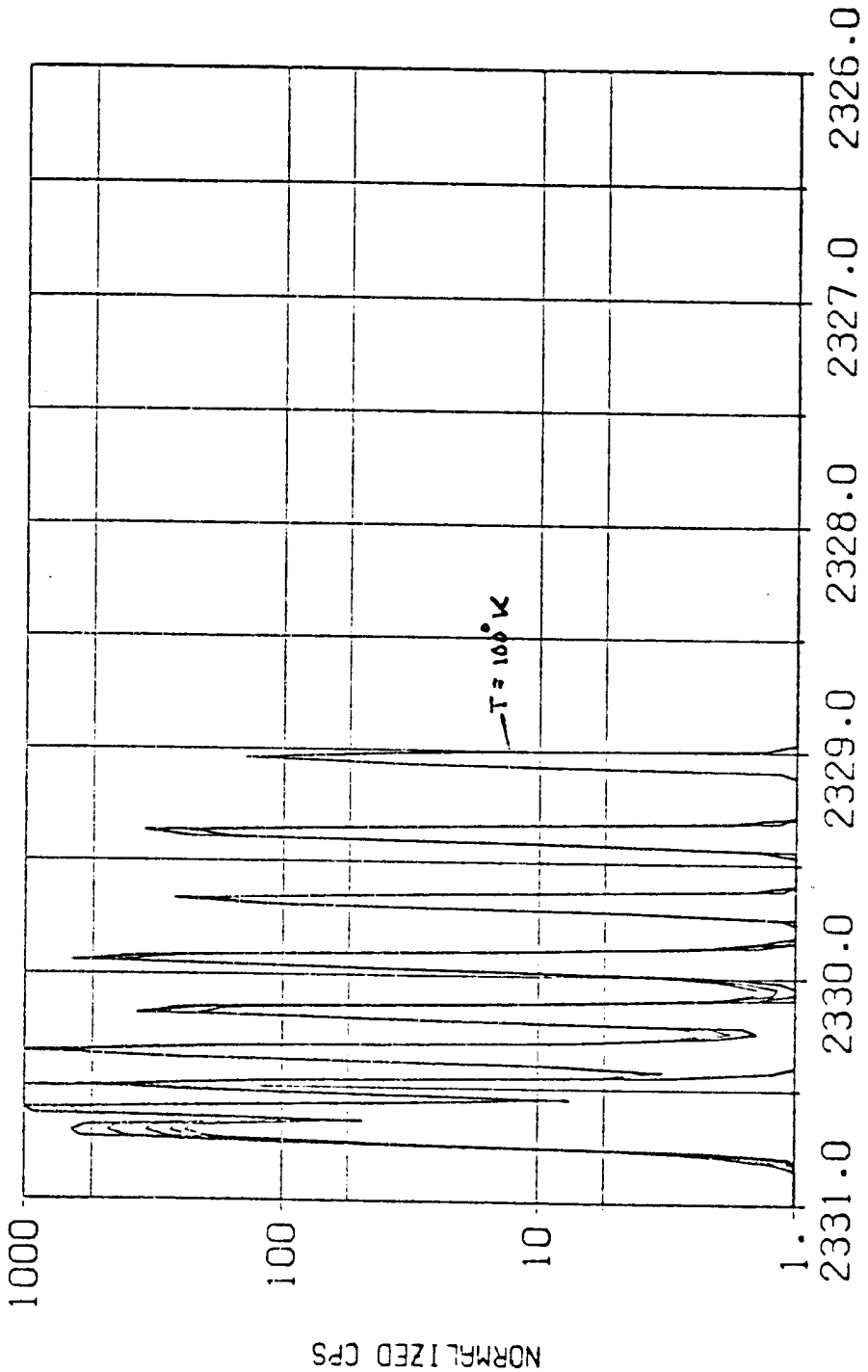

FIGURE 25. N_2 SRS: (N,Z1) = 0.002 AMAGATS, 0.020 CM-1

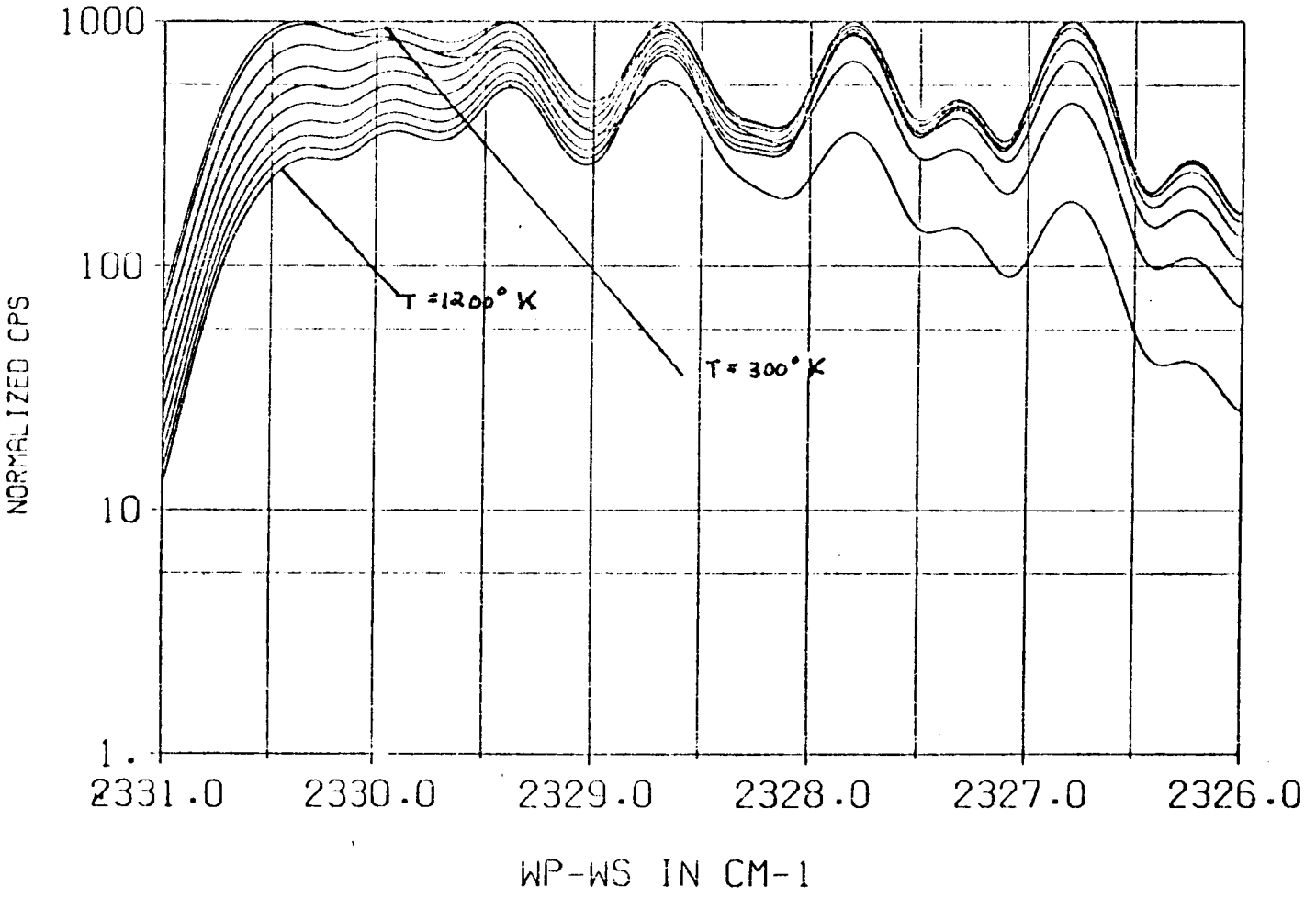

FIGURE 26. N_2 CARS: (N,Z1) = 1.0 AMAGATS, 0.200 CM-1

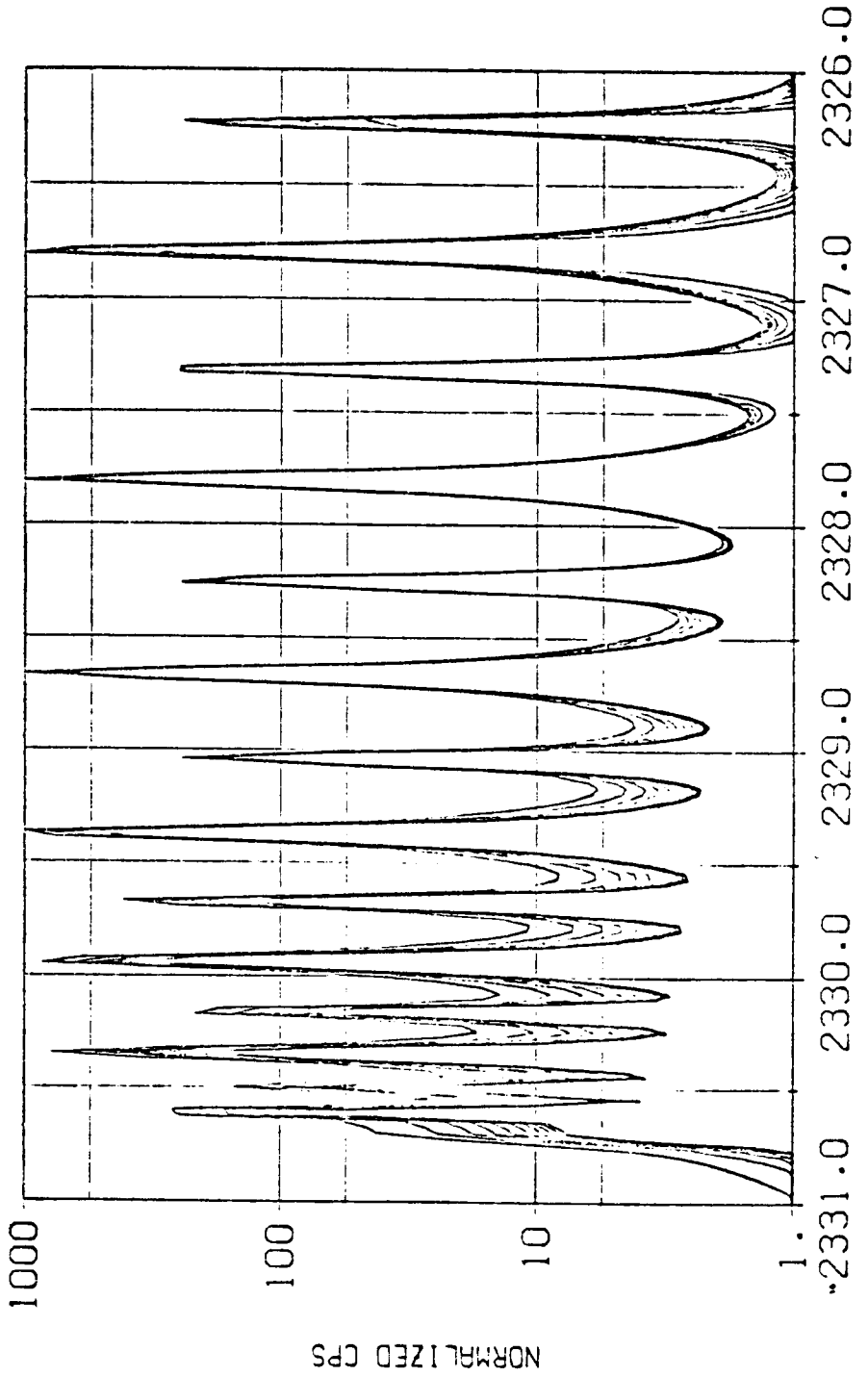

FIGURE 27. N_2 CARS: (N,Z1) = 0.100 AMAGATS, 0.020 CM-1

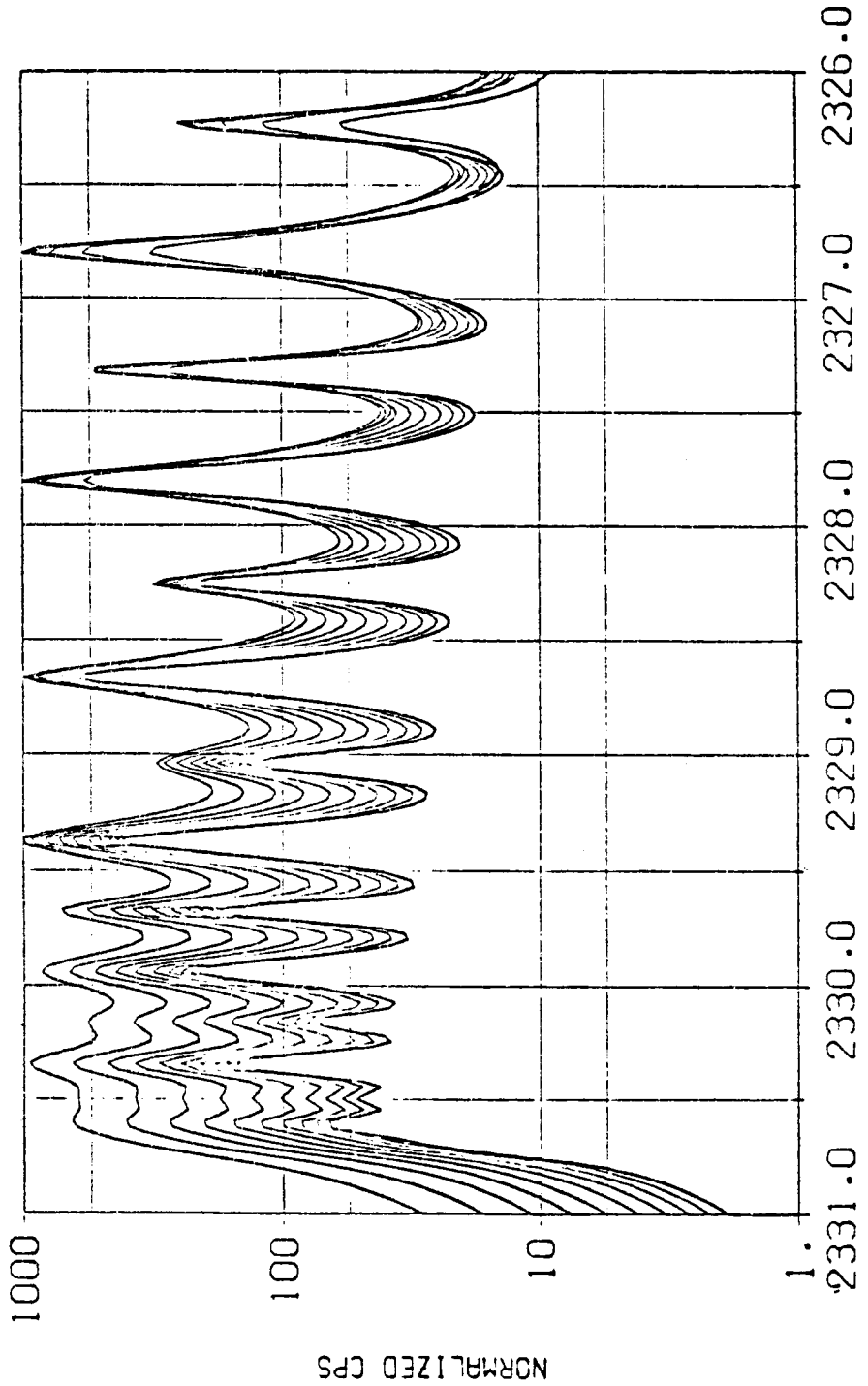

FIGURE 28. N_2 CARS: (N,Z1) = 1.0 AMAGATS, 0.020 CM-1

CHAPTER 6

RATIOING TECHNIQUES IN (N, T) MEASUREMENT

6.1 Linewidth Effects

Considering the case of two widely separated peaks such that the resonances do not interfere and additionally the non-resonant background is relatively small, one detects a peak signal at either of the peaks 1, 2 given by

$$S_{CARS} \simeq \frac{N^2}{z\Gamma_{1,2}}[\Delta_{1,2}a_{1,2}]^2 \sqrt{\pi}\ \mathrm{Re}\ \overline{W}(\overline{z}_{1,2}) \qquad (6.1.1a)$$

$$S_{SRS} \simeq \frac{N}{z\Gamma}[\Delta_{1,2}a_{1,2}]\ \sqrt{\pi}\ \mathrm{Re}\ \overline{W}(z_{1,2}) \qquad (6.1.1b)$$

where only the resonant $1/\Gamma$ term in Equation (2.3.21) is retained. Assuming for the sake of clarity that one has laser linewidths sufficiently small such that the asymptotic assumption holds,

$$R_{CARS} = \frac{S_1}{S_2} = [\frac{\Delta_1 a_1 \Gamma_2}{\Delta_2 a_2 \Gamma_1}]^2 \qquad (6.1.2a)$$

$$R_{SRS} = \frac{\Delta_1 a_1 \Gamma_2}{\Delta_2 a_2 \Gamma_1}. \qquad (6.1.2b)$$

Representing the population difference by the ground level partition function for computation ease,

$$\Delta_1/\Delta_2 \simeq \mathrm{EXP}\ [(E_2 - E_1)/kT] \qquad (6.1.3)$$

or in wavenumbers,

$$\frac{\Delta_1}{\Delta_2} \simeq \text{EXP}\left[\frac{1.438}{T}(E_2 - E_1)\right] \tag{6.1.4}$$

where the factor 1.438 is the second radiation constant.

Thus

$$\frac{d(\Delta_1/\Delta_2)}{dT} = \frac{E_1 - E_2}{T^2}(1.438)\frac{\Delta_1}{\Delta_2}. \tag{6.1.5}$$

To obtain a change of 1% in $\frac{\Delta_1}{\Delta_2}$ for a 1% change in T, one requires

$$\left|\frac{1.438(E_1 - E_2)}{T}\right| = 1. \tag{6.1.6}$$

Thus, at 1500K, the representative energy levels must be separated by $\simeq$1000 cm^{-1} for a one-to-one change.

From Equations (6.1.2a) and (6.1.2b) it is clear that measurement error in the linewidths will induce a significant temperature error. Since

$$U_{CARS} = \frac{\Delta_1}{\Delta_2} = \frac{\Gamma_1 a_2}{\Gamma_2 a_1} R_{CARS}^{\frac{1}{2}} \tag{6.1.7a}$$

$$U_{SRS} = \frac{\Gamma_1 a_2}{\Gamma_2 a_1} R_{SRS} \tag{6.1.7b}$$

a random error of 10% in the selected linewidths will be reflected in a 20% error in the U ratio. If one selects two peaks such that the change in U reflects change in temperature, then the 20% ratio error will induce an error of 20% in the measured value of temperature.

Similarly, if one predicts number density by a system efficiency convolved with detected signal, thelinewidth uncertainties will significantly effect measurement accuracies in number density.

By selecting a linewidth from the next vibrational transition at high temperature, one may reduce the effect of linewidth error by going to a less than unity ratio in Equation (6.1.5). However, one must overcome the experimental problem of a much wider spread in frequency between the two peaks. If one selects only rotational bands from Q-branch transitions, in N_2 with an anharmonicity of 0.0187 cm^{-1}, a separation of 1000 cm^{-1} in energy is $\simeq$20 cm^{-1} in frequency. At 100°K rather than 1500°K, only a 1 cm^{-1} spread is necessary.

From the previous discussion, reduction of error due to linewidth uncertainties in collisional-dominated regimes is desirable. One method of accomplishing this is by determining the functional (N, T) dependence of the linewidths; if sufficiently accurate, a non-linear fitting of experimental/theoretical profile will reduce measurement error. However, a scan of frequencies is necessary.

6.2 FM Normalization

By implementing an FM modulated SRS technique which explicitly depends on the Lorentzian $(x^2 + 1)^{-1}$ shape in collisional regimes, linewidths of the selected peaks may be determined quite accurately. Rewriting Equation (6.1.1b) in the asymptotic region,

$$SRS \simeq \frac{N}{\Gamma} \Delta[x^2 + 1]^{-1}. \qquad (6.2.1)$$

Frequency modulating the laser difference frequency by

$$X = X_0 + V_0 \text{ SIN } \omega_m t \tag{6.2.2}$$

where V_0 is the normalized modulation depth introduces an AM modulation of the detected signal as in laser stabilization. One may show by expanding $(x^2 + 1)^{-1}$ in a Taylor series that in general n'th harmonic information will be contained in (n + 2k) derivatives for k > 0. However, if V_0 is sufficiently small, one may only consider the nth term. Thus, the first harmonic information will be contained in the first derivative and so forth.

One may write the first and second harmonics as

$$K_1 \simeq \frac{-2X}{(x^2 + 1)^2} V_0 \text{ SIN } \omega_m t \tag{6.2.3a}$$

$$K_2 \simeq \frac{(1 - 3x^2)}{(x^2 + 1)^3} V_0^2 \text{ COS } 2\ \omega_m t \tag{6.2.3b}$$

By ratioing the peak values of K_1 and K_2, one defines a quantity

$$H = \frac{K_2}{K_1} = \frac{3x^2 - 1}{x(x^2 + 1)}. \tag{6.2.4}$$

The first and second derivatives are

$$\frac{\partial H}{\partial x} = \frac{V_0}{2}\left[\frac{1 + 6x^2 - 3x^4}{(x^3 + x)^2}\right] \tag{6.2.5}$$

$$\frac{1}{2}\frac{\partial^2 H}{\partial x^2} = \frac{V_0}{2}\left[\frac{3x^6 - 15x^4 - 3x^2 - 1}{(x^3 + x)^3}\right]. \tag{6.2.6}$$

The maximum value of H occurs at the point

$$x^2 = 1 + \frac{2}{3}\sqrt{3} \simeq 2.1547 \qquad (6.2.7)$$

and expanding H in a Taylor series,

$$H \simeq 1.18\frac{V_0}{2}\ 1.0 - .40\Delta x^2 \ . \qquad (6.2.8)$$

Since

$$\Delta x = -x\,\frac{\Delta\Gamma}{\Gamma} \qquad (6.2.9)$$

a 10% error in determining Γ will result in a value for x of .146 and

$$\Delta H \simeq 1\%. \qquad (6.2.10)$$

Implementing the technique will require an FM modulation that can be conveniently furnished by a standard electro-optic modulator and a two-channel lock-in amplifier. By using the normalization technique, the effective Lorentzian error can be measured to an accuracy of $.8(\Delta\Gamma/\Gamma)^2$.

The two peak ratioing techniques can be done with an FM modulated Stokes beam and two separated frequencies and two optical detector channels. In that case, the Δ_1/Δ_2 ratio may be written for $x \simeq x_{MAX}$

$$\Delta_1/\Delta_2 \simeq \frac{[(\omega_2 - \omega_p + \omega_s)^2 + \Gamma_2^2]^2(\omega_1 - \omega_p + \omega_s')}{[(\omega_1 - \omega_p + \omega_s')^2 + \Gamma_1^2]^2(\omega_2 - \omega_p + \omega_s)}. \qquad (6.2.11)$$

Assuming ignorable frequency errors.

$$\delta[\Delta_1/\Delta_2] = 4\Delta_1/\Delta_2 \left| \frac{\Delta\Gamma_2\Gamma_2}{(\omega_2 - \omega_p + \omega_s)^2 + \Gamma^2} + \text{term (1)} \right|. \qquad (6.2.12)$$

With .8% measurement accuracy and $x \simeq 1.46$,

$$\frac{\delta[\Delta_1/\Delta_2]}{[\Delta_1/\Delta_2]} \simeq 1\%.$$

The FM normalization scheme greatly reduces linewidth errors in a Lorentzian regime which is indeed the regime in which they are significant.

CHAPTER 7

PARAMETERIZATION OF NON-LINEAR PROFILE FITTING

In order to determine number density and temperature from an experimental profile by a weighted fitting technique, implementation of some non-linear algorithm is necessary for a non-linear problem such as (N, T) determination by CARS and SRS.

In a single variable, linear situation, a modified Newton scheme is quite satisfactory for the usual closely convergent regimes; i.e., the answer is relatively well known a priori. The usual non-linear algorithms proceed by some sort of multivariate Newton's method, in which a derivative is a fundamental part.

Since the closed form derivative usually is not only less costly in computational time but also may accelerate convergence, the determination of closed-form derivatives is desirable. Additionally, from these derivatives and a reasonable knowledge of the solution vector, regression analysis may be applied to determine error limits.

$|X_{CARS}(\delta)|^2$ can formally be considered a five-parameter non-linear equation for case B) since

$$S_J(X_{NR}, N, T, P_p, P_s) = P_p^2 P_s |X_{CARS}(\delta_J)|^2 \qquad (7.1)$$

where the subscript J indicates S measured at $\delta = \omega_p - \omega_{s_j}$. Only B) will be considered due to higher achievable resolution and the general experimental trend toward it. The mathematical statement of the profile fit is

$$E_{CARS} = \sum_J W_J[Y_J - S_J(X_{NR}, N, T, P_p, P_s)]^2 \qquad (7.2)$$

where Y_J, δ_J represents the experimental observed point and frequency, respectively. Normalization will clearly remove the $P_p^2 P_s$ dependence. However, these two variables remain in (7.2) to reflect the noise contribution of the pump and Stokes lasers.

To extract (N, T) data, one would generally use a computationally efficient (28), non-linear least square algorithm to solve Eq. (7.2).

Similarly, to Equation (7.2),

$$E_{SRS} = \Sigma W_J[Y_J - T_J(N, T, P_p, P_s)]^2, \qquad (7.3)$$

$$T_J = -P_p P_s X''_{SRS}(\delta_J). \qquad (7.4)$$

Re-examining (7.1), the actual Y_J's will have statistical noise introduced as a result of three factors:

1) Laser power level fluctuations

2) Background noise

3) $\sqrt{N}$ signal variation

4) Linewidth uncertainty.

Since in general one achieves a tighter fit (i.e., smaller error bars, for less statistical noise), factor (2) demonstrates the superiority of perpendicular polarizations for a CARS experiment. When the pump and Stokes beams are in this configuration, 2.1.5 indicates the $\hat{\ell}_{as}$ is perpendicular to $\hat{\ell}_p$ and parallel to $\hat{\ell}_s$. Separating ω_{as} from ω_p for high pump powers for $P_{as} \simeq 10^{-14} P_p$ is

not easy and the crossed polarization reduces background pump leakage on the order of two magnitudes. Therefore, there is much less statistical noise. Additionally, a mixed pump polarization (28) can reduce X_{NR} a factor of four or five.

To simplify calculations, it is possible to combine the variances associated with 1) and 3). With $\bar{\beta}$ the normalizing factor such that $S\ell$, $T\ell_{MAX} = 1.0$,

$$S_\ell = \bar{\beta}[X_{NR}^2 + 2X_{NR}X_\ell \sum_J \bar{K}_J \sqrt{\pi}\ \mathrm{Im}\ \bar{W}(\bar{Z}_{JL})$$

$$+ X_\ell{}^2 \sum_J \bar{K}_J^2 \sqrt{\pi}\ \mathrm{Re}\ \bar{W}(\bar{Z}_{JL})/\bar{Y}_J$$

$$+ 2X\ell^2 \sum_J \bar{K}_J \sqrt{\pi}\ \mathrm{Im}\ \bar{W}(\bar{Z}_{JL}) \sum_{K\neq} \bar{K}_K \frac{\bar{D}_{KJ}}{\bar{D}_{KJ}^2 + (\bar{Y}_K + \bar{Y}_J)^2}$$

$$+ 2X\ell^2 \Sigma\ \bar{K}_J \sqrt{\pi}\ \mathrm{Re}\ \bar{W}(\bar{Z}_{JL}) \sum_{K\neq} \bar{K}_K \frac{\bar{Y}_K + \bar{Y}_J}{\bar{D}_{KJ}^2 + (\bar{Y}_K + \bar{Y}_J)^2}] \qquad (7.5)$$

where $Z_J l = \dfrac{W_J - \delta l}{z l}$ and l is the profile frequency index. The real utility of the closed form expression is in the calculation of $\vec{\nabla}(S\ell)$ where the gradient operator represents differentiation with respect to the fitting parameters. One can immediately write

$$\frac{\partial S\ell}{\partial \bar{\beta}} = \frac{S\ell}{\bar{\beta}}, \qquad (7.6)$$

and

$$\frac{\partial S\ell}{\partial X_{NR}} = 2\bar{\beta}[X_{NR} + X\ell \sum_J \bar{K}_J\ \pi\ \mathrm{Im}\ \bar{W}_{JL}]. \qquad (7.7)$$

Evaluation of the (N, T) derivatives is much more complex. To begin, note that

$$\frac{d}{d\bar{T}} = \Sigma \frac{\partial \bar{Y}_J}{\partial \bar{T}} \frac{d}{d\bar{Y}_J} + \frac{\partial}{\partial \bar{T}} \tag{7.8}$$

and similarly for (N). The problem of determining the derivatives with respect to the Y_J's is solvable; noting that it may be shown from the series expansion of $\bar{W}_J$l that

$$\text{Re } \frac{\partial \bar{W}}{\partial \bar{Y}} = \frac{\partial}{\partial Y} \text{ Re } \bar{W}; \tag{7.9}$$

the derivatives of the real and imaginary parts of the complex error function are given by (24)

$$\text{Re } \bar{W})Y = 2Y \text{ Re } \bar{W} + 2X \text{ Im } \bar{W} - \frac{2}{\sqrt{\pi}},$$

$$\text{Im } \bar{W})Y = -2X \text{ Re } \bar{W} + 2Y \text{ Im } \bar{W}. \tag{7.10}$$

Differentiating the first sum in Equation (7.5) with respect to Y_J, one obtains

$$4 \, X\ell \, \sqrt{\pi} \, X_{NR} \, \bar{K}_J(\bar{Y}_J \text{ Im } \bar{W}_{JL} - \bar{X}_{JL} \text{ Re } \bar{W}_{JL}). \tag{7.11}$$

From the second sum, the Y_J derivative is

$$X\ell^2 \sqrt{\pi} \, \bar{K}_J^2 \frac{1}{\bar{Y}_J}\{\text{Re } \bar{W}_{JL}(2\bar{Y}_J - \frac{1}{\bar{Y}_J}) + 2\bar{X}_{JL} \text{ Im } \bar{W}_{JL} - \frac{2}{\sqrt{\pi}}\}. \tag{7.12}$$

Since this term in Equation (7.12) is the resonance term for Z_Jl = Y_J, it is instructive to examine the asymptotic behavior of the derivative for the case zl << Γ_{RES}. Asymptotically,

$$\sqrt{\pi} \, \bar{Y}_J \text{ Re } \bar{W}(i\bar{Y}_J) \simeq 1 - \frac{1}{2\bar{Y}_J^2} \tag{7.13}$$

with the result that the resonance derivative varies as $-2/\Gamma_{RES}^3$

which is what one would expect for a resonance term varying asymptotically as $1/\Gamma_{RES}^2$.

Differentiating with respect to Y_J, the third and fourth summations give

$$4X\ell^2\ \overline{K}_J\ \sqrt{\pi}\ (\overline{Y}_J\ \mathrm{Im}\ \overline{W}_{JL} - \overline{X}_{JL}\ \mathrm{Re}\ \overline{W}_{JL})\ \sum_{K\neq}$$

$$4X\ell^2\ \overline{K}_J\ \sqrt{\pi}\ (\overline{Y}_J\ \mathrm{Re}\ \overline{W}_{JL} + \overline{X}_{JL}\ \mathrm{Im}\ \overline{W}_{JL} - \frac{2}{\sqrt{\pi}})\sum_{K\neq} \qquad (7.14)$$

with the addition of two terms from the third and fourth summations. involving the Y_J dependence of the two $\sum_{K\neq}$ sums. The third term $\{K\neq\}$ is

$$\sum_{K\neq}\ \overline{K}_K\ \overline{D}_{KJ}/[\overline{D}_{KJ}^2 + (\overline{Y}_K + \overline{Y}_J)^2]. \qquad (7.15)$$

Differentiating with respect to Y_J gives

$$-2\ \Sigma\ \overline{K}_K\ \overline{D}_{KJ}(\overline{Y}_K + \overline{Y}_J)/[\ \ ]^2. \qquad (7.16)$$

One simplifies calculation by defining

$$ZKM(J) = \sum_{K\neq}\ \overline{K}_K\ \overline{D}_{KJ}/[\ \ ]$$

$$ZKM)_y(J) = -2\ \sum_{K\neq}\ \overline{K}_K\ \overline{D}_{KJ}(\overline{Y}_K + \overline{Y}_J)/[\ \ ]^2. \qquad (7.17)$$

Since ZKM(J) need only be evaluated at one point in the profile--i.e., it is not a function of 1, clear computation advantages exist in terms of minimizing mathematical operations to write additionally for the fourth sum

$$ZKC(J) = \sum_{K\neq} \bar{K}_K(\bar{Y}_J + \bar{Y}_K)/[\quad] , \tag{7.18}$$

and similarly to Equation (7.17),

$$ZKC)_y(J) = \sum_{K\neq} \bar{K}_K\{1/[\quad] - 2(\bar{Y}_J + \bar{Y}_K)^2/[\quad]^2\} \tag{7.19}$$

which may be simplified as

$$ZKC)_y(J) = \sum_{K\neq} \bar{K}_K(\bar{D}^2_{KJ} - (\bar{Y}_J + \bar{Y}_K))^2/[\quad]^2. \tag{7.20}$$

Since the (N, T) dependence of Y_J may be determined from Equation (4.1.2), the remaining T derivatives involve $\bar{K}_K)_T$. Collecting terms, one has finally

$$\begin{aligned} S\ell)_T = {} & \beta\mathfrak{E}2X_{NR}X\ell \sum_J \bar{K}_J \sqrt{\pi}[\frac{\bar{K}_J)_T}{\bar{K}_J} \operatorname{Im} \bar{W}_{JL} + \operatorname{Im} \bar{W}_{JL})_{Y_J} \bar{Y}_J)_T] \\ & + X\ell^2 \sum_J \frac{\bar{K}_J^2\sqrt{\pi}}{\bar{Y}_J}[\frac{2\bar{K}_J)_T}{\bar{K}_J} \operatorname{Re} \bar{W}_{JL} - \frac{\operatorname{Re} \bar{W}_{JL}}{\bar{Y}_J} \bar{Y}_J)_T + \operatorname{Re} \bar{W}_{JL})_{\bar{Y}_J} \bar{Y}_J)_T] \\ & + 2X\ell^2 \sum_J \bar{K}_J \sqrt{\pi}\{[\frac{\bar{K}_J)_T}{\bar{K}_J} \operatorname{Im} \bar{W}_{JL} + \operatorname{Im} \bar{W}_{JL})_{\bar{Y}_J} \bar{Y}_J)_T]ZKM(J) \\ & + \operatorname{Im} \bar{W}_{JL}\ ZKM)_T(J)\} + 2X\ell^2 \sum_J \bar{K}_J \sqrt{\pi}\{[\frac{\bar{K}_J)_T}{\bar{K}_J} \operatorname{Re} \bar{W}_{JL} \\ & + \operatorname{Re} \bar{W}_{JL})_{\bar{Y}_J} \bar{Y}_J)_T]ZKC(J) + \operatorname{Re} \bar{W}_{JL}\ ZKC)_T(J)\}\mathfrak{E} \end{aligned} \tag{7.21}$$

where as usual $)_X$ indicates differentiation with respect to X. The terms $ZKM)_T(J)$ and $ZKC)_T(J)$ may be written as

$$ZKM)_T(J) = \sum_{K\neq} \bar{K}_K \bar{D}_{KJ}/[\bar{D}^2_{KJ} + (\bar{Y}_K + \bar{Y}_J)^2] \times$$

$$\{\frac{\bar{K}_K)_T}{\bar{K}_K} - 2(\bar{Y}_K + \bar{Y}_J)(Y_K)_T + Y_J)_T)/[\ \ ]\} \qquad (7.22a)$$

and

$$ZKC)_T(J) = \sum_{K\neq} \bar{K}_K(\bar{Y}_K + \bar{Y}_J)/[\ \ ] \times$$

$$\{\frac{\bar{K}_K)_T}{\bar{K}_K} + \frac{Y_J)_T + Y_K)_T}{\bar{Y}_J + \bar{Y}_K} - \frac{2(Y_K + Y_J)(Y_K)_T + Y_J)_T)}{[\ \ ]}\}. \qquad (7.22b)$$

Although these equations may seem rather awkward, there exist computational advantages in writing Equations (7.21) and (7.22) as they are. Using a fast calculational algorithm for the complex error function (29) reduces convolution time, but using the form in Appendix C has one disadvantage. Calculation of the derivates as in Equation (7.10) diverges from accuracies on the order of 1 ppm as $|z| > 100$. To maintain closed-form consistency, the finite difference derivative and the closed form derivative should approach one another as the T, N difference approaches zero. To this end, avoiding double precision arithmetic is possible by calculating Re $\bar{W}_{JL})_{\bar{Y}_J}$ and Im $\bar{W}_{JL})_{\bar{Y}_J}$ as in Appendix C.

Considering Equation (7.22), note that the quantity $[\bar{D}^2_{KJ} + (\bar{Y}_K + \bar{Y}_J)^2]$ is a common denominator and need only be

computed once as one performs the indicated summations in Equations (7.17), (7.18), (7.22). As previously, the $\vec{z}$ functions and derivatives need only be computed at one point in the profile.

The derivative with respect to (N) is similarly calculated by writing

$$S\ell)_N = \frac{2\bar{\beta}S\ell}{N} + \bar{\beta}\{2X_{NR}\, X\ell \sum_J \bar{K}_J \sqrt{\pi}\ \mathrm{Im}\ \bar{W}_{JL})_{\bar{Y}_J}\bar{Y}_J)_N$$

$$+ X\ell^2 \sum_J \frac{\sqrt{\pi}\bar{K}_J^2}{\bar{Y}_J}\{\mathrm{Re}\ \bar{W}_{JL})_{Y_J} - \frac{\mathrm{Re}\ \bar{W}_{JL}}{\bar{Y}_J}\}\bar{Y}_J)_N$$

$$+ X\ell^2 \sum_J \sqrt{\pi}\ \bar{K}_J\{\mathrm{Im}\ \bar{W}_{JL})_{\bar{Y}_J}\bar{Y}_J)_N\ ZKM(J) + \mathrm{Im}\ \bar{W}_{JL}\ ZKM)_N(J)\}$$

$$+ X\ell^2 \sum \sqrt{\pi}\ \bar{K}_J\{\mathrm{Re}\ \bar{W}_{JL})_{\bar{Y}_J}\bar{Y}_J)_N\ ZKC(J) + \mathrm{Re}\ \bar{W}_{JL}\ ZKC)_N(J)\}\}. \tag{7.23}$$

where the $\frac{2\bar{\beta}S\ell}{N}$ term comes from the N^2 signal dependence and

$$ZKM)_N(J) = \sum_{K\neq} \bar{K}_K\ \bar{D}_{KJ}\{-2(\bar{Y}_K + \bar{Y}_J)(\bar{Y}_K)_N + \bar{Y}_J)_N)\}/[\ \ ]^2$$

$$ZKC)_N(J) = \sum \bar{K}_K(\bar{Y}_K + \bar{Y}_J)\{\frac{\bar{Y}_K)_N + \bar{Y}_J)_N}{\bar{Y}_J + \bar{Y}_K}$$

$$- \frac{2(\bar{Y}_K + \bar{Y}_J)(\bar{Y}_K)_N + \bar{Y}_J)_N)}{[\ \ ]}\}/[\ \ ]. \tag{7.24}$$

The profile term Sl is now written as

$$S\ell = \overline{\beta}[X_{NR}^2 + 2X\ell\ X_{NR} \sum_J \overline{K}_J\ \sqrt{\pi}\ \mathrm{Im}\ \overline{W}_{JL}$$

$$+ X\ell^2 \sum_J \sqrt{\pi}\ \overline{K}_J^2\ \mathrm{Re}\ \overline{W}_{JL}/\overline{Y}_J$$

$$+ 2X\ell^2 \sum_J \overline{K}_J\ \sqrt{\pi}\ \mathrm{Im}\ \overline{W}_{JL}\ ZKM(J)$$

$$+ 2X\ell^2 \sum_J \overline{K}_J\ \sqrt{\pi}\ \mathrm{Re}\ \overline{W}_{JL}\ ZKC(J) \qquad (7.25)$$

which considerably simplifies Equation (7.5).

The casual observer might wonder at the utility of these rather complicated equations, but remembering the usefulness of writing $Z\underset{\rightarrow}{K}M$, $Z\underset{\rightarrow}{K}C$ and associated derivatives, calculation of the profile height at one point along with the fitting derivatives involves only one summation of twelve or so individual terms neglecting the $\vec{z}$ vector calculations. Multiplying the terms by appropriate constants gives one the profile height and derivatives.

The remaining (N, T) derivatives are $\overline{Y}_J)_{T,N}$ and $\overline{K}_J)_T$. Remembering that

$$\overline{K}_J = \eta_J a_J \Delta J \qquad (7.26)$$

and that the t dependence of the line strength factor A_J is ignorable (Appendix D),

$$\bar{K}_J)_T = n_J a_J \Delta\ )_T. \tag{7.27}$$

Writing Δ_J, the population difference as

$$\Delta_J = P_{vJ} - P_{v+1\ J}, \tag{7.28}$$

for the Q branch vibrational transition v = 0, v = 1,

$$P_{0J} = EXP(-E_{0J}\ KT)/\sum_i EXP(-E_{0i}/KT) \tag{7.29}$$

and

$$P_{1J} = EXP(-E_{1J}/KT)/\sum_i EXP(-E_{1i}/KT). \tag{7.30}$$

In the equilibrium case where rotation and vibrational temperatures are equal,

$$\Delta_J)_T = \frac{1}{KT^2}[E_{0J}P_{0J} - E_{1J}P_{1J} - \langle E\rangle \Delta J] \tag{7.31}$$

which may be rewritten as

$$\Delta_J)_T = \frac{1}{KT^2}[\Delta J(E_{0J} - \langle E\rangle) - \lambda C\omega_J\ P_{1J}] \tag{7.32}$$

where ω_J is in cm^{-1}. Ignoring the contribution of P_{1J} for moderate temperature, $\Delta J)_T$ will be positive for $E_{0J} > \bar{E}$; negative for $E_{0J} < \bar{E}$. This is as one would expect since the higher J levels become more heavily populated as the temperature increases.

For the non-equilibrium case in which the rotational and vibrational temperature are not equal, Eq. (7.31) becomes

$$\Delta_J)_{T_V,T_R} = \frac{1}{kT^2_{V,R}} \{(E - \langle E\rangle)_{0,J} P_{0J}$$

$$- (E - \langle E\rangle)_{1,J} P_{1J}\} \qquad (7.33)$$

where the v,R indicates differentiation with respect to either T_V or T_R and

$$P_{vJ} \simeq EXP[- \frac{E_V}{KT_V} - \frac{E_R}{KT_R}]. \qquad (7.34)$$

Equation (7.32) may at first hand seem to require costly computational time, but calculating the partition function alone involves P_{0J} and P_{1J}; the population difference derivative adds very little computational effort.

Calculating the (N, T) derivatives of the Y_J gives from section 4.1; writing (4.1.2) as

$$Y = \frac{1}{2z1} \{\beta\ell(1 + \varepsilon\ell n2) + [\beta\ell^2(1 - \varepsilon\ell n2)^2 + 4\beta_g^2]^{\frac{1}{2}}\} \qquad (7.35)$$

simplifies the necessary calculations.

Remembering that

$$\beta)_T = \frac{-\beta\ell}{2T}$$

and

$$\beta_g)_T = \frac{\beta g}{2T} \qquad (7.36)$$

the $Y)_T$ derivative becomes

$$Y)_T = \frac{1}{4z\bar{1}T}\{-\beta\ell(1 + \varepsilon\ell n^2) + \frac{-\beta\ell^2(1 - \varepsilon\ell n2)^2 + 4\beta_g^2}{[\beta\ell^2(1 - \varepsilon\ell n2)^2 + 4\beta_g^2]^{\frac{1}{2}}}\}. \quad (7.37)$$

To demonstrate validity of the derivative for the cases where either $\beta\ell >> \beta_g$ or vice versa, for $\beta\ell/\beta_g$ approaching infinity, $Y)_T \simeq [\frac{\beta\ell}{z\bar{1}}])_T$ as one requires; for $\beta_g >> \beta\ell$, $Y)_T \simeq [\beta_g/z1])_T$.

Since $\beta\ell)_N = \beta\ell)_N$,

$$Y)_N = \frac{1}{2z\bar{1}N}\{\beta\ell(1 + \varepsilon\ell n2) + \frac{\beta\ell^2(1 - \varepsilon\ell n2)}{[\quad]^{\frac{1}{2}}}\} \quad (7.38)$$

As in the population difference (T) derivative, the (N, T) derivatives add little computational time since $\beta\ell$, β_g and $[\ ]^{\frac{1}{2}}$ need be calculated to produce Y_J regardless of the derivatives.

From the preceding discussion the SRS profile and derivatives may be immediately written as

$$T\ell = CX\ell \sum_J \bar{K}_J \, Re \, \bar{W}_{JL} \sqrt{\pi}$$

$$T\ )_T = CX\ell \, \Sigma \sqrt{\pi} \, \bar{K}_J\{\frac{\bar{K}_J)_T}{\bar{K}_J} Re \, \bar{W}_{JL} + Re \, \bar{W}_{JL})_{Y_J} Y_J)_T\} \quad (7.39)$$

and for the (N) derivative remembering that C depends linearly on N,

$$T\ell)_N = \frac{T\ell}{N} + CX\ell \sum \pi \overline{K}_J \text{ Re } \overline{W}_{JL})_{\overline{Y}_J} \overline{Y}_J)_N. \qquad (7.40)$$

Computationally, calculation of a profile point and closed-form derivatives is very fast. At any one l value, single precision IBM 370/65 times varies from 3 to 10 milliseconds per point depending on temperature. The temperature dependence of profile and derivative time results from the difference in J level populations versus temperature. Generating one point in the profile takes only on the order of 2.5 milliseconds. The closed form derivative forms take an additional 2.5 ms. versus the additional 7.5 ms. for (T, N, X_{NR}) finite difference derivatives. The closed form derivatives save a factor of two and the closed form convolution about a factor of sixty or so from previous calculations (20). Timewise, a factor of about two orders of magnitude is the resulting saving. The real significance is in profile fitting which may take fifty to a hundred functional evaluations.

For two hundred data points, the profile and derivatives consume about one sec. of CPU time. Considering average convergence to require sixty functional evaluations, convergence will be achieved in about one minute versus the two hours necessary without the closed form. The most significant feature in this much CPU savings is the possibility of using small and relatively inexpensive systems rather than taking large amounts of expensive main frame time.

CHAPTER 8

MULTIVARIATE NON-LINEAR REGRESSION ANALYSIS

8.1 Basic Theory

Certain definitions are of great utility in simplifying the following discussion:

$\vec{C}$	parameter vector
$\vec{z}$	measured experimental profile vector
$\vec{x}$	independent variable $(\omega_p - \omega_{si})$
$\vec{\varepsilon}$	error vector
$\vec{y}$	mathematical profile vector
Ω	variance (σ_i^2)

A general statement of the non-linear fitting problem is to minimize a weighted error function with respect to the parameter vector. At any one point

$$z_i = y_i\ (x_i, \vec{C}) + \varepsilon_i. \tag{8.1.1}$$

The total error including weighting is given as

$$S = \sum_i W_i\ \varepsilon_i^2. \tag{8.1.2}$$

Since non-linear parameter fitting by a Gauss-Newton or a modified Gauss-Newton method proceeds by linearization of $\vec{y}$ (29), it is sufficient for error analysis to consider the cases of near convergence. As one would expect, the problem is then

reduced to the much simpler one of linear regression analysis (33). The linearized form of Equation (8.1.1) is

$$z_i = y_i(x_i, \vec{C}_0) + \vec{\nabla}_C y_i \cdot \delta\vec{C} + \varepsilon_i \tag{8.1.3}$$

with

$$\vec{\nabla}C = \hat{C}_1 \frac{\partial}{\partial C_1} + \hat{C}_2 \frac{\partial}{\partial C_2} + \cdot \cdot \hat{C}_N \frac{\partial}{\partial C_N} \tag{8.1.4}$$

and

$$\delta C_i = C_i - C_{0i}. \tag{8.1.5}$$

Letting

$$v_i = z_i - y_i,$$

$$\vec{v} = \underline{\alpha}\delta\vec{C} + \vec{\varepsilon} \tag{8.1.6}$$

where

$$diJ = \frac{\partial y_i}{\partial C_J}. \tag{8.1.7}$$

The total weighted error S can then be written as

$$S = (\vec{v} - \underline{\alpha}\delta\vec{C})^T \underline{W} (\vec{v} - \underline{\alpha}\delta\vec{C}) \tag{8.1.8}$$

where $\underline{W}$ is the weighting matrix.

Expanding this equation term by term,

$$S = \vec{v}^T\underline{W}\vec{v} - 2\vec{\delta C}^T\underline{\alpha}^T\underline{W}\vec{v} + \vec{\delta C}^T\underline{\alpha}^T\underline{W}\vec{\delta C}. \tag{8.1.9}$$

For n points and v variables, $\underline{\alpha}$ is an (n x v) matrix; $\underline{W}$, (n x n); $\vec{v}$, (n x 1); and $\vec{\delta}C$, (v x 1). $\underline{\alpha}^T\underline{W}\underline{\alpha}$ is then a symmetric (v x v) matrix.

Minimizing (8.1.9) with respect to the parameter vector $\vec{\delta}C$,

$$\underline{\alpha}^T\underline{W}\vec{v} = \underline{\alpha}^T\underline{W}\underline{\alpha}\vec{\delta}C \tag{8.1.10}$$

which defines the normal equations for the parameters C.

If in general the columns of $\underline{\alpha}^T\underline{W}\underline{\alpha}$ are linearly independent, an inverse for this (r x r) square matrix does exist. Since columns c, j involve differentiation with respect to C_i and C_j, the columns are indeed linearly independent. Equation (8.1.10) has the immediate solution:

$$\vec{\delta}C = (\underline{\alpha}^T\underline{W}\underline{\alpha})^{-1}\ \underline{\alpha}^T\underline{W}\vec{v}. \tag{8.1.11}$$

Defining $\underline{M}$ as $\underline{\alpha}^T\underline{W}\underline{\alpha}$, Equation (8.1.11) becomes

$$\vec{\delta}C = \underline{M}^{-1}\underline{\alpha}^T\underline{W}\vec{v}. \tag{8.1.12}$$

For the physically realistic case of uncorrelated measurements with unequal weights, $W_{iJ} = W_{ii}\delta_{iJ}$ and

$$m_{lm} = \sum_i^N \alpha_{il}\alpha_{im}\, W_{ii}. \tag{8.1.13}$$

In the case of a linear transformation, it may be shown (32) if

$$\vec{y} = \underline{A}\vec{x} \tag{8.1.14}$$

then

$$\underline{\Omega}_y = \underline{A}\ \underline{\Omega}_x\ \underline{A}^T \tag{8.1.15}$$

with the reminder that $\underline{\Omega}_{y,x}$ are the covariance matrices of y and x, respectively. Applying Equation (8.1.15),

$$\underline{\Omega}_c = \underline{M}^{-1}[\underline{\alpha}^T\underline{W}\underline{\Omega}_v\underline{W}^T\underline{\alpha}](\underline{M}^{-1})^T. \tag{8.1.16}$$

The two usually followed weighting procedures are a) equal weight or b) inversely proportional to the variance. The form of the variance matrix is now of paramount importance. The variance matrix associated with the physical measurement of a spectral profile is of necessity diagonal since a measurement at one point should not effect another. The variance due to the uncertainties of the line broadening parameters is likewise diagonal since variance for one value of J should not be correlated with any other. Regardless of the source of the variance, $\underline{\Omega}$ is diagonal.

In case a) Equation (8.1.16) is now written as

$$m_{lm} = \sum_i^N \alpha_{il}\alpha_{im} = m_{ml}, \tag{8.1.17}$$

$$P_{JK} = \sum_i^N \alpha_{iJ}\alpha_{iK}\Omega_{ii}, \tag{8.1.18}$$

$$\underline{\Omega}_{EQ} = \underline{M}^{-1}\underline{P}\ \underline{M}; \tag{8.1.19}$$

in case b), $W_{ii} = 1/\Omega_{ii}$ or more formally $\underline{W} = \underline{\Omega}^{-1}v$ and (8.1.16) becomes the simple equation

$$\underline{\Omega}_{C} = \underline{M}^{-1} \tag{8.1.20}$$

with $m_{lm} = \sum_{i}^{N} \alpha_{il}\alpha_{im}/\Omega_{ii}$.

To further illustrate these results, for one variable θ,

$$\Omega(\theta)_{EQ} = \sum_{i} \left(\frac{\partial f_i}{\partial \theta}\right)^2 \Omega_{ii} / \{\sum_{i} \left(\frac{\partial f_i}{\partial \theta}\right)^2\}^2 \tag{8.1.21}$$

$$\Omega(\theta)_{UNEQ} = \{\sum_{i} \left(\frac{\partial f_i}{\partial \theta}\right)^2 / \Omega_{ii}\}^{-1} \tag{8.1.22}$$

which is in exact agreement with the more familiar one variable case as demonstrated by Saleh (33).

For the two variable case (T, N), Equation (8.1.13) yields

$$m_{TT} = \sum_{i} \left(\frac{\partial y_c}{\partial T}\right)^2 / \Omega_{ii}, \tag{8.1.23}$$

$$m_{nn} = \sum_{i} \left(\frac{\partial y_i}{\partial N}\right)^2 / \Omega_{ii}, \tag{8.1.24}$$

$$m_{TN} = \Sigma \left(\frac{\partial y_i}{\partial T}\right)\left(\frac{\partial y_c}{\partial N}\right) / \Omega_{ii}. \tag{8.1.25}$$

It is easy enough to calculate $\underline{M}^{-1}$ with the result

$$\underline{M}^{-1} = [m_{TT}m_{NN} - M_{TN}^2]^{-1}\begin{bmatrix} m_{nn} & -m_{TN} \\ -m_{TN} & m_{TT} \end{bmatrix}; \qquad (8.1.26)$$

for case b) the calculation of the variances is straightforward

$$\Omega_{TT} = m_{nn}/[m_{TT}M_{nn} - m_{TN}^2], \qquad (8.1.27)$$

$$\Omega_{nn} = m_{TT}/[\quad]. \qquad (8.1.28)$$

For case a)

$$\Omega_{TT} = \frac{m'^2_{nn}P_{TT} + m'^2_{TN}P_{NN} - 2m'_{TN}m'_{nn}P_{TN}}{[\quad]^2} \qquad (8.1.29)$$

$$\Omega_{NN} = \frac{m'^2_{TT}P_{NN} + m'^2_{TN}P_{TT} - 2m'_{TN}m'_{TT}P_{TN}}{[\quad]^2} \qquad (8.1.30)$$

where the ' denotes evaluating m by Equation (8.1.17).

Although the profile fitting involves a normalization factor $\overline{\beta}$, the derivative with respect to β is simply $Y_i/\overline{\beta}$. For high count rate, high signal-to-noise situations, the variance due to $\overline{\beta}$ may be ignored and the preceding analysis is quite accurate enough. However, if it is necessary to include the normalization factor $\overline{\beta}$ as an independent variable in noisy conditions, for case b)

$$\Omega_{\beta\beta} = m_{TT}m_{NN} - m_{TN}^2 / \{m_{\beta\beta}[\quad]_{T,N}$$

$$+ m_{TT}[\quad]_{\beta,N} - m_{nn}[\quad]_{\beta,T}$$

$$+ 2[m_{TN}m_{\beta N}m_{T\beta} - m_{TT}m_{\beta\beta}m_{nn}]\} \qquad (8.1.31)$$

and similar expression for Ω_T and Ω_N with the indices exchanged. The variance associated with β may be thought of as the implicit error in choosing a normalization point from noisy data.

Examining Equations (8.1.21) and (8.1.27), it is readily apparent that two parameter fitting introduces greater variance since

$$1/m_{TT} \leq 1/[m_{TT} - \frac{m_{TN}^2}{m_{NN}}]. \qquad (8.1.32)$$

Indeed, if the RHS of (32) is negative, then convergence by linearization is not possible for the two variable case although one may always find a positive variance for one variable. The possible advantage of equal weighting is due to the fact the denominator are always positive and therefore convergence regimes may exist for one method that do not for the other.

In general b) is much superior to a) (33). Consider the simple case with

$$f_i(\theta) = \tau\theta_i$$

$$\Omega_i = \tau^2\theta_i^2 \tag{8.1.34}$$

and evaluate Ω_θ for equal and unequal with the result

$$\Omega_{\theta EQ} = \sum_i \theta_i^2$$

$$\Omega_{\theta UNEQ} = [\sum_i (1/\theta_i^2)]^{-1}. \tag{8.1.35}$$

Clearly for $\theta > 1$, $\Omega_{\theta UNEQ} < \Omega_{\theta EQ}$.

If one does not have a priori estimates of experimental error, a somewhat different approach is necessary. WHat one really knows is the goodness of fit or

$$S_{MIN} = \vec{V}_{MIN}^T \underline{W} \vec{V}, \tag{8.1.36}$$

and the estimated covariance may then be expressed as (32)

$$\underline{\Omega}_C = \frac{1}{n - r} \vec{V}^T \underline{W} \vec{V} \underline{M}. \tag{8.1.37}$$

8.2 Application to Experimental Error

From an experimentally observed CARS or SRS profile, the effective covariance matrix may be calculated. The Y variance associated with background noise may be written as

$$\Omega_{Y_i} = Y_{MAX}/(S/N) + (1 + \tau)Y_i + \Omega_{\alpha_i} \tag{8.2.1}$$

where Y_{MAX} is the normalized maximum; S/N is the signal to noise ratio, and τ is a coefficient introduced to reflect the laser power level uncertainty.

The meaning of signal-to-noise ratio needs more explicit definition; in an experimentally observed profile, N/S is the ratio of background noise to maximum observed signal. For example, if the background noise is observed at 10 counts/sec and Y_{MAX} at the rate of 1000 counts/sec, the S/N ratio is 100/1.

The variance associated with Y_i is the standard variance from a large N poisson or Gaussian distribution. The factor τ for a CARS experiment is typically 3×10^{-2} for a Stokes laser error of 1% and a pump laser error of 1% since τ_{CARS} varies as twice the pump error plus the Stokes error to reflect the $P_p^2 P_s$ signal dependence. With identical laser uncertainties, $\tau_{SRS} = 2 \times 10^{-2}$ demonstrating the $P_p P_s$ signal variation. Note that the terms represented by

$$\Omega_i = Y_{MAX}/(S/N) + (1 + \tau)Y_i \tag{8.2.2}$$

have the usual N count dependence. In a large N Poisson distribution, if Y_i is scaled by a factor of γ, Ω_i is also scaled by the same factor (32, 33). From Equations (8.1.27) and (8.1.28), the variance in the (T, N) variable will be scaled inversely to with the usual result in percentage of error if

$$ERR - T = (\Omega_{TT})^{\frac{1}{2}}/T, \tag{8.2.3}$$

then

$$ERR - T \simeq 1/\ \gamma \tag{8.2.4}$$

which demonstrates the usual $1/\ N$ reduction in error.

The remaining term in Equation (8.2.1) does not show the signal dependence. For the CARS and SRS profiles, the Ω_α term is included to account for the effects of uncertainty in the pressure broadening coefficients. If Ω_{α_J} is the mean square variance associated with the pressure broadening coefficient for the Jth rotational level in a vibrational manifold, then

$$\Omega_{i(\alpha)} = \sum_J \left(\frac{\partial f}{\partial \alpha_J}\right)^2 \Omega_{\alpha_J}. \tag{8.2.5}$$

From the closed form expressions for the CARS profile, the derivatives may be evaluated as

$$\frac{\partial S_\ell}{\partial \alpha_J} = \overline{\beta} Y_J)_\alpha \{ 2X_{NR} X_\ell \overline{K}_J \ \mathrm{Im}\ \overline{W}_{JL}$$

$$+ X\ell^2 \overline{K}_J^2 \ \sqrt{\pi}\ \frac{\mathrm{Re}\ \overline{W}_{JL}}{\overline{Y}_J} (\mathrm{Re}\ \overline{W}_{JL})_{YJ} / \mathrm{Re}\ \overline{W}_{JL} - \frac{1}{\overline{Y}_J})$$

$$+ 2X\ell^2 \overline{K}_J \ \sqrt{\pi}\ \mathrm{Im}\ \overline{W}_{JL}) Y_J\ ZKM(J)$$

$$+ 2X\ell^2 \overline{K}_J \ \sqrt{\pi}\ \mathrm{Re}\ \overline{W}_{JL}) Y_J\ ZKC(J) + \varepsilon \} \tag{8.2.6}$$

where the ε term represents the ignorable contribution of the $\vec{z})Y_J$ derivatives.

$Y_J)_\alpha$ may be found from Equation (4.1.2) as

$$Y_J)_\alpha = \frac{1}{2zl}\{N(1 + \varepsilon\ell n2) + \frac{\beta\ell n(1 + \varepsilon\ell n2)^2}{\beta\ell^2(1 + \varepsilon\ell n2)^2 + 4\beta_g^2}^{\frac{1}{2}}\} . \quad (8.2.7)$$

To examine the effects of γ, the scaling factor,

$$Y_J)_\alpha \simeq N/zl \quad (8.2.8)$$

with the result that

$$\Omega_{i(\alpha)} \simeq \Sigma(\frac{\partial S_\ell}{\partial \alpha_J})^2(N \ \Omega_{\alpha J}/zl)^2. \quad (8.2.9)$$

As one expects, as $N \to 0$, $\Omega_{i(\alpha)} \to 0$ which physically implies the non-collisional error is determined by Ω' and scaled as $1/\sqrt{N}$.

However, if S_ℓ is scaled by a factor γ, $\Omega_{i(\alpha)}$ is scaled by a factor of γ^2 which implies that the error in fitting (T, N) in the case where $\Omega_{i(\alpha)}$ dominates is constant regardless of count rate. Thus, unless one operates in low densities such that $\beta_\ell << \beta_g$, there is an implicit error due to the mean square error in the pressure broadening coefficients.

CHAPTER 9

ERROR ANALYSIS

9.1 Explanation of Error Tables

To facilitate reader comprehension, an explanation of the error tables is in order. The terminology CARS (T, N) indicates that the profile height was considered a function of (T, N) simultaneously; i.e., both number density and temperature are considered to be unknown. The terminology CARS (T), (N) indicates that the profile height is either a function of (T) or a function of (N); one is measuring a single variable. The same variable terminology applies to SRS.

The β factor refers to the 10^3 counts normalized peak intensity. The peak counts were calculated on a 1 watt pump, 100 mw Stokes laser basis and the collection times were assumed to be such that one counts 10^3 events in the peak channel.

For the case where one does not consider linewidth uncertainties, errors must be scaled by $\beta^{-\frac{1}{2}}$. Thus, taking an error value from the table, if $\beta = 100$, the actual error would be 1/10 of the tabular value. For a particular linewidth parameter, errors for two different (N) values should be scaled by $(\beta_1/\beta_2)^{-\frac{1}{2}}$.

The term S/N indicates signal-to-noise ratio which is defined as the ratio of the peak counts to the background level. A S/N of 10 with a normalized maximum of 1000 counts would imply a background variance of 100 counts.

The letter "N" represents number density in amagats.

Additionally, all the error values were based on a 200 data point, 5 cm^{-1} scan range in the profile.

9.2 Count Rate Versus Number Density

Although CARS and SRS have been mentioned in the literature (2, 10) as non-linear optical processes with respective N^2 and N density dependences, this is not precisely the case. The β factors in the error tables are directly related to the number density dependence since under a given set of pump and Stokes laser conditions, the maximum count/sec varies as does β. Remembering that β is the normalizing factor and that S1, T1 MAX = 10^3 counts/sec illustrates this fact.

In the case of pure N_2, examining the β values in Tables 1, 2, 3 demonstrates the fact for certain experimental regimes, CARS does not show an N^2 dependence. In the asymptotic case,

$$PEAK_{CARS} \simeq N^2/\Gamma_p^2 \qquad (9.2.1)$$

which by inserting the pressure broadened linewidth becomes

$$PEAK_{CARS} \simeq N^2/(a + bN)^2. \qquad (9.2.2)$$

Clearly in the regimes where $bN >> a$, the peak value is relatively independent of the number density.

For SRS, Equation (9.2.3) is

$$PEAK_{SRS} \simeq N/(a + bN) \qquad (9.2.3)$$

with essentially the same result as demonstrated in Tables 7, 8, 9; i.e., if bN >> a, the N^2 and N dependencies of CARS and SRS are not correct.

For the intermediate regions, a ≃ bN, one sees a mixed dependence not easily typified. However, examining the β values for the smaller values of N, the usual N^2, N dependencies are quite correct. This is as one would expect for a >> bN. Note additionally that at which number density the N^2, N dependencies occur depends also on the temperature as is expected from the mixed $T^{\frac{1}{2}}$ and $T^{-\frac{1}{2}}$ variation of the total linewidth from Chapter 4.

The case of CO as a trace constituent is quite different. Making the physically reasonable assymption that foreign gas broadening will vastly predominate for relative number densities of 1:100 and less, the total linewidth is quite independent of the trace constituent number density.

Thus, SRS will demonstrate a strict N signal dependence. Equation (9.2.3) becomes for the mixture trace,

$$PEAK_{SRS} \simeq N/b' \qquad (9.2.4)$$

from which arises the strict N dependence.

For non-asymptotic regimes, it is much more difficult to qualitize the CARS number dependence. Writing the CARS dependence, one has

$$PEAK_{CARS} \simeq X_{NR}^2 + k_1 X_{NR} N + k_2 N^2 \qquad (9.2.5)$$

where k_1 and k_2 are constants. If one measures the total received signal less the background signal proportional to X_{NR}^2, there are three distinct experimental regimes:

(1) N^2 predominates

(2) mixed N^2, N

(3) N predominate.

This is best demonstrated by examining the β factors in Tables 13, 14, 15. In the asymptotic region (3), Equation (9.2.5) becomes

$$PEAK_{CARS} \simeq X_{NR}^2 + k_1 X_{NR} N \qquad (9.2.6)$$

which would imply a N signal level dependence if one subtracts the large background. Tables 21 and 22 so illustrate.

As a concluding note, the presence of values of number density for which the signal level does not vary appreciably may actually increase the uncertainties in the measurement of number density if one includes the actual received signal ala Equations (9.2.2) and (9.2.3). If this does occur, strict profile matching which normalizes the N^2, N dependencies will increase

the value of the (N) derivative. Since the derivative is proportional to the inverse of the derivative squared, the larger normalized derivative will decrease the measurement error. Conversely, in Doppler-dominated regions, one must include the N^2, N dependence to maximize the value of the (N) derivative.

9.3 Effects of the z1 Parameter

To examine the utility of both narrow and broad laser sources or more accurately, asymptotic or non-asymptotic in regards to the complex error function, (N, T) errors were calculated in N_2 as an instructive case. The z1, z2, z3 parameters of 2×10^{-3}, 2×10^{-2}, 2×10^{-1} are the same as those used in generating the theoretical profiles discussed in Chapter 4. Since widely different power levels may be associated with each linewidth, absolute error values were not determined.

Examining Tables 1, 2, 3 there are two distinct ranges for the β factors. In the N^2 regions, one is in a Doppler-dominated regime and the absolute errors neglecting scaling are identical. This is as one would expect because only the peak count rate is affected by (N); the spectral profile is then essentially a function of (T).

This statement may be visually confirmed for Figures 29-32 which are scaled error data for the z1 values of 0.050 and 0.010 cm^{-1} as represented by the experimental CARS apparatus of Moya

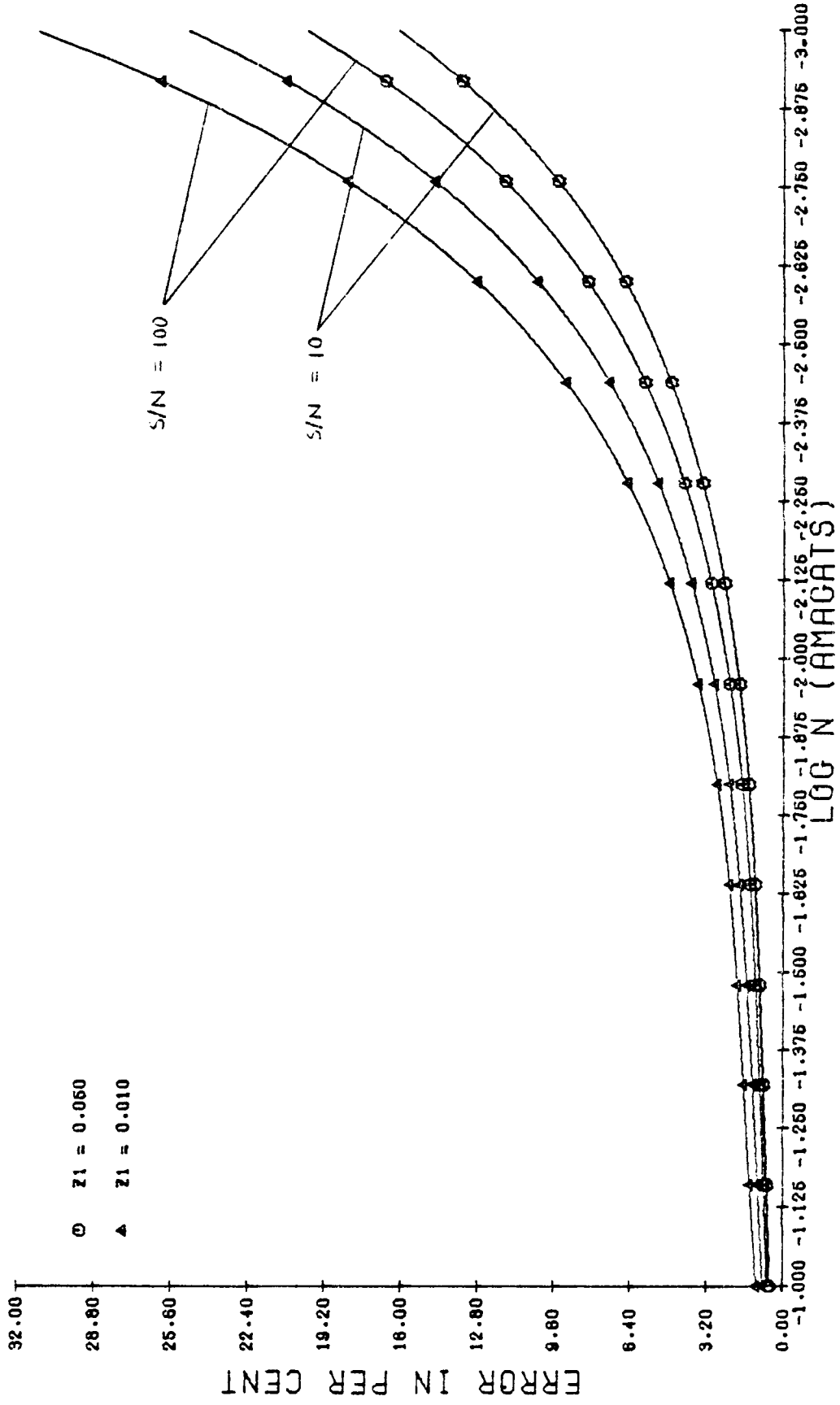

FIGURE 29. CARS (N,T) ERROR IN (N) AT 100°K

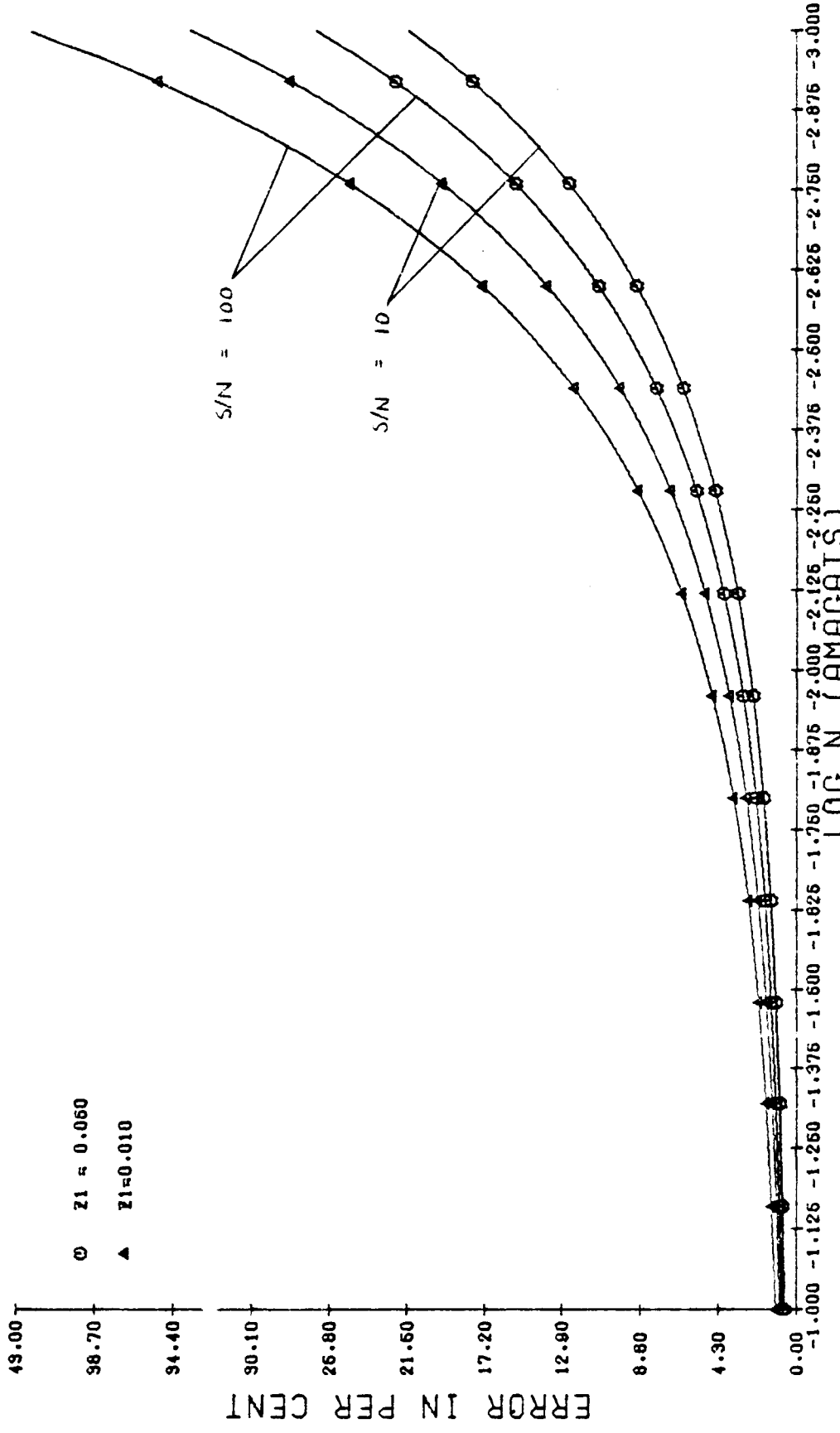

FIGURE 30. CARS (N,T) ERROR IN (T) AT 100°K

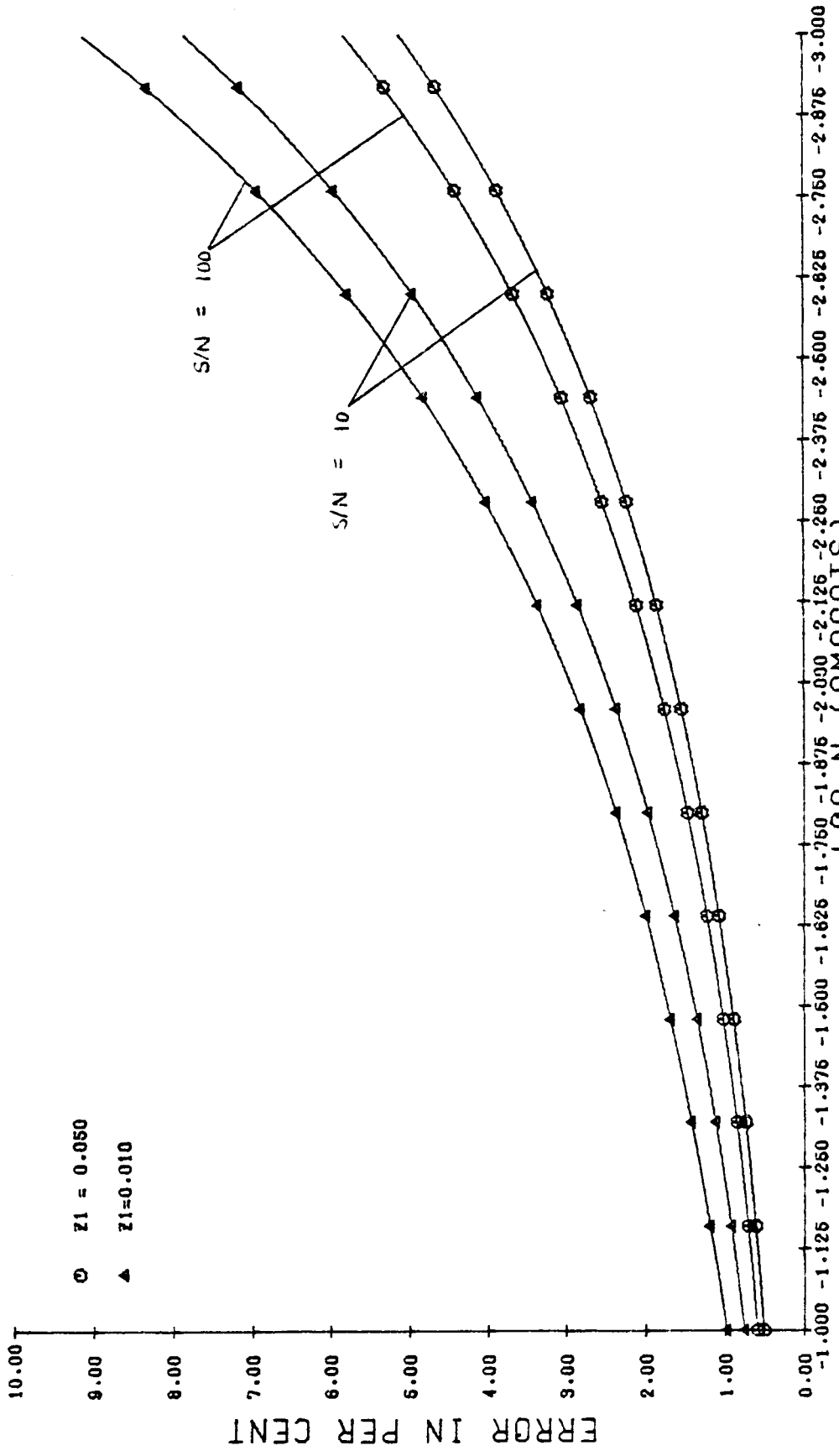

FIGURE 31. SRS (N,T) ERROR IN (N) AT 100°K

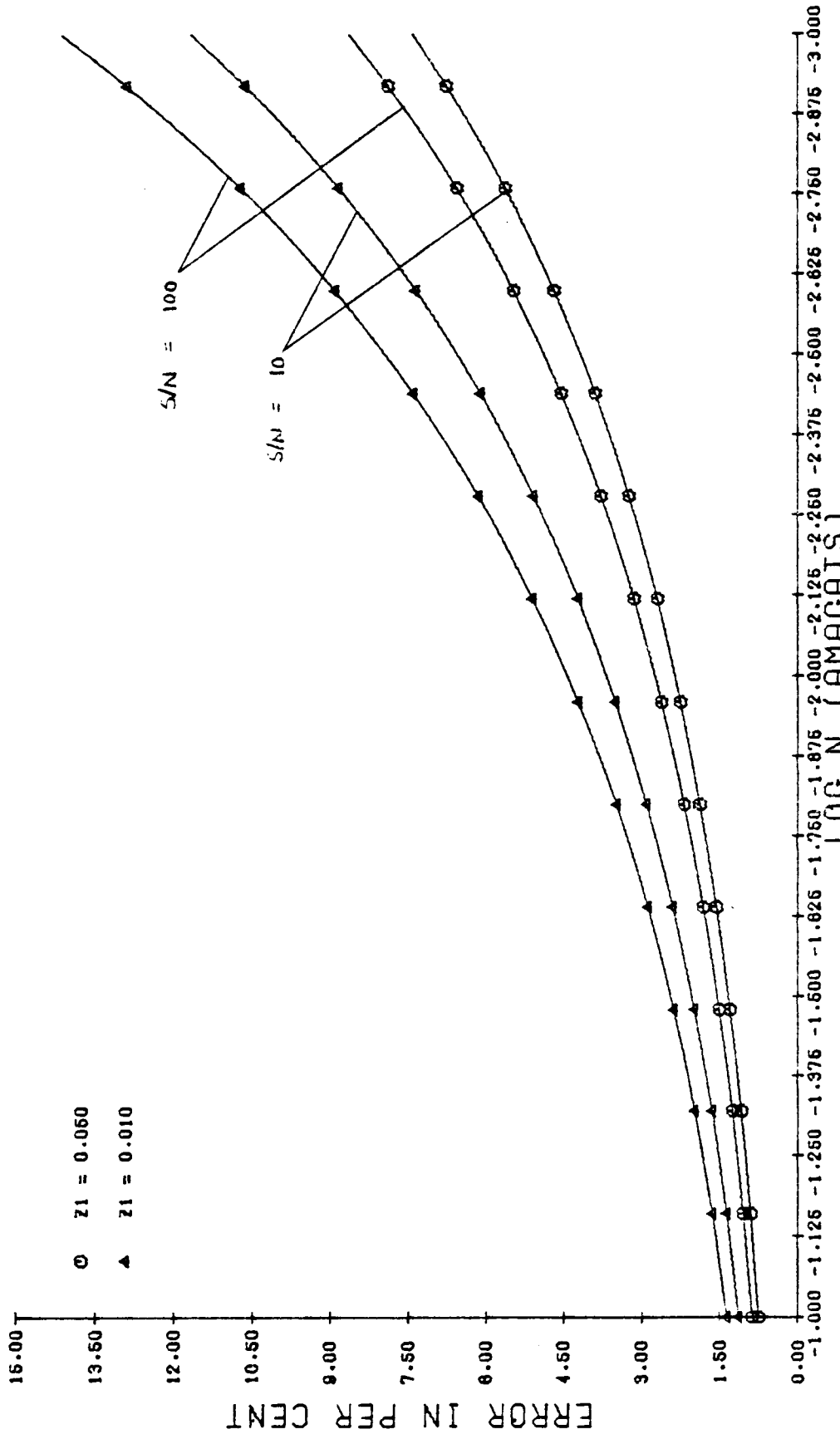

FIGURE 32. SRS (N,T) ERROR IN (T) AT 100°K

and Nitsch. Close scrutiny will reveal the 1/N and $1/N^{\frac{1}{2}}$ asymptotic regimes which correspond to N^2, N signal dependence for CARS and SRS, respectively. Errors are simultaneous (N, T) type.

For the pictorial data, it is clear that the higher zl value of 0.050 cm^{-1} has less implicit error and additionally is less influenced by a higher S/ ratio. This is true for both CARS and SRS. Note that the zl = 0.050 case is non symptotic and the zl = 0.010 is asymptotic ($\Gamma/zl >> 1$) as shown visually in the representative profiles in Figures 33, 34.

One may question these conclusions in other regimes. Considering CARS (T, N) the last row of Tables 1, 2, 3 quite agree with the graphs of Figs. 29 and 30. The higher z values not only possess less implicit error due to Gaussian noise but are also less effected by noisy conditions. This holds true for (T) and (N).

The same conclusion is true in separate (T) and (N) CARS measurement as evidenced by the last row of Tables 4, 5, 6. The higher values of zl are also less effected by Gaussian and detector noise in the SRS process. The 1/N signal region asymptotic error values or again the last row of Tables 7-12 which displays (T, N) and (T), (N) error data.

This conclusion may seem quite surprising; at first consideration, one might expect the higher zl-broader profiles to have a smaller (N) derivative due to the masking influence of an

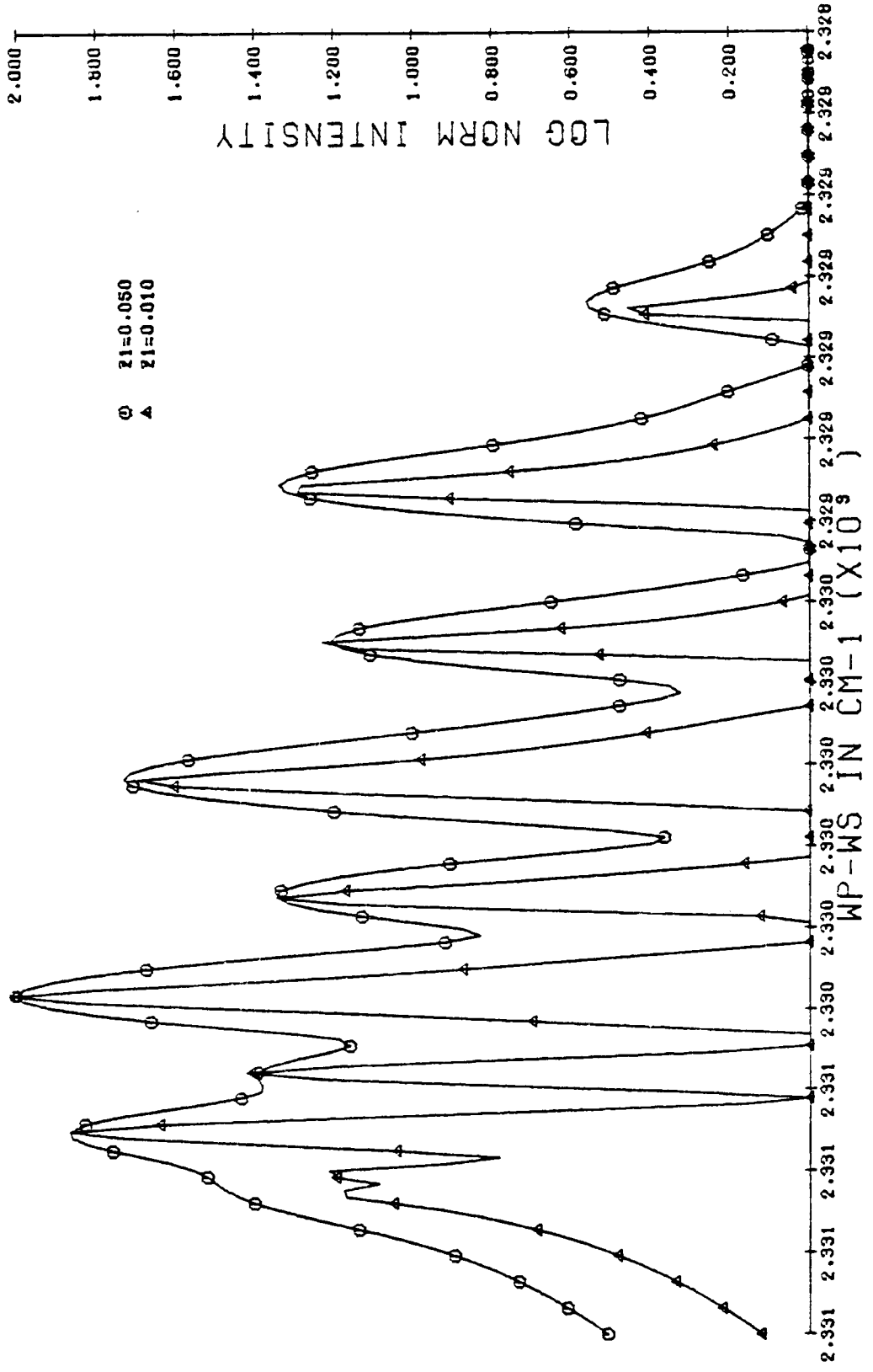

FIGURE 33. CARS 100°K, 0.1 AMAGAT PROFILE

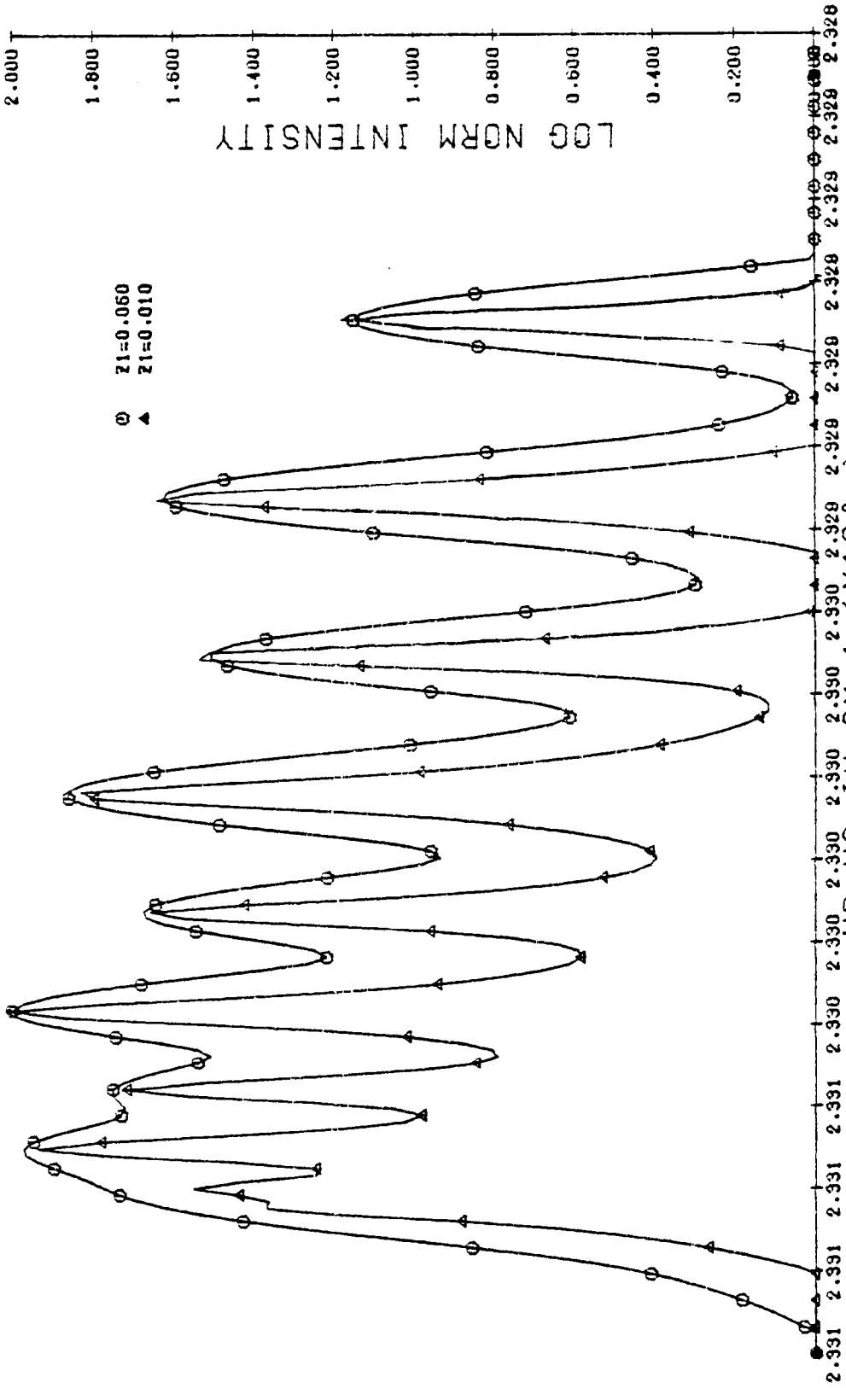

FIGURE 34. SRS 100°K, 0.1 AMAGAT PROFILE

effective laser linewidth comparable to the Raman linewidths. However, in the asymptotic regions, the major contribution to the Raman linewidth is Doppler. Since the (N) derivative is then only determined by received signal, the normalized (N) derivatives are essentially equivalent.

In the regions where the linewidth is of the same form [a(T) + b(T)N], but N is not ignorable, the signal dependence is not of the N^2, N type. For areas in which the collisional broadening is significant, the (N) and (T) derivative will be decidedly different from the Doppler regime values. These regions are characterized by (T, N) values of (60°K, N > 2 x 10^{-4}), (300°K, N > 10^{-3}) and (1200°K, N > 10^{-2}). If one assymes that the pump powers are scaled by a ratio of at least 1.7:1.1:1 for zl = 0.200, 0.020, 0.002 cm^{-1}, in even the simultaneous (N, T) case, the zl = 0.200 cm^{-1} case has less implicit error in CARS as inspection of Tables 1-6 will indicate. Equal power levels are enough to demonstrat the superiority of the highest zl value in SRS in Tables 7-12.

As a verification of the regression analysis, note that in all cases in Tables 1-12, the error is less in (T), (N) measurement than (T, N) measurement, in agreement with Equation 8.1.32. At least for the case of pure gases, the higher z values assuming that linewidth uncertainties are ignorable for the moment, offer true experimental advantage. For Doppler dominated (T, N) regimes,

linewidth uncertainties are indeed ignorable; in these regions, the $1/\beta$ scaling is an accurate estimate and the higher zl values are quite clearly advantageous for either (T, N) or (T), (N) measurements.

To first appearances, this statement seemingly contradicts the visual evidence from the spectral profiles. However, note that the total counts are much higher in the $zl = 2 \times 10^{-1}$ case than for either value $zl = 2 \times 10^{-2}$, 2×10^{-3}. Since one readily scales errors as $1/\sqrt{N_{TOTAL}}$ if Ω_α is ignorable, z3 errors should be somewhat less if the (T, N) derivatives are not too different.

In further support of the z3 advantage, visual examination of these graphs clearly indicates that the $zl = 2 \times 10^{-1}$, 2×10^{-2}, 2×10^{-3} parameters have successively greater contributions from the higher frequency Fourier components. The effect of noisy data is to introduce error in the measurement of indeed these higher frequency components; therefore, the more peaked profiles or lower zl valued profiles will be more susceptible to measurement error introduced by noise. Tables 1-12 for the S/N values of 1, 10, 100 demonstrate that this statement is correct for both one and two variable fitting procedures.

A somewhat more mathematical description is to assume one is fitting a profile similar to ℓ^{-x^2/D^2} from x = 0 to XF. D in this case is essentially proportional to $1/Y_J$ where Y_J is the dimensionless factor Γ_J/zl. Physically, a large value of D will give a broader profile. One may immediately write

$$\frac{\partial}{\partial D} \ell^{-x^2/D^2} = \frac{2x^2}{D^2} \ell^{-x^2/D^2} \tag{9.3.1}$$

with the result that

$$\Omega_{DD} = D[4 \int_0^{x_f/D} (\frac{x}{D})^4 \ell^{-2x^2/D^2} d(\frac{x}{D})]^{-1}. \tag{9.3.2}$$

Assuming that $X_f/D >> 1$, the integral is a constant, and Equation (9.3.2) then defines an error in measuring D given by

$$ERR - D/D = (\Omega_{DD})^{\frac{1}{2}}/D \simeq D^{-\frac{1}{2}} \simeq Y^{\frac{1}{2}}. \tag{9.3.3}$$

Since measuring either one or two parameters of which Y_J is an explicit function is tantamount to measuring D, clearly the higher D values have less intrinsic errors in a parameter measurement by a fitting technique. This rather simple argument further reinforces the contention that the higher zl values are relatively better in an (T, N) measurement.

Considering the mixture CO in N_2, the influence of the zl linewidth parameter will be essentially the same since X_{NR} does not affect the SRS spectral profile. Again the z2 and z3 errors are much the same if one includes the $(\beta P_p)^{\frac{1}{2}}$ scaling factor; the zl high resolution error is much worse after scaling for all S/N ratios. As for the pure gas case, the z3 low resolution error is less affected by decreasing the S/N ratio. Tables 13 and 14

for (T) values of 60°K, 300°K, 1200°K present the unscaled SRS error data.

Only one number density of 10^{-2} was included in the experimental regimes since the fitting procedure was calculated with the postulate that for relative number densities CO/N_2 of 10^{-2} or less, the dominating Raman linewidths are due to foreign gas collisions. With the further assumption that the number density of the major constituent is constant, the Raman linewidths will vary only with temperature; this functional dependence is estimated by a $T^{-\frac{1}{2}}$ dependence of the collisional linewidth and a $T^{\frac{1}{2}}$ dependence for the Doppler linewidth. For the stated set of conditions, SRS will exhibit a strict N dependent signal level variation and the β factor will so vary.

The CARS process errors differed primarily from those associated with SRS due to the instability of a non-linear fitting technique in regimes where the X^2_{NR} term predominates. The CARS error data in Tables 15-22 were calculated with the same assumptions as the preceding paragraph.

In the low N regimes where one can not fit the CARS profile, the contributting factor is the large background signal due to X_{NR}, the non-resonant susceptibility. Since one is fitting a large constant signal with a relatively small added modulated signal, the background considerably enlarges the total variances Ω'.

The β factors in Tables 15-17 are for total signal level. In actually fitting a mixture CARS profile, one would subtract

the non-resonant background signal. However, the variance so associated must be included in error calculations. To demonstrate the low signal level N dependence, on must subtract the constant level of $(.11 \times 10^{-5})$ from the relevant total β values. Scaling the raw error data by the factor $[(\beta - \beta_{MIN})P_p^2]$ is necessary to compare error data; the inevitable result is to again demonstrate the slight advantage of z3 with respect to z2, both of which are much superior to z1.

It is quite clear from Tables 15-20 that for the trace constituent, CARS is severely limited in simultaneous (T, N) measurement as well as (T) measurement. This fact is not really as damaging as one might expect; the major constituent can certainly be used as a medium from which one may extract the necessary temperature data. Examining only the (N) errors in Tables 18-20 for z1, z2, z3 these errors will approach in the N varying regions the corresponding values .17, .16, and .16 for S/N = 1. Since one must additionally scale for power levels, z3 is again quite superior. However, one can still make a density determination with the presence of a large background signal if enough power is available or one collects data under low enough noise conditions for a greater period of time.

For conditions where the S/N ratio demonstrates an appreciable noise content in the data, the z3 case offers the least error irregardless of the effect of the non-resonant susceptibility. Both the CARS and SRS processes may be used more advantageously

with a broader zl parameter for the measurement of temperature and/or number density. However, in the case of mixtures where the N signal dependence dominates for CARS and SRS, SRS is clearly much superior as a measurement technique.

9.4 Influence of X_{NR}

From the previous section, the reduction of the non-resonant susceptibility would appear to offer certain advantages. Using the polarization technique as mentioned in Chapter 2.3, it is certainly possible to reduce X_{NR} by a factor of 10^2. Assuming that such is the case, the raw errors were calculated for a CO/N^2 mixture for a typical zl parameter as in the Moya experiments of 0.050; the two X_{NR} values were 10^{-18} cm^3/erg and 10^{-20} cm^3/erg. The unscaled results are displayed in Tables 21 and 22. The values indicated are actually $(\beta - \beta_{MIN})$ in accordance with the fitting technique of subtracting the background contribution of X_{NR}^2.

The reduced X_{NR} case is much superior from $N = 10^{-2}$ to the unstable region in Table 21. For simultaneous measurement of (T, N), reduction of X_{NR} greatly lessens the implicit error regardless of the relative contribution of the N and N^2 terms as defined in section 2. From the reduced X_{NR} column in Table 21 the change from the N^2 to the N region may be seen.

This result is as one would expect; reduction of X_{NR} in the simultaneous measurement extends the experimental regions in

which one may actually fit profiles since the ratio of signal to Gaussian noise is improved. Reduction of X_{NR} may be considered to be a change from a mixture to a pure gas case in which the N^2 signal dependence dominates. One would indeed expect a significant improvement in (T, N) fitting by reducing X_{NR}.

Considering profiles as a one parameter function, the reduced X_{NR} case offers a clear advantage in determining (T) as can be seen from Table 22. Additionally, the regimes in which it is possible to measure (T) are extended. However, if one is only interested in a trace gas number density measurement, the use of polarization CARS does not improve the error. The convergence limit in each case is .16, .12, .111 for S/N ratios of 1, 10, 100 from Table 22.

Strangely enough, this is not in contrast with what one should expect. Ignoring the effects of laser linewidths and considering only a single resonance,

$$S_{CARS} = K_0(X_{NR}^2 + 2N\bar{X}'X_{NR} + N^2\bar{X}^2) \tag{9.4.1}$$

where K_0 is the normalizing factor and $\bar{X}$ the unit susceptibility (cm^6/erg). In the regime for which

$$N\bar{X}'X_{NR} >> \bar{X}'', \tag{9.4.2}$$

$$S_{CARS} \simeq K_0(X_{NR}^2 + 2N\bar{X}'X_{NR}). \tag{9.4.3}$$

The (N) derivative is

$$\frac{\partial S}{\partial N} = 2K_0 \bar{X}' X_{NR}, \tag{9.4.4}$$

and

$$\Omega_{NN} = [(\frac{\partial S}{\partial N})^2/\Omega_s]^{-1} \tag{9.4.5a}$$

$$\Omega_{NN} = (4K_0 \bar{X}'^2)^{-1}. \tag{9.4.5b}$$

The error in (N) measurement is

$$(\Omega_{NN})^{\frac{1}{2}}/N = 1/(2N\bar{X}' \sqrt{K_0}). \tag{9.4.6}$$

Thus the (N) error is independent of X_{NR} so long as the $\bar{X}'$ term dominates.

This same sort of analysis may be carried out for polarization CARS. In N_2, polarization reduces the peak values of X" by ½ with the result

$$S_{pCARS} \simeq K_0 \tfrac{1}{4} N^2 \bar{X}''^2. \tag{9.4.7}$$

The factor of ½ is roughly the same for all diatomic gases. Thus, the (N) error is

$$(\Omega'_{NN})^{\frac{1}{2}}/N = 1/(N\bar{X}''\sqrt{K_0}). \tag{9.4.8}$$

Remembering that the normalized form for $\bar{X}^{(3)}$ in terms of the laser difference frequency is

$$\bar{X} \simeq \frac{1}{\Gamma}\frac{X + i}{X^2 + 1}, \tag{9.4.9}$$

then $\bar{X}'_{MAX} = \frac{1}{2}\bar{X}''_{MAX}$ and the (N) error is essentially equal. If one considers multiple resonances, the difference frequency may be so selected that X_i, X_j have the same sign and

$$\bar{X}'_{MAX} > \tfrac{1}{2}\bar{X}''_{MAX}.$$

Hence the (N) error may be increased by PCARS.

The real utility of PCARS lies in reducing the dynamic range of the system which must be weighed against additional experimental complexities.

9.5 Effects of Linewidth Uncertainities

The preceding error calculations were based on the assumption that the imprecisions in measurement of the pressure broadening coefficients were ignorable in calculating functional variances. In considering the detection of a trace constituent, this is a valid assumption if one actually measures the relevant linewidths.

This assumption is also valid for experimental regimes in which Doppler broadening is the dominating factor in determining the Raman linewidth. However, for the pure gas case where collisional broadening is a significant factor, the uncertainties in the pressure broadening coefficients as shown in Table 24.

Including the effect of these uncertainties increases the variance from Ω' to Ω_α where Ω is defined as in (8.2.9). Since Ω_α is constant regardless of the scale factor β, the measurement precision is limited by this component of variance for regions where it is indeed significant. At T = 300°K, error data were calcualted for the low resolution (Moya) and the high resolution (Nitsch) cases with zl values of 0.050 and 0.010 cm^{-1}, respectively. As one can see from Tables 25, 26 the inclusion of Ω_α is only significant for (T = 300°K, $N > 10^{-3}$).

For the N = 1.0 regime, in partial contradiction of the masking argument advanced in 3.1 as to peak height errors, the (T, N) error with no assumptions as to β is very close for the zl = 0.010 and zl = 0.050 cases. The (T), (N) errors are also essentially equal; however, if one assumes a pump power ratio of 2.2 for the two cases, the greater zl will be superior. In the other N regions, the larger zl value will be clearly superior and the masking hypothesis is more obviously demonstrable.

The SRS process is treated similarly in Table 27, 28. The zl = 0.050 case is demonstrably superior in each of the regimes

from N = 1 to 10^{-3} after which the errors are scaled as the number density. Since according to section 3.2, the SRS process should indeed mask the linewidths errors more than CARS for equal values of zl, this conclusion is consistent with the masking hypothesis.

Including the effects of Ω_α does not change the greater inherent measurement accuracy in two versus one parameter fitting. However, in the collisionally broadened and mixed broadened regimes, the inherent accuracy of either CARS or SRS is limited by the precision in determining the variation of the Raman linewidth as a function of the species number density.

For comparable S/N ratios, SRS is less effected by Ω_α as can be seen by comparing Tables 25, 26 and 27, 28 for values of N = 1, 10^{-1}. This is true for both zl linewidths. The $1/\Gamma$ dependence of SRS is indeed less affected by errors than the $1/\Gamma^2$ dependence of CARS. However, in the well known linewidth regimes ($\Omega_\alpha \simeq 0$), for the same peak count rate, SRS has more (T, N) and (T), (N) parameter errors than does CARS. The actual utility of either technique depends on the given experimental regime and the expected count rate.

9.6 CARS Versus SRS

CARS and SRS are both non-linear optical techniques explicitly dependent on the Raman transition linewidth. Since this transition linewidth is in itself a function of number density and temperature, the effect of number density and temperature must be

considered not only in the β factors and population difference, but also in the Raman linewidths. The differing functional dependences are responsible for the somewhat different values of error in (T, N) regimes.

For CW experimentation, SRS is vastly superior to CARS due to the respective relative detected signal intensities of 10^6 for pump power of 1 watt and Stokes power of 100 mw. Since SRS has less intrinsic error than CARS due to Raman linewidth uncertainties and since the Ω' errors are scaled relative to $1/\sqrt{N}$, SRS is a much superior technique even for the pure gas case if one is operating under identical S/N ratios.

If one considers mixtures, SRS has the distinct advantage that it is not susceptible to high background variances due to a large non-resonant susceptibility.

However, typical S/N ratios for CARS and SRS are not equal for identical Stokes and pump lasers, CARS may employ both spatial and electronic filtering to reduce background noise. Since the SRS signal is a modulation of the Stokes beam, one necessarily must modulate the pump laser and electronically detect the SRS signal. If one compares the SRS and CARS processes for respective S/N ratios of 1 and 10 to reflect the filtering advantage inherent in CARS, SRS and CARS are approximately equal in the regimes where collisional broadening uncertainties are significant.

In areas where one may ignore collisional broadening, SRS has more error for (T, N) and (T), (N) measurement than does CARS

if the maximum count rates are equal. However, this stipulation is difficult to physically justify for CW lasers. Owyoung and Ezekial have obtained N_2 and O_2 SRS atmospheric data with relatively low power sources; to date, only Hirsch has generated CW CARS data and intracavity operation was necessary.

In terms of detection, the presence of the SRS Stokes beam background necessitates a detection system with a dynamic range of 10^4 to 10^5 (2). Although photosensitive diodes regularly achieve dynamic ranges of 10^6 in radiometers, P.M. tubes can normally achieve a dynamic range $\simeq 10^3$. Experimental differences other than the spatial filtering inherent in CARS do exist.

Although possible to use pulsed lasers on SRS, detection difficulties in electronic filtering indicate that CARS would be a better technique not only due to signal detection, but also since one may take advantage of higher pump powers up to a typical saturation level of 14 kw (4).

For temperature and/or number density measurement, the use of CW or pulsed lasers would indicate whether one should utilize the SRS or the CARS process. Additionally, for (T, N) measurement, if the laser modes are stockastically populated, the broader linewidths offer more noise immunity along with masking the effect of Raman linewidths uncertainties.

CHAPTER 10

CONCLUSIONS

The intention of this dissertation was to derive closed form expressions for the theoretical power in CARS and SRS for regimes in which the laser sources possess linewidths finite compared to the characteristic Raman transition linewidth.

The theoretical and experimental spectral profiles were compared as a method of determining the utility of the expressions outside of the two-order-of-magnitude improvement in CPU time.

From the convolution expressions, the technique of multivariate non-linear regression analysis was applied to determine realistic errors for regimes of (N, T) of experimental interest using N_2 and CO as representative molecules.

In pursuing the general purposes of this dissertation, a normalization technique for microsecond measurement of Lorentzian linewidths in SRS was developed as a possible means of reducing linewidths influences in (N, T) measurement by ratioing.

Additionally, the subject of non-linear errors was extensively investigated by the use of regression analysis. From such analysis, laser linewidths greater than or equal to the transition linewidth were demonstrated to be beneficial in reducing Gaussian noise, detector noise, and the implicit errors due to measurement inaccuracies in the (T, N) dependence of the transition.

As an addendum, polarization CARS was considered with the result that in detecting trace constituents, the real advantage lies in reduction of detector dynamic range.

LIST OF REFERENCES

1. Tolles, W. M., Turner, R. D., Applied Spectroscopy, Volume 31, No. 2 (1977).

2. Owyoung, A., ERDA, Sand-77-0005 (1977).

3. Shaub, W. M., Nibler, J. W., Harvey, A. B., J. Chem. Phys., Volume 67, No. 5 (1977).

4. Ecbreth, A. C., Bonizyk, P. A., Shirley, J. A., EPA-600/7-78-104 (1978).

5. Moya, F., ESA TT-331 (1976).

6. Owyoung, A., Jones, E. D., Optical Letters, Volume 1 (1977).

7. Owyoung, A., Opt. Commun., Volume 22 (1977).

8. Private Communication from S. Ezekiel.

9. Dewitt, R. W., Harvey, A. B., Tolles, W. M., NRL Memorandum Report 3260 (1976).

10. Nibler, J., "Coherent Anti-Stokes Raman Spectroscopy," Raman Spectroscopy of Gases and Liquids, ed. by A. Weber (Springer, New York, 1979).

11. Tolles, W. M., Nibler, J., Mcdonald, J. R., Harvey, A. B., Applied Spectroscopy, Volume 31, No. 4 (1977).

12. Shen, Y. R., "Stimulated Raman Scattering," Light Scattering in Solids, ed. by M. Cardona (Springer, New York, 1975).

13. Bloembergen, N., Nonlinear Optics, 3rd edition (W. A. Benjamin, New York, 1977).

14. Andersen, H. S., Hudson, B. S., "The Raman Effect," in Molecular Spectroscopy, ed. by D. A. Long, Volume 5 (Chemical Society, New York, 1975).

15. Flytzanis, C., "Third-Order Susceptibilities," in Quantum Electronics: A Treatise, ed. by H. Rabin (Academic Press, New York, 1969).

16. Perlussi, J. H., Vanderwood, P. C., J. Quant. Spectros. Radiat. Transfer, Vol. 18 (1977).

17. Wang, C. S., "The Stimulated Raman Process," in Quantum Electronics: A Treatise, ed. by H. Rabin (Academic Press, New York, 1969).

18. Levenson, M. D., Bloembergen, N., Phys. Dev. B., Volume 10, No. 10 (1974).

19. Lotem, H., Lynch, R. T., Bloembergen, N., Phys. Rev. A., Volume 14, No. 5 (1974).

20. Yuratich, M. A., Hanna, D. C., Mol. Phys., Volume 33, No. 33 (1977).

21. Hall, R. J., Combustion and Flame, Volume 35, No. 1 (1979).

22. Stappaerts, C., IEEE J. Quant. Electronics, QE-12, Page 330 (1976).

23. Nitsch, W., Krefer, W., Opt. Commun., Volume 23, No. 2 (1977).

24. Henesian, M. A., Kuberskii, L., Byer, R. L., J. Chem. Phys., Volume 65, No. 12 (1975).

25. Abramowitz, M., Stegan, I. A., Handbook of Mathematical Functions, Chapter7 (NBS, Washington, 1972).

26. Kilekopf, J., J.O.S.A., Volume 63, No. 8 (1973).

27. Gray, C. G., Van Kranendonk, J., Can. J. Phys., Volume 4 (1966).

28. Song, J. J., Eesley, G. L., Levenson, M. D., Applied. Phys. Lett., Volume 29, No. 9 (1976).

29. Byrne, G. D., Hall, C. A., Numerical Solutions of System of Non-linear Algebraic Equations, Chapter 5 (Academic Press, London, 1975).

30. Drayson, S. R., J. Quant. Spectrosc. Radiat. Transfer, Volume 16 (1976).

31. Hui, A. K., Armstrong, B. H., Wray, A. A., J. Quant. Spectrosc. Radiat. Transfer, Volume 19 (1978).

32. Meyer, S. L., Data Analysis for Scientists and Engineers, Chapter 33 (Wiley and Sons, Inc., 1975).

33. Saleh, B., Photoelectron Statistics, Chapters 1 and 2 (Springer-Verlaag, New York, 1978).

34. Private communication from W. H. Fletcher.

35. Hirth, A., Vollratii, K., Optics Communications, Volume 18 (1976).

36. Private communication from M. A. Henesian.

37. Fenner, W. R., Hyatt, H. A., J.O.S.A., Volume 63 (1973).

38. Herzberg, G., Spectra of Diatomic Molecules, pages 502-581 (D. Van Nostrand Co., Inc., New York, 1950).

APPENDIXES

APPENDIX A

TABLES

TABLE 1

N_2 ERROR - CARS (T, N), T = $60^{o}K$

ERRORS IN %

ERROR-T, ERROR-N

N	Z1=0.002	Z2=0.020	Z3=0.200
B,2 x 10^{-1}	(.88)	(.81)	(.38)
X/N=1	3.02, 1.91	2.97, 1.83	4.00, 1.85
10	1.66, 1.03	1.63, 1.00	1.93, 0.91
100	1.35, 0.84	1.33, 0.82	1.34, 0.68
B,2 x 10^{-2}	(.45)	(.14)	(.311 x 10^{-1})
S/N=1	7.01, 7.43	3.10, 2.60	2.62, 1.31
10	3.83, 3.66	1.76, 1.62	1.28, 0.75
100	2.96, 2.66	1.45, 1.37	0.90, 0.65
B,2 x 10^{-3}	(.35 x 10^{-1})	(.70 x 10^{-2})	(.14 x 10^{-2})
S/N=1	18.90,14.00	2.94, 2.72	2.48, 2.03
10	9.11, 6.81	1.72, 1.58	1.20, 0.97
100	6.17, 4.69	1.45, 1.33	0.85, 0.71
B,2 x 10^{-4}	(.47 x 10^{-3})	(.90 x 10^{-4})	(.18 x 10^{-4})
S/N=1	22.32,18.89	2.93, 2.84	2.46, 2.20
10	10.11, 8.57	1.72, 1.64	1.19, 1.05
100	6.61, 5.63	1.45, 1.38	0.84, 0.75
B,2 x 10^{-5}	(.49 x 10^{-5})	(.93 x 10^{-6})	(.18 x 10^{-6})
S/N=1	22.64,19.37	2.93, 2.84	2.46, 2.22
10	10.20, 8.73	1.72, 1.65	1.19, 1.05
100	6.65, 5.72	1.45, 1.38	0.84, 0.75
B,2 x 10^{-6}	(.49 x 10^{-7})	(.93 x 10^{-8})	(.18 x 10^{-8})
S/N=1	22.68,19.42	2.93, 2.84	2.46, 2.22
10	10.21, 8.75	1.72, 1.65	1.19, 1.05
100	6.65, 5.72	1.45, 1.38	0.84, 0.75

TABLE 2

N_2 ERROR - CARS (T, N), T = 300°K

ERRORS IN %

ERROR-T, ERROR-N

N	Z1=0.002	Z2=0.020	Z3=0.200
B,1.0	(1.09)	(1.05)	(.77)
S/N=1	1.11, 0.79	1.10, 0.77	1.84, 0.98
10	0.64, 0.46	0.63, 0.45	1.04, 0.56
100	0.54, 0.39	0.54, 0.39	0.90, 0.49
$B,10^{-1}$	(.70)	(.32)	$(.52 \times 10^{-1})$
S/N=1	2.81, 3.14	1.90, 1.71	0.94, 0.63
10	1.68, 1.64	1.08, 1.03	0.56, 0.39
100	1.37, 1.23	0.89, 0.84	0.50, 0.35
$B,10^{-2}$	$(.58 \times 10^{-1})$	$(.16 \times 10^{-1})$	$(.22 \times 10^{-2})$
S/N=1	3.19, 3.54	2.11, 1.91	1.01, 0.93
10	2.03, 2.16	1.23, 1.11	0.58, 0.51
100	1.71, 1.79	1.03, 0.93	0.48, 0.42
$B,10^{-3}$	$(.81 \times 10^{-3})$	$(.22 \times 10^{-3})$	$(.30 \times 10^{-4})$
S/N=1	3.31, 3.94	2.21, 2.14	1.06, 1.04
10	2.08, 2.41	1.26, 1.22	0.59, 0.56
100	1.75, 1.98	1.06, 1.01	0.49, 0.46
$B,10^{-4}$	$(.84 \times 10^{-5})$	$(.23 \times 10^{-5})$	$(.31 \times 10^{-6})$
S/N=1	3.33, 3.98	2.22, 2.17	1.06, 1.05
10	2.09, 2.41	1.27, 1.23	0.59, 0.57
100	1.75, 2.00	1.06, 1.02	0.49, 0.46
$B,10^{-5}$	$(.85 \times 10^{-7})$	$(.23 \times 10^{-7})$	$(.31 \times 10^{-8})$
S/N=1	3.33, 3.98	2.22, 2.17	1.06, 1.06
10	2.09, 2.41	1.27, 1.23	0.59, 0.57
100	1.75, 2.00	1.06, 1.02	0.49, 0.46

TABLE 3

N_2 ERROR - CARS (T, N), T = 1200°K

ERRORS IN %

ERROR-T, ERROR-N

N	Z1=0.002	Z2=0.020	Z3=0.200
B,1.0	(1.23)	(1.06)	(.26)
S/N=1	2.63, 4.26	2.99, 5.06	2.33, 3.49
10	1.57, 2.33	1.66, 2.56	1.41, 2.13
100	1.33, 1.86	1.37, 1.98	1.27, 1.92
$B,10^{-1}$	(.28)	(1.26)	$(.17 \times 10^{-1})$
S/N=1	4.51, 8.26	5.68, 8.92	2.56, 3.88
10	2.48, 4.25	3.02, 4.79	1.51, 2.32
100	2.04, 3.29	2.29, 3.60	1.31, 2.02
$B,10^{-2}$	$(.59 \times 10^{-2})$	$(.21 \times 10^{-2})$	$(.26 \times 10^{-3})$
S/N=1	6.85,12.11	6.16, 9.58	2.43, 3.71
10	3.32, 5.77	3.44, 5.42	1.46, 2.25
100	2.52, 4.23	2.67, 4.21	1.27, 1.96
$B,10^{-3}$	$(.63, \times 10^{-4})$	$(.22 \times 10^{-4})$	$(.27 \times 10^{-5})$
S/N=1	7.14,12.57	6.20, 9.64	2.42, 3.69
10	3.45, 5.96	3.49, 5.49	1.45, 2.24
100	2.59, 4.35	2.71, 4.28	1.27, 1.96
$B,10^{-4}$	$(.64 \times 10^{-6})$	$(.22 \times 10^{-6})$	$(.27 \times 10^{-7})$
S/N=1	7.18,12.63	6.20, 9.64	2.41, 3.69
10	3.45, 5.98	3.49, 5.49	1.45, 2.24
100	2.59, 4.36	2.72, 4.28	1.27, 1.95
$B,10^{-5}$	$(.64 \times 10^{-8})$	$(.22 \times 10^{-8})$	$(.27 \times 10^{-9})$
S/N=1	7.18,12.63	6.20, 9.65	2.42, 3.69
10	3.46, 5.98	3.49, 5.49	1.45, 2.23
100	2.59, 4.36	2.72, 4.28	1.26, 1.95

TABLE 4

N_2 ERROR - CARS (T), (N), T = 60°K

ERRORS IN %

ERROR-T, ERROR-N

N	Z1=0.002	Z2=0.020	Z3=0.200
2×10^{-1}			
S/N=1	1.87, 1.28	1.78, 1.20	1.26, 0.69
10	1.11, 0.72	1.08, 0.70	0.88, 0.46
100	0.96, 0.60	0.94, 0.59	0.82, 0.42
2×10^{-2}			
S/N=1	6.47, 6.92	2.96, 2.50	1.47, 0.99
10	3.81, 3.65	1.70, 1.59	0.90, 0.67
100	2.92, 2.62	1.41, 1.34	0.79, 0.62
2×10^{-3}			
S/N=1	3.62, 2.43	1.61, 1.49	0.70, 0.61
10	2.37, 1.71	1.07, 0.98	0.49, 0.42
100	2.09, 1.58	0.96, 0.88	0.46, 0.39
2×10^{-4}			
S/N=1	2.56, 2.02	1.35, 1.30	0.58, 0.53
10	1.73, 1.42	0.90, 0.86	0.40, 0.37
100	1.57, 1.33	0.81, 0.77	0.38, 0.34
2×10^{-5}			
S/N=1	2.48, 1.98	1.32, 1.29	0.57, 0.53
10	1.69, 1.40	0.89, 0.85	0.40, 0.36
100	1.53, 1.31	0.81, 0.76	0.37, 0.34
2×10^{-6}			
S/N=1	2.48, 1.98	1.32, 1.29	0.57, 0.53
10	1.68, 1.40	0.89, 0.85	0.40, 0.36
100	1.52, 1.30	0.80, 0.76	0.37, 0.34

TABLE 5

N_2 ERROR - CARS (T), (N), T = 300°K

ERRORS IN %

ERROR-T, ERROR-N

N	Z1=0.002	Z2=0.020	Z3=0.200
1.0			
S/N=1	0.72, 0.55	0.70, 0.54	0.63, 0.43
10	0.44, 0.33	0.44, 0.33	0.43, 0.28
100	0.40, 0.29	0.39, 0.28	0.39, 0.26
10^{-1}			
S/N=1	2,80, 3.14	1.89, 1.70	0.67, 0.56
10	1.66, 1.63	1.07, 1.02	0.42, 0.37
100	1.34, 1.20	0.89, 0.83	0.37, 0.34
10^{-2}			
S/N=1	1.59, 1.82	1.15, 1.04	0.38, 0.36
10	1.11, 1.22	0.74, 0.67	0.26, 0.24
100	1.03, 1.08	0.66, 0.59	0.24, 0.22
10^{-3}			
S/N=1	1.30, 1.58	0.98, 0.95	0.32, 0.33
10	0.92, 1.08	0.63, 0.61	0.22, 0.22
100	0.86, 0.97	0.57, 0.54	0.21, 0.20
10^{-4}			
S/N=1	1.27, 1.56	0.97, 0.94	0.32, 0.32
10	0.90, 1.06	0.62, 0.61	0.22, 0.21
100	0.84, 0.96	0.56, 0.54	0.21, 0.20
10^{-5}			
S/N=1	1.27, 1.56	0.97, 0.94	0.32, 0.32
10	0.90, 1.06	0.62, 0.61	0.22, 0.21
100	0.84, 0.96	0.56, 0.54	0.21, 0.20

TABLE 6

N_2 ERROR - CARS (T), (N), T = 1200°K

ERRORS IN %

ERROR-T, ERROR-N

N	Z1=0.002	Z2=0.020	Z3=0.200
1.0			
S/N=1	1.23, 1.96	1.11, 1.84	0.42, 0.62
10	0.66, 0.96	0.60, 0.90	0.26, 0.38
100	0.51, 0.70	0.48, 0.67	0.23, 0.34
10^{-1}			
S/N=1	1.14, 2.08	0.81, 1.28	0.28, 0.43
10	0.76, 1.29	0.5I, 0.80	0.18, 0.28
100	0.66, 1.07	0.44, 0.69	0.16, 0.25
10^{-2}			
S/N=1	0.94, 1.65	0.64, 1.00	0.21, 0.32
10	0.63, 1.08	0.40, 0.63	0.13, 0.21
100	0.57, 0.95	0.35, 0.56	0.12, 0.19
10^{-3}			
S/N=1	0.91, 1.61	0.62, 0.97	0.20, 0.31
10	0.61, 1.06	0.39, 0.62	0.13, 0.20
100	0.55, 0.93	0.35, 0.54	0.12, 0.19
10^{-4}			
S/N=1	0.91, 1.60	0.62, 0.97	0.20, 0.31
10	0.61, 1.05	0.39, 0.61	0.13, 0.20
100	0.55, 0.93	0.34, 0.54	0.12, 0.18
10^{-5}			
S/N=1	0.91, 1.60	0.62, 0.97	0.20, 0.31
10	0.61, 1.05	0.39, 0.61	0.13, 0.20
100	0.55, 0.93	0.34, 0.54	0.12, 0.18

TABLE 7

N_2 ERROR - SRS (T, N), T = 60°K

ERRORS IN %

ERROR-T, ERROR-N

N	Z1=0.002	Z2=0.020	Z3=0.200
B,2 x 10^{-1}	(.31 x 10^{9})	(.30 x 10^{9})	(.17 x 10^{9})
S/N=1	2.85, 1.88	2.79, 1.82	2.40, 1.24
10	1.67, 1.04	1.64, 1.02	1.44, 0.76
100	1.47, 0.87	1.44, 0.86	1.27, 0.68
B,2 x 10^{-2}	(.21 x 10^{9})	(.68 x 10^{8})	(.19 x 10^{8})
S/N=1	10.12, 6.47	3.85, 2.46	2.30, 1.25
10	5.50, 3.37	2.28, 1.51	1.36, 0.77
100	4.36, 2.47	2.01, 1.30	1.19, 0.69
B,2 x 10^{-3}	(.39 x 10^{8})	(.78 x 10^{7})	(.19 x 10^{7})
S/N=1	14.72, 7.72	3.94, 2.51	2.29, 1,25
10	7.87, 4.72	2.38, 1.57	1.35, 0.77
100	6.10, 3.85	2.11, 1.40	1.18, 0.69
B,2 x 10^{-4}	(.41 x 10^{7})	(.79 x 10^{6})	(.19 x 10^{6})
S/N=1	14.23, 7.95	3.93, 2.52	2.29, 1.25
10	7.64, 4.81	2.38, 1.57	1.35, 0.77
100	6.00, 4.00	2.11, 1.40	1.18, 0.69
B,2 x 10^{-5}	(.42 x 10^{6})	(.79 x 10^{5})	(.19 x 10^{5})
S/N=1	14.14, 7.95	3.93, 2.52	2.29, 1.25
10	7.61, 4.81	2.38, 1.57	1.35, 0.77
100	6.00, 4.00	2.11, 1.40	1.18, 0.69
B,2 x 10^{-6}	(.42 x 10^{5})	(.78 x 10^{4})	(.19 x 10^{4})
S/N=1	14.14, 7.95	3.93, 2.52	2.29, 1.25
10	7.61, 4.81	2.38, 1.57	1.35, 0.77
100	6.00, 4.00	2.11, 1.40	1.18, 0.69

TABLE 8

N_2 ERROR - SRS (T, N), T = $300^{o}K$

ERRORS IN %

ERROR-T, ERROR-N

N	Z1=0.002	Z2=0.020	Z3=0.200
B,1.0	$(.36 \times 10^{9})$	$(.35 \times 10^{9})$	$(.26 \times 10^{9})$
S/N=1	1.27, 0.88	1.24, 0.86	1.15, 0.71
10	0.77, 0.49	0.76, 0.49	0.68, 0.41
100	0.68, 0.42	0.67, 0.41	0.59, 0.37
$B,10^{-1}$	$(.28 \times 10^{9})$	$(.13 \times 10^{9})$	$(.29 \times 10^{8})$
S/N=1	4.24, 2.95	2.46, 1.60	1.18, 0.76
10	2.48, 1.57	1.45, 0.96	0.69, 0.44
100	2.03, 1.20	1.25, 0.80	0.60, 0.39
$B,10^{-2}$	$(.66 \times 10^{8})$	$(.16 \times 10^{8})$	$(.29 \times 10^{7})$
S/N=1	4.86, 4.49	2.70, 1.72	1.18, 0.76
10	2.90, 2.59	1.61, 1.06	0.69, 0.44
100	2.36, 2.06	1.39, 0.93	0.60, 0.39
$B,10^{-3}$	$(.73 \times 10^{7})$	$(.17 \times 10^{7})$	$(.29 \times 10^{6})$
S/N=1	4.87, 4.73	2.70, 1.72	1.18, 0.76
10	2.85, 2.73	1.61, 1.06	0.69, 0.44
100	2.28, 2.19	1.39, 0.94	0.60, 0.39
$B,10^{-4}$	$(.74 \times 10^{6})$	$(.17 \times 10^{6})$	$(.29 \times 10^{5})$
S/N=1	4.87, 4.74	2.70, 1.72	1.18, 0.76
10	2.85, 2.74	1.61, 1.06	0.69, 0.44
100	2.28, 2.19	1.39, 0.94	0.60, 0.39
$B,10^{-5}$	$(.74 \times 10^{5})$	$(.17 \times 10^{5})$	$(.29 \times 10^{4})$
S/N=1	4.37, 4.74	2.70, 1.72	1.18, 0.76
10	2.85, 2.74	1.61, 1.06	0.69, 0.44
100	2.28, 2.10	1.39, 0.94	0.60, 0.39

TABLE 9

N_2 ERROR - SRS (T, N), T = 1200°K

ERRORS IN %

ERROR-T, ERROR-N

N	Z1=0.002	Z2=0.020	Z3=0.200
B,1.0	$(.38 \times 10^{9})$	$(.33 \times 10^{9})$	$(.83 \times 10^{8})$
S/N=1	3.30, 3.63	3.55, 4.06	2.36, 2.58
10	1.98, 2.02	2.01, 2.12	1.60, 1.74
100	1.72, 1.67	1.71, 1.71	1.50, 1.62
$B,10^{-1}$	$(.17 \times 10^{9})$	$(.70 \times 10^{8})$	$(.91 \times 10^{7})$
S/N=1	4.83, 6.96	6.47, 7.43	2.79, 3.07
10	2.77, 3.53	3.42, 3.93	1.86, 2.04
100	2.34, 2.66	2.55, 2.84	1.73, 1.89
$B,10^{-2}$	$(.23 \times 10^{8})$	$(.76 \times 10^{7})$	$(.91 \times 10^{6})$
S/N=1	5.92, 9.29	6.99, 8.02	2.82, 3.10
10	3.04, 4.53	3.77, 4.39	1.88, 2.06
100	2.33, 3.26	2.76, 3.18	1.75, 1.91
$B,10^{-3}$	$(.23 \times 10^{7})$	$(.76 \times 10^{6})$	$(.91 \times 10^{5})$
S/N=1	6.10, 9.57	7.07, 8.10	2.82, 3.10
10	3.10, 4.67	3.82, 4.45	1.89, 2.06
100	2.36, 3.35	2.79, 3.22	1.75, 1.91
$B,10^{-4}$	$(.23 \times 10^{6})$	$(.76 \times 10^{5})$	$(.91 \times 10^{4})$
S/N=1	6.11, 9.60	7.07, 8.11	2.82, 3.10
10	3.11, 4.67	3.82, 4.45	1.89, 2.06
100	2.36, 3.36	2.79, 3.22	1.75, 1.91
$B,10^{-5}$	$(.23 \times 10^{5})$	$(.76 \times 10^{4})$	$(.91 \times 10^{3})$
S/N=1	6.11, 9.60	7.07, 8.11	2.82, 3.10
10	3.11, 4.67	3.82, 4.45	1,89, 2.06
100	2.36, 3.36	2.79, 3.22	1.75, 1.91

TABLE 10

N_2 ERROR - SRS (T), (N), T = 60°K

ERRORS IN %

ERROR-T, ERROR-N

N	Z1=0.002	Z2=0.020	Z3=0.200
2×10^{-1}			
S/N=1	2.36, 1.56	2.36, 1.53	1.98, 1.02
10	1.45, 0.90	1.46, 0.91	1.30, 0.69
100	1.29, 0.76	1.29, 0.78	1.18, 0.63
2×10^{-2}			
S/N=1	10.07, 6.44	3.52, 2.24	1.85, 1.01
10	5.20, 3.18	2.11, 1.40	1.21, 0.68
100	3.95, 2.24	1.86, 1.20	1.10, 0.63
2×10^{-3}			
S/N=1	7.01, 3.68	3.53, 2.25	1.83, 1.00
10	4.34, 2.60	2.19, 1.45	1.20, 0.68
100	3.83, 2.42	1.97, 1.31	1.09, 0.63
2×10^{-4}			
S/N=1	6.02, 3.36	3.52, 2.25	1.83, 1.00
10	3.80, 2.39	2.19, 1.45	1.20, 0.68
100	3.38, 2.25	1.96, 1.31	1.09, 0.63
2×10^{-5}			
S/N=1	5.93, 3.34	3.52, 2.25	1.83, 1.00
10	3.75, 2.37	2.19, 1.45	1.20, 0.68
100	3.34, 2.23	1.96, 1.31	1.09, 0.63
2×10^{-6}			
S/N=1	5.92, 3.33	3.52, 2.25	1.83, 1.00
10	3.74, 2.37	2.19, 1.45	1.20, 0.68
100	3.34, 2.23	1.96, 1.31	1.09, 0.63

TABLE 11

N_2 ERROR - SRS (T), (N), T = 300°K

ERRORS IN %

ERROR-T, ERROR-N

N	Z1=0.002	Z2=0.020	Z3=0.200
1			
S/N=1	1.04, 0.73	1.03, 0.71	0.93, 0.57
10	0.66, 0.43	0.66, 0.42	0.61, 0.37
100	0.60, 0.37	0.60, 0.37	0.56, 0.34
10^{-1}			
S/N=1	3.97, 2.77	2.26, 1.47	0.92, 0.59
10	2.21, 1.40	1.33, 0.88	0.61, 0.39
100	1.75, 1.04	1.13, 0.72	0.44, 0.36
10^{-2}			
S/N=1	3.20, 2.96	2.35, 1.50	0.92, 0.59
10	2.19, 1.97	1.46, 0.96	0.61, 0.39
100	1.98, 1.72	1.29, 0.86	0.55, 0.36
10^{-3}			
S/N=1	2.80, 2.72	2.34, 1.49	0.92, 0.59
10	1.93, 1.85	1.45, 0.96	0.61, 0.39
100	1.76, 1.68	1.28, 0.86	0.55, 0.36
10^{-4}			
S/N=1	2.77, 2.70	2.34, 1.49	0.92, 0.59
10	1.91, 1.84	1.45, 0.96	0.61, 0.39
100	1.73, 1.67	1.28, 0.86	0.55, 0.36
10^{-5}			
S/N=1	2.77, 2.70	2.34, 1.49	0.92, 0.59
10	1.91, 1.84	1.45, 0.96	0.61, 0.39
100	1.73, 1.67	1.28, 0.86	0.55, 0.36

TABLE 12

N_2 ERROR - SRS (T), (N), T = 1200°K

ERRORS IN %

ERROR-T, ERROR-N

N	Z1=0.002	Z2=0.020	Z3=0.200
1.0			
S/N=1	1.32, 1.45	1.17, 1.34	0.41, 0.45
10	0.70, 0.71	0.64, 0.67	0.28, 0.31
100	0.56, 0.55	0.53, 0.52	0.26, 0.29
10^{-1}			
S/N=1	2.11, 3.05	1.40, 1.61	0.43, 0.47
10	1.37, 1.74	0.87, 1.00	0.29, 0.32
100	1.21, 1.37	0.77, 0.85	0.27, 0.30
10^{-2}			
S/N=1	1.79, 2.80	1.38, 1.58	0.43, 0.47
10	1.21, 1.80	0.86, 1.00	0.29, 0.32
100	1.12, 1.57	0.77, 0.88	0.27, 0.30
10^{-3}			
S/N=1	1.75, 2.75	1.37, 1.58	0.43, 0.47
10	1.19, 1.79	0.85, 1.00	0.29, 0.32
100	1.10, 1.57	0.77, 0.88	0.27, 0.30
10^{-4}			
S/N=1	1.75, 2.74	1.37, 1.58	0.43, 0.47
10	1.19, 1.79	0.85, 1.00	0.29, 0.32
100	1.10, 1.57	0.77, 0.88	0.27, 0.30
10^{-5}			
S/N=1	1.75, 2.74	1.37, 1.58	0.43, 0.47
10	1.19, 1.79	0.85, 1.00	0.29, 0.32
100	1.10, 1.57	0.77, 0.88	0.27, 0.30

TABLE 13

CO ERROR - SRS (T, N)

ERRORS IN %

ERROR-T, ERROR-N

N	Z1=0.002	Z2=0.020	Z3=0.200
$T=60^{o}K$			
$B,10^{-2}$	$(.62 \times 10^{7})$	$(.62 \times 10^{7})$	$(.61 \times 10^{7})$
S/N=1	5.17, 1.87	5.19, 1.88	5.98, 1.85
10	3.09, 1.24	3.10, 1.24	3.57, 1.24
100	2.48, 1.02	2.48, 1.02	2.82, 1.01
$T=300^{o}K$			
$B,10^{-2}$	$(.37 \times 10^{7})$	$(.36 \times 10^{7})$	$(.30 \times 10^{7})$
S/N=1	1.11, 0.71	1.11, 0.66	1.26, 0.68
10	0.66, 0.45	0.66, 0.44	0.70, 0.41
100	0.59, 0.41	0.58, 0.40	0.60, 0.37
$T=1200^{o}K$			
$B,10^{-2}$	$(.27 \times 10^{7})$	$(.24 \times 10^{7})$	$(.80 \times 10^{6})$
S/N=1	2.37, 2.59	2.74, 2.64	2.03, 2.21
10	1.62, 1.69	1.62, 1.69	1.43, 1.53
100	1.41, 1.53	1.42, 1.53	1.35, 1.44

TABLE 14

CO ERROR - SRS (T), (N)

ERRORS IN %

ERROR-T, ERROR-N

N	Z1=0.002	Z2=0.020	Z3=0.200
$T=60^{o}K$			
10^{-2}			
S/N=1	3.53, 1.28	3.54, 1.28	4.01, 1.24
10	2.09, 0.84	2.10, 0.84	2.37, 0.82
100	1.84, 0.76	1.84, 0.76	2.06, 0.74
$T=300^{o}K$			
10^{-2}			
S/N=1	1.09, 0.70	1.08, 0.68	1.15, 0.62
10	0.66, 0.45	0.66, 0.44	0.70, 0.41
100	0.59, 0.41	0.58, 0.42	0.60, 0.37
$T=1200^{o}K$			
10^{-2}			
S/N=1	0.915,0.87	0.82, 0.79	0.36, 0.39
10	0.53, 0.55	0.49, 0.51	0.26, 0.28
100	0.45, 0.49	0.42, 0.46	0.24, 0.26

TABLE 15

CO ERROR - CARS (T, N), T = $60^{o}K$

ERRORS IN %

ERROR-T, ERROR-N

N	Z1=0.002	Z2=0.020	Z3=0.200
B,10^{-2}	(.36 x 10^{-3})	(.36 x 10^{-3})	(.36 x 10^{-3})
S/N=1	5.04, 1.09	5.07, 1.09	6.01, 1.11
10	2.89, 0.58	2.90, 0.58	3.33, 0.57
100	2.53, 0.48	2.54, 0.48	2.86, 0.47
B,10^{-3}	(.59 x 10^{-5})	(.59 x 10^{-5})	(.56 x 10^{-5})
S/N=1	4.12, 1.23	4.14, 1.23	4.56, 1.23
10	2.84, 0.80,	2.85, 0.80	3.15, 0.79
100	2.68, 0.74	2.69, 0.74	2.96, 0.74
B, 10^{-4}	(.13 x 10^{-5})	(.13 z 10^{-5})	(.13 x 10^{-5})
S/N=1	13.20, 6.96	13.30, 6.98	14.70. 7.26
10	9.83, 5.14	9.85, 5.15	10.90, 5.35
100	9.42, 4.92	9.45, 4.92	10.40, 5.11
B,10^{-5}	(.11 x 10^{-5})	(.11 x 10^{-5})	(.11 x 10^{-5})
S/N=1			
10			
100	ERROR PROPAGATION IS UNSTABLE FOR N 10^{-4}; (T,N) CANNOT BE MEASURED SIMULTANEOUSLY		
B,10^{-6}			
S/N=1			
10	B = .111 x 10^{-5}		
100			
B,10^{-7}			
S/N=1			
10			
100			

TABLE 16

CO ERROR - CARS (T, N), T = 300°K

ERRORS IN %

ERROR-T, ERROR-N

N	Z1=0.002	Z2=0.020	Z3=0.200
$B,10^{-2}$	$(.11 \times 10^{-3})$	$(.10 \times 10^{-3})$	$(.80 \times 10^{-4})$
S/N=1	0.98, 0.60	0.98, 0.59	3.87, 2.23
10	0.56, 0.37	0.56, 0.37	2.15, 1.21
100	0.49, 0.33	0.49, 0.33	1.85, 1.03
$B,10^{-3}$	$(.30 \times 10^{-5})$	$(.29 \times 10^{-5})$	$(.20 \times 10^{-5})$
S/N=1	1.36, 1.56	1.37, 1.60	4.27, 7.08
10	0.90, 1.07	0.91, 1.09	3.09, 5.12
100	0.83, 1.00	0.85, 1.02	2.93, 4.84
$B,10^{-4}$	$(.12 \times 10^{-5})$	$(.13 \times 10^{-5})$	$(.12 \times 10^{-5})$
S/N=1	11.90,13.80	12.00,14.00	13.50,24.90
10	8.56, 9.85	8.70, 9.97	9.65,16.90
100	8.14, 9.21	8.3q, 9.43	9.13,13.90
$B,10^{-5}$	$(.11 \times 10^{-5})$	$(.11 \times 10^{-5})$	$(.11 \times 10^{-5})$
S/N=1			
10			
100			
$B,10^{-6}$			
S/N=1	UNSTABLE AS A FUNCTION OF (T,N)		
10			
100			

TABLE 17

CO ERROR - CARS (T, N), T = 1200°K

ERRORS IN %

ERROR-T, ERROR-N

N	Z1=0.002	Z2=0.020	Z3=0.200
$B,10^{-2}$	$(.65 \times 10^{-4})$	$(.57 \times 10^{-4})$	$(.16 \times 10^{-5})$
S/N=1	2.48, 1.81	2.40, 1.78	1.85, 1.88
10	1.47, 1.15	1.43, 1.12	1.28, 1.29
100	1.24, 1.01	1.21, 0.99	1.20, 1.22
$B,10^{-3}$	$(.23 \times 10^{-5})$	$(.22 \times 10^{-5})$	$(.14 \times 10^{-5})$
S/N=1	5.64, 3.96	6.92, 4.96	12.00,11.80
10	3.68, 2.67	4.52, 3.31	8.37, 8.21
100	3.39, 2.47	4.17, 3.07	7.82, 7.67
$B,10^{-4}$	$(.12 \times 10^{-5})$	$(.12 \times 10^{-5})$	$(.11 \times 10^{-5})$
S/N=1			
10			
100			
$B,10^{-6}$			
S/N=1	UNSTABLE AS A FUNCTION OF (T,N)		
10			
100			

TABLE 18

CO ERROR - CARS (T), (N), T = $60^{o}K$

ERRORS IN %

ERROR-T, ERROR-N

N	Z1=0.002	Z2=0.020	Z3=0.200
10^{-2}			
S/N=1	4.37, 0.59	4.39, 0.59	4.88, 0.57
10	2.78, 0.37	2.79, 0.37	3.14, 0.37
100	2.52, 0.32	2.53, 0.32	2.84, 0.32
10^{-3}			
S/N=1	3.57, 0.32	3.58, 0.32	3.76, 0.31
10	2.58, 0.20	2.58, 0.20	2.73, 0.20
100	2.45, 0.18	2.46, 0.18	2.61, 0.18
10^{-4}			
S/N=1	11.80, 0.17	11.80, 0.17	12.90, 0.17
10	8.75, 0.13	8.76, 0.13	9.55, 0.13
100	8.38, 0.12	8.40, 0.12	9.16, 0.12
10^{-5}			
S/N=1			
10			
100			
10^{-6}			
S/N=1	UNSTABLE AS A FUNCTION OF (T), (N)		
10			
100			

TABLE 19

CO ERROR - CARS (T), (N), T = 300°K

ERRORS IN %

ERROR-T, ERROR-N

N	Z1=0.002	Z2=0.020	Z3=0.200
10^{-2}			
S/N=1	0.85, 0.38	0.83, 0.37	0.78, 0.32
10	0.51, 0.24	0.50, 0.24	0.55, 0.20
100	0.44, 0.22	0.44, 0.21	0.51, 0.19
10^{-3}			
S/N=1	1.11, 0.24	1.11, 0.23	0.93, 0.17
10	0.71, 0.16	0.72, 0.16	0.70, 0.13
100	0.66, 0.15	0.66, 0.15	0.65, 0.12
10^{-4}			
S/N=1	0.66, 0.17	0.67, 0.17	0.75, 0.16
10	0.48, 0.12	0.49, 0.12	0.56, 0.12
100	0.46, 0.12	0.47, 0.12	0.54, 0.12
10^{-5}			
S/N=1			
10			
100			
10^{-6}			
S/N=1	UNSTABLE AS A FUNCTION OF (T), (N)		
10			
100			

TABLE 20

CO ERROR - CARS (T), (N), T = 1200°K

ERRORS IN %

ERROR-T, ERROR-N

N	Z1=0.002	Z2=0.020	Z3=0.200
10^{-2}			
S/N=1	0.69, 0.50	0.63, 0.46	0.27, 0.21
10	0.41, 0.32	0.38, 0.30	0.18, 0.15
100	0.35, 0.28	0.33, 0.26	0.17, 0.14
10^{-3}			
S/N=1	1.55, 0.27	1.54, 0.26	1.51, 0.18
10	1.06, 0.17	1.07, 0.17	1.10, 0.13
100	1.00, 0.16	1.00, 0.16	1.05, 0.13
10^{-4}			
S/N=1	11.70, 0.17	11.90, 0.16	19.20, 0.16
10	8.60, 0.12	8.82, 0.12	14.30, 0.12
100	8.23, 0.12	8.44, 0.12	13.70, 0.12
10^{-5}			
S/N=1			
10			
100			
10^{-6}			
S/N=1			
10	UNSTABLE AS A FUNCTION OF (T), (N)		
100			

TABLE 21

CO ERROR - CARS (T, N); X_{NR}

Z1 = 0.050

ERRORS IN %

ERROR-T, ERROR-N

N	$X_{NR} = 10^{-18}$	$X_{NR} = 10^{-20}$
B, 10^{-2}	$(.36 \times 10^{-3})$	$(.89 \times 10^{-4})$
S/N=1	5.20, 1.08	1.06, 0.54
10	2.96, 0.57	0.59, 0.33
100	2.59, 0.47	0.50, 0.29
B, 10^{-3} $(.88 \times 10^{-6})$	$(.48 \times 10^{-5})$	$(.89 \times 10^{-6})$
S/N=1	3.99, 0.95	1.05, 0.55
10	2.78, 0.61	0.59, 0.33
100	2.63, 0.56	0.50, 0.29
B, 10^{-4} $(.10 \times 10^{-7})$	$(.22 \times 10^{-6})$	$(.89 \times 10^{-8})$
S/N=1	13.10, 3.70	0.99, 0.60
10	9.70, 2.72	0.57, 0.37
100	9.30, 2.60	0.51, 0.33
B, 10^{-5}	$(.21 \times 10^{-7})$	$(.26 \times 10^{-9})$
S/N=1		1.40, 1.35
10	UNSTABLE	0.95, 0.94
100		0.90, 0.88
B, 10^{-6}	$(.21 \times 10^{-8})$	$(.21 \times 10^{-11})$
S/N=1		12.20, 6.74
10	UNSTABLE	8.95, 4.89
100		8.57, 4.67
B, 10^{-7}	$(.21 \times 10^{-9})$	$(.21 \times 10^{-11})$
S/N=1		
10	UNSTABLE	UNSTABLE
100		

TABLE 22

CO ERROR - CARS (T), (N); X_{NR}

Z1 = 0.050

ERRORS IN %

ERROR-T, ERROR-N

N	$X_{NR} = 10^{-18}$	$X_{NR} = 10^{-20}$
10^{-2}		
S/N=1	4.48, 0.55	0.83, 0.37
10	2.85, 0.35	0.51, 0.24
100	2.58, 0.30	0.45, 0.22
10^{-3}		
S/N=1	3.61, 0.27	0.82, 0.37
10	2.61, 0.17	0.51, 0.24
100	2.48, 0.16	0.45, 0.21
10^{-4}		
S/N=1	11.90, 0.17	0.76, 0.32
10	8.81, 0.12	0.48, 0.20
100	8.45, 0.11	0.44, 0.18
10^{-5}		
S/N=1	UNSTABLE, 0.16	1.08, 0.20
10	0.12	0.72, 0.13
100	0.11	0.68, 0.13
10^{-6}		
S/N=1	UNSTABLE, CONSTANT	6.95, 0.16
10		5.11, 0.12
100		4.89, 0.11
10^{-7}		
S/N=1	UNSTABLE, CONSTANT	66.40, 0.16
10		49.40, 0.12
100		47.40, 0.11
		UNSTABLE

TABLE 23

PRESSURE BROADENING COEFFICIENTS*

		a	$(\Lambda a)^{\frac{1}{2}}$
N_2			
	J= 6	0.1477	0.0183
	7	0.1242	0.0374
	8	0.1502	0.0205
	9	0.1120	0.0116
	10	0.1222	0.0047
	11	0.1107	0.0177
	12	0.1263	0.0263
	13	0.1222	0.0511
	14	0.0962	0.0124
	15	0.1283	0.0281
O_2			
	3	0.1811	0.0431
	5	0.1481	0.0275
	7	0.1385	0.0252
	9	0.1306	0.0223
	11	0.1259	0.0374
	13	0.1319	0.0374
	15	0.1394	0.0507
	17	0.1283	0.0342
	19	0.1190	0.0356

*Linewidth data furnished by W. H. Fletcher

TABLE 24

CARS N_2 PEAK HEIGHT ERROR

	HIGH RESOLUTION Z1=0.010			(2 ERR-A)/A	LOW RESOLUTION Z1=0.050		
	Exp.	Theory	Err.		Exp.	Theory	Err.
Q(2)	0.868	0.9820	0.114	0.200	1.000	1.000	0.000
Q(3)	0.667	0.8021	0.132	0.200	-	-	-
Q(4)	0.923	0.9757	0.53	0.200	0.909	0.9512	0.042
Q(5)	0.522	0.6411	0.119	0.200	0.590	0.6179	0.028
Q(6)	1.000	1.000	0.000	0.207	0.910	0.9550	0.045
Q(7)	0.474	0.6658	0.192	0.610	0.535	0.6013	0.066
Q(8)	0.944	0.9368	-0.007	0.272	0.732	0.8927	0.161
Q(9)	0.437	0.6081	0.171	0.206	0.453	0.5467	0.093
Q(10)	0.808	0.9508	0.143	0.164	0.726	0.8941	0.168
Q(11)	0.306	0.4725	0.167	0.318	0.279	0.4051	0.126
Q(12)	0.632	0.7164	0.084	0.414	0.608	0.6672	0.059

TABLE 25

N_2 CARS VARIANCE ERROR, z1 = 0.050

$T = 300^{o}K$

ERRORS IN %

N,B	Λ (T,N) ; (T),(N)	$\Lambda + \Lambda_d$ (T,N) ; (T),(N)
1.0, (.956)		
S/N=1	1.13,0.75 ; 0.67,0.50	3.00,2.00 ; 1.46,0.96
10	0.64,0.44 ; 0.43,0.31	1.86,1,29 ; 1.04,0.63
100	0.55,0.39 ; 0.39,0.28	1.49,1.07 ; 0.94,0.55
10^{-1}, (.157)		
S/N=1	1.50,1.16 ; 1.33,1.04	3.76,3.12 ; 3.23,2.79
10	0.85,0.69 ; 0.77,0.63	2.72,2.08 ; 2.21,1.76
100	0.70,0.58 ; 0.65,0.54	2.17,1.57 ; 1.77,1.29
10^{-2}, ($.435 \times 10^{-2}$)		
S/N=1	1.57,1.47 ; 0.74,0.69	1.91,1.79 ; 1.01,0.95
10	0.87,0.82 ; 0.46,0.43	1.20,1.12 ; 0.71,0.67
100	0.73,0.67 ; 0.41,0.38	1.01,0.92 ; 0.64,0.59
10^{-3}, ($.505 \times 10^{-4}$)		
S/N=1	1.61,1.56 ; 0.68,0.66	1.61,1.56 ; 0.69,0.67
10	0.89,0.86 ; 0.43,0.41	0.90,0.87 ; 0.43,0.42
100	0.73,0.70 ; 0.38,0.37	0.74,0.71 ; 0.39,0.37

TABLE 26

N_2 CARS VARIANCE ERROR, z1 = 0.010

T = 300°K

ERRORS IN %

N,B	Λ (T,N) ; (T),(N)	$\Lambda - \Lambda_d$ (T,N) ; (T),(N)
1.0, (1.080)		
S/N=1	1.12,0.79 ; 0.72,0.55	2.96,1.82 ; 1.44,0.93
10	0.64,0.46 ; 0.45,0.33	1.80,1.09 ; 0.98,0.60
100	0.54,0.39 ; 0.40,0.29	1.44,0.88 ; 0.86,0.51
10^{-1}, (.398)		
S/N=1	2.33,1.98 ; 2.18,1.85	5.96,4.22 ; 5.39,3.83
10	1.35,1.14 ; 1.27,1.08	3.49,2.19 ; 3.06,1.92
100	1.11,0.92 ; 1.05,0.86	2.47,1.54 ; 2.15,1.34
10^{-2}, ($.127 \times 10^{-1}$)		
S/N=1	2.27,2.21 ; 1.15,1.12	3.32,3.09 ; 1.87,1.75
10	1.40,1.34 ; 0.77,0.74	2.20,1.99 ; 1.37,1.24
100	1.17,1.10 ; 0.70,0.66	1.76,1.52 ; 1.21,1.05
10^{-3}, ($.149 \times 10^{-3}$)		
S/N=1	2.30,2.32 ; 1.06,1.07	2.32,2.34 ; 1.07,1.08
10	1.42,1.41 ; 0.71,0.71	1.44,1.42 ; 0.73,0.72
100	1.18,1.16 ; 0.65,0.63	1.20,1.17 ; 0.66,0.64

TABLE 27

N_2 SRS VARIANCE ERROR, z1 = 0.050

T = 300°K

ERRORS IN %

N,B	Λ (T,N) ; (T),(N)	$\Lambda + \Lambda_a$ (T,N) ; (T),(N)
1.0, ($.311 \times 10^9$)		
S/N=1	1.17,0.79 ; 0.98,0.66	2.07,1.26 ; 1.66,1.01
10	0.72,0.46 ; 0.63,0.41	1.56,0.95 ; 1.32,0.77
100	0.64,0.39 ; 0.58,0.36	1.45,0.84 ; 1.25,0.73
10^{-1}, ($.678 \times 10^8$)		
S/N=1	1.79,1.14 ; 1.56,1.00	1.97,1.27 ; 1.72,1.11
10	1.05,0.69 ; 0.95,0.62	1.27,0.83 ; 1.15,0.76
100	0.92,0.59 ; 0.84,0.54	1.13,0.74 ; 1.05,0.69
10^{-2}, ($.760 \times 10^7$)		
S/N=1	1.89,1.20 ; 1.62,1.03	1.89,1.20 ; 1.62,1.03
10	1.10,0.72 ; 0.99,0.65	1.11,0.73 ; 1.00,0.65
100	0.95,0.63 ; 0.88,0.59	0.96,0.63 ; 0.88,0.58
10^{-3}, ($.767 \times 10^6$)		
S/N=1	1.89,1.20 ; 1.62,1.03	1.89,1.20 ; 1.62,1.03
10	1.11,0.72 ; 0.99,0.65	1.11,0.72 ; 0.99,0.65
100	0.95,0.63 ; 0.87,0.58	0.95,0.63 ; 0.88,0.58

TABLE 28

N_2 SRS VARIANCE ERROR, z1 = 0.010

T = 3000°K

ERRORS IN %

N,B	Λ (T,N) ; (T),(N)	$\Lambda + \Lambda_d$ (T,N) ; (T),(N)
1.0, ($.358 \times 10^9$)		
S/N=1	1.26,0.87 ; 1.04,0.72	2.26,1.29 ; 1.72,0.99
10	0.77,0.49 ; 0.66,0.43	1.61,0.89 ; 1.31,0.72
100	0.68,0.42 ; 0.60,0.37	1.48,0.81 ; 1.24,0.68
10^{-1}, ($.180 \times 10^9$)		
S/N=1	3.18,2.14 ; 2.90,1.95	4.78,3.09 ; 4.18,2.71
10	1.85,1.21 ; 1.69,1.10	3.29,2.05 ; 2.80,1.75
100	1.55,0.96 ; 1.51,0.88	2.82,1.68 ; 2.42,1.44
10^{-2}, ($.254 \times 10^8$)		
S/N=1	3.38,2.29 ; 2.82,1.91	3.49,2.32 ; 2.96,1.97
10	1.99,1.39 ; 1.75,1.23	2.11,1.44 ; 1.90,1.30
100	1.63,1.16 ; 1.51,1.08	1.75,1.22 ; 1.65,1.15
10^{-3}, ($.263 \times 10^7$)		
S/N=1	3.37,2.31 ; 2.78,1.91	3.37,2.31 ; 2.78,1.91
10	1.98,1.41 ; 1.73,1.23	1.98,1.41 ; 1.73,1.23
100	1.61,1.18 ; 1.49,1.09	1.61,1.18 ; 1.49,1.10

APPENDIX B

EXPONENTIALS

$$\text{EXP}\,[x, y; z] = \text{EXP}\left(-\frac{(x - y)^2}{z^2}\right) \tag{1}$$

$$\text{EXP}\,[x, y; z]\ \text{EXP}\,[x, v; w] =$$

$$\text{EXP}\left\{-\left[\frac{x^2(w^2 + z^2) - 2(w^2y + z^2v) + w^2y^2 + z^2v^2}{z^2w^2}\right]\right\} \tag{2}$$

$$\text{Quantity within brackets} = \left[\frac{w^2 + z^2}{w^2z^2}\left(x - \frac{w^2y + z^2v}{w^2 + z^2}\right)^2 + \frac{(v - y)^2}{w^2 + z^2}\right] \tag{3}$$

Eq. (2) R.H.S. becomes

$$\text{EXP}\left(-\frac{(v - y)^2}{w^2 + z^2}\right)\ \text{EXP}\ -\left[\frac{w^2 + z^2}{w^2z^2}\left(x - \frac{w^2y + z^2v}{w^2 + z^2}\right)^2\right] \tag{4}$$

$$\text{EXP}[x, y; z]\ \text{EXP}\,[x, v; w] = \text{EXP}\,[v, y;\ w^2 + z^2]\ x$$

$$\text{EXP}\left[x, \frac{w^2y + z^2v}{w^2 + z^2}; \frac{zw}{w^2 + z^2}\right] \tag{5}$$

APPENDIX C

THE COMPLEX ERROR FUNCTION

For the calculation of the complex error function necessary for the CARS and SRS profile, the regimes of z are

$$\text{A)}\quad \mathrm{Im}\, z \equiv 0,\ \mathrm{Re}\, z > 0$$

$$\text{B)}\quad \mathrm{Im}\, z \equiv 0,\ \mathrm{Re}\, z < 0. \tag{1}$$

Evaluating $\bar{W}(z)$ for case A0 may be done in the quotient form (30)

$$R(v) = \left(\sum_i^p a_i v^i\right)/\left(v^{p+1} + \sum_i^p b_i v^i\right) \tag{2}$$

where $v = y - ix$ and $\bar{W} = R$. For $p = 5$, the relative error in calculating $\bar{W}$ is a 10^{-9} for $0 \leq |v| \leq 10^5$. To extend the analysis to case B), note that

$$-x + iy = -(x + iy)^*. \tag{3}$$

Since $\bar{W}(-z^*) = [\bar{W}(z)]^*$, then

$$\bar{W}_B = \bar{W}_A(x + iy)^* \tag{4}$$

and similarly for derivatives. $\mathrm{Re}\bar{W})_y$ and $\mathrm{Dm}\bar{W})_y$ may be calculated from (2).

The a_i and b_i coefficients are given ala Hui.

Coefficients for rational approximation of (2) are

	a	b
0	37.24429446739879	37.2442945086
1	57.90331938807185	99.9290005933
2	43.16280063072749	118.6763981260
3	18.64649990312317	80.6459493922
4	4.67506018267650	33.5501020941
5	0.56418958297228	8.2863279156

APPENDIX D

LINE STRENGTH FACTOR

Calculating the line strength factor for diatomic molecules requires some detailed analysis. The expression for the Raman cross section is (37, 38)

$$\sigma^{B}_{v,J} = K(\nu^{B}_{v,J})^{4} S_v S^{B}_{J} \tag{1}$$

where $\nu^{B}_{v,J}$ is the wavelength of the scattered light and B indicates the branch {O, Q, S} of the vibrational manifold. The expressions for the S factors are (37, 38)

$$S_v = v + 1 \tag{2}$$

$$S^{Q}_{J} = a_0 + \frac{J(J+1)}{(2J-1)(2J+3)} \tag{3}$$

$$S^{S}_{J} = \frac{3}{2}\frac{(J+1)(J+2)}{(2J+1)(2J+3)} \tag{4}$$

$$S^{O}_{J} = \frac{3}{2}\frac{J(J-1)}{(2J+1)(2J-1)} \tag{5}$$

where a_0 is the trace scattering constant.

To obtain the line strength factor the usual room temperature, v = 0 vibrational level calculations, from Fenner (37),

$$\frac{\sigma^{S}_{v} + \sigma_{v}}{\sigma^{Q}_{v}} = 0.3 \qquad O_2,\ N_2 \tag{6}$$

Defining $f_{v,J}$ as EXP $(-E_{vJ}/KT)$,

$$\frac{\sigma_0^S + \sigma_0^Q}{\sigma_0^Q} = \frac{\Sigma f_{0,J}(\sigma_{0,J}^S + \sigma_{0,J}^Q)}{\Sigma f_{0,J}\sigma_{0,J}^Q} . \tag{7}$$

Note that the rotational partition function for diatomic molecules used in many calculations is $(2J + 1)f_{v,J}$.

From Equations (1) and (6),

$$\frac{\Sigma f_{0,J}[(v_{0,J}^S)^4 S_J^S + (v_{0,J}^0)^4 S_J^0]}{\sum_J f_{0,J}(v_{0,J}^Q)^4 S_J^Q} = 0.3. \tag{8}$$

Writing S_J^Q as $Q_J + a_0$ with

$$Q_J = \frac{J(J + 1)}{(2J - 1)(2J + 3)}. \tag{9}$$

Equation (8) becomes

$$a_0 = \frac{\Sigma f_{0,J}[(v_{0,J}^S)^4 S_J^S + (v_{0,J}^0)^4 S_J^0]}{0.3 \sum_J f_{0,J}(v_{0,J}^Q)^4}$$

$$- \frac{\Sigma f_{0,J}(v_{0,J}^Q)^4 Q_J}{\sum_J f_{0,J}(v_{0,J}^Q)^4}. \tag{10}$$

For either anti-Stokes or Stokes scattering,

$$v_{0,J}^B = v_{EXCITING} = \Delta v_J^B. \tag{11}$$

The results of solving Equation (10) for N_2, O_2 and CO are:

$$a_0(N_2) = 2.2594 - (T - 260)(1.43 \times 10^{-5}) \quad (12)$$

$$a_0(O_2) = 2.2571 - (T - 260)(1.04 \times 10^{-5}) \quad (13)$$

$$a_0(CO) = 2.2591 - (T - 260)(1.41 \times 10^{-5}) \quad (14)$$

where the partition function has been calculated from the energy expression in Herzberg (38), and the computer calculations were run from 60°K to 1260°K. Note from the above expression that the trace scattering constant has a very weak temperature dependence.

VITA

Patrick Elliott Perkins was born in Syracuse, New York, on February 24, 1951. He was graduated from Sandy Springs High School in Atlanta, Georgia, in May, 1968. The following September he entered Emory University. He transferred to the Georgia Institute of Technology from which he received a Bachelor of Science in Physics in 1973. In the fall of 1973, he began study at New Mexico Institute of Mining and Technology for a Master's degree in Physics which he completed in December, 1974.

He entered the graduate program at the University of Tennessee Space Institute in June, 1975. He obtained a Master's degree in Computer Science in August 1976. He received the Doctor of Philosophy degree with a major in Physics in March 1980.

The author is a member of the Optical Society of America and is presently employed at Sanders Associates, Inc. in Nashua, New Hampshire.